The Journal of
Gemmology
2008 / Volume 31 / Nos. 1/2

The Gemmological Association of Great Britain

The Gemmological Association of Great Britain

27 Greville Street, London EC1N 8TN
T: +44 (0)20 7404 3334 **F:** +44 (0)20 7404 8843
E: information@gem-a.com **W:** www.gem-a.com

Registered Charity No. 1109555
Registered office: Palladium House, 1-4 Argyll Street, London W1F 7LD

The Journal of Gemmology

The Editor is glad to consider original articles shedding new light on subjects of gemmological interest for publication in *The Journal of Gemmology*. A Guide to the preparation of typescripts for publication in *The Journal* is given on our website, or contact the Production Editor at the Gemmological Association of Great Britain.

Thortveitite – a new gemstone

R. Chapman, I.F. Mercer, A.H. Rankin and J. Spratt

Abstract: A water-worn pebble of good clarity purchased in Bangkok started the quest that identified this as gem-quality thortveitite, a scandium yttrium silicate. A faceted stone and a cleavage fragment, both from the original pebble, have been tested. Results from standard gemmological tests on the faceted stone did not match those from any known gemstone. The stone and fragment were subsequently identified as high-scandium thortveitite. The unusual chemistry indicates a possible synthetic origin; however, a natural origin is suggested by the presence of three-phase inclusions in a planar array (feather) within the faceted stone.

Keywords: electron microprobe, Raman spectroscopy, scandium, thortveitite, three-phase inclusions

Introduction

A specimen of purple gem-quality material was purchased in Bangkok in a mixed parcel of rough of stated African origin. It was not possible to establish the geographic source of this rough prior or subsequent to its acquisition in 2004.

When purchased, the specimen was a water-worn pebble that showed no discernible crystal form. It had a mid-purple colour which varied with distinct pleochroism. A 12.3 mm × 9.1 mm × 8.95 mm faceted gemstone of 10.01 ct was cut from the pebble. Standard gemmological tests on this faceted stone gave results which did not match published data of any known gemstone. Prior to cutting, the rough was accidentally dropped on concrete and a fragment cleaved from its side. This small cleavage fragment was eventually used for initial electron microprobe analysis and Raman spectroscopy. Subsequently the faceted stone and the cleavage fragment were subjected to further testing. The material was identified as thortveitite, but with a composition richer in scandium than shown in a range of published analyses of the mineral thortveitite. Mineral specimens of thortveitite are normally small (up to a few millimetres), often acicular, variously coloured, occasionally transparent but more often opaque to translucent. This unusual high-scandium material has gem potential and the results of our investigation are presented as a reference point in the event of discovery of further rough or cut gem-quality stones. This in turn might enable further research to establish its origin.

Figure 1: Double refraction and small cleavages in facet edges viewed through the crown facets of the thortveitite. © R. Chapman.

Standard gemmological tests and observations

The gemmological properties determined using standard gemmological tests and observation on the faceted stone are set out in *Table I*.

Figure 1 illustrates the back facet edges of the faceted material, looking through the table facet. There is a series of small cleavage nicks along pavilion facet junctions that give the appearance of blurred facet edges. A similar phenomenon is seen with some cut spodumene.

Laboratory tests and observations

The cleavage fragment of thortveitite was split into two and each was analysed by electron microprobe at the Natural History Museum, London. The analyses were obtained using wavelength dispersive X-ray spectrometry (WDX) on a Cameca SX50 electron microprobe. The conditions used were 15kV (accelerating voltage) 15nA (probe current) with a 10 µm spot size. The data shown in *Table II* are the average of 10 analyses of the cleavage fragment (five from each of the two separated samples). Weight % Oxide values shown as <dt were determined but were below the instrumental detection limit.

The material was identified as thortveitite, $(Sc,Y)_2Si_2O_7$. This specimen is

Figure 2: Appearance of the faceted thortveitite in daylight (left) and incandescent light (right).

rich in scandium but contains almost no yttrium.

A comparison with recently published electron microprobe data on natural thortveitite from various localities worldwide is shown in *Table III*. From this, it is apparent that the silica and alumina contents for the studied sample lie within the known range, but that the yttrium content (0.1wt% Y_2O_3) is at least an order of magnitude lower. The scandium content (52.9% Sc_2O_3) is significantly higher than those previously reported. Other notable differences include a lower Fe_2O_3 content and, with the exception of one sample from Baveno, Italy, a lower Yb_2O_3 content. Other REEs are below the detection limit of the instrument used.

Laser Raman microspectroscopy was carried out at the School of Earth

Table I: Gemmological properties of the faceted thortveitite.

Colour	Purplish blue of moderate saturation in daylight *(Figure 2a)*; purple of intense saturation in incandescent light *(Figure 2b)*. Face-up colour in daylight with Gem Dialogue: 70% grey, 20% purple (B2P). No evidence of colour zoning was readily visible
Visual appearance	High vitreous lustre with pronounced pleochroism. Distinct pleochroic colours of: violet, blue and straw-yellow *(Figure 3)*.
Clarity	Good clarity with a colourless fine linear inclusion *(Figure 4)*.
Hardness	When cutting the gemstone, this mineral appeared to have comparable hardness with quartz. It polished easily and well. A Mohs' hardness estimate was not obtained.
Cleavage	A small cleavage 'nick' in the table *(Figure 5)* indicated the presence of cleavage in at least two directions.
Specific gravity	3.48
Refractive indices	$\alpha = 1.753$ $\beta = 1.793$ $\gamma = 1.809$
Birefringence	0.056 The extent of observed DR is illustrated in *Figure 6*.
Optic sign	Biaxial negative
Absorption spectrum	Two very fine lines in the green at around 535 nm plus a band in the deep blue at 425 nm.
UV luminescence	None observed under either long-wave or short-wave UV light.
Inclusions	Across the centre of the photomicrograph *(Figure 4)* some lens-shaped lighter patches have the appearance of twinning patterns. In one corner there is a planar feather containing a cloud of small inclusions *(Figure 8)*. There is also another small, irregular group of similar inclusions. A prominent colourless linear inclusion *(Figure 3)* extends from the planar feather across the stone. It is seen to be discontinuous under 30× magnification, with a 'string of pearls' appearance, and is surrounded along its length by a very sparse 'halo' of extremely small inclusions which appears to have dispersed from the linear inclusion.

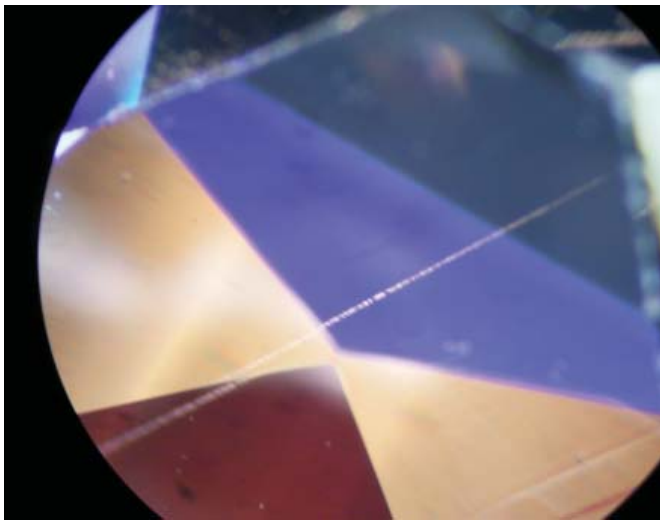

Figure 3: Distinct pleochroism displayed by the faceted thortveitite. A colourless linear inclusion is prominent across the centre of the picture.

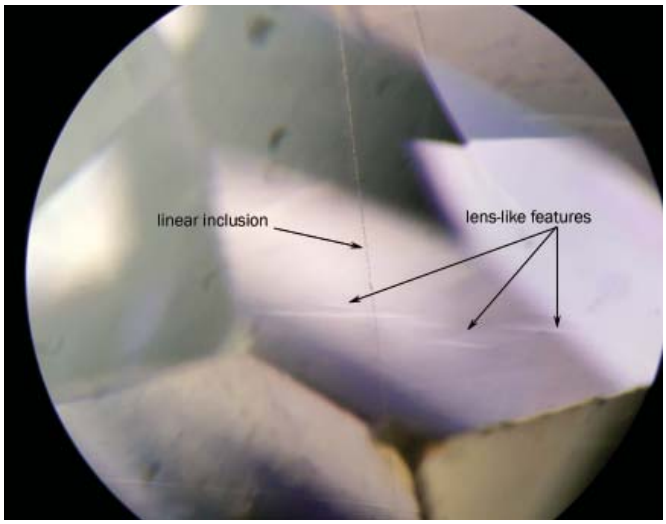

Figure 4: Linear inclusion and lens-like features in the faceted thortveitite.

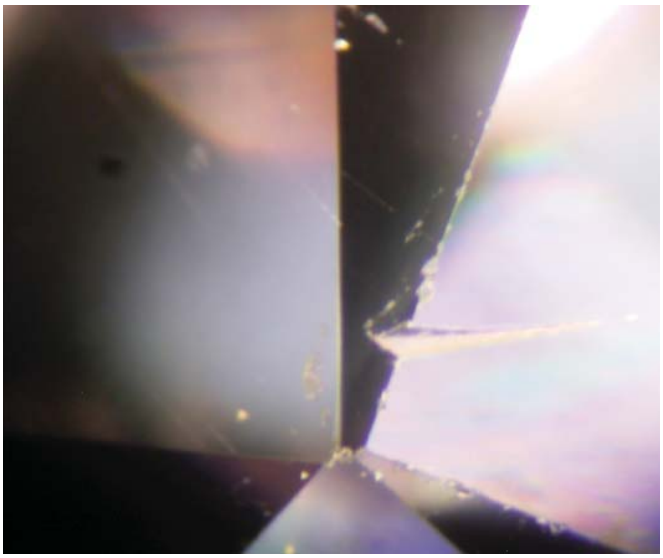

Figure 5: Presence of at least two directions of cleavage illustrated by the presence of this small cleavage nick on the edge of the table of the faceted thortveitite.

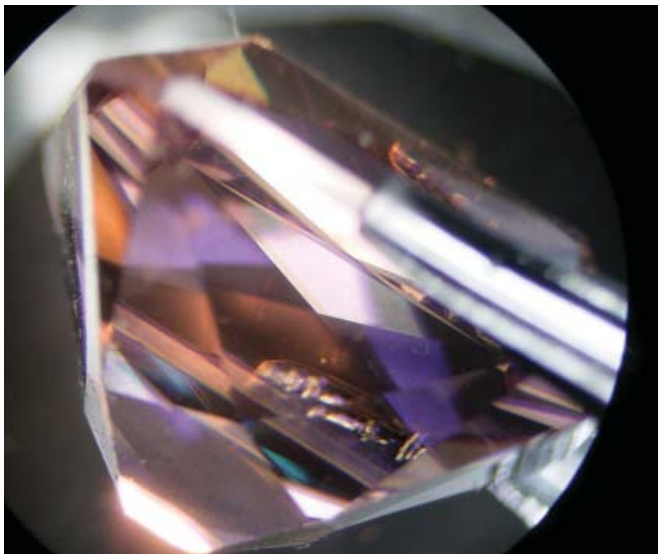

Figure 6: The distinct double refraction effect seen through the faceted thortveitite.

Sciences, Kingston University, UK, on the uncut surface of part of the small, cleaved, elongate crystal fragment (*c.* 0.3 mm × 2 mm) using a Renishaw RM1000 Raman Spectrometer equipped with a CCD detector and a 633 nm He-Ne ion laser. The system was operated in confocal mode with the laser focused on or below the surface of the sample through a 50× objective lens of an Olympus petrological microscope. Under these conditions the Raman analysis was restricted to an area of less than *c.* 30 μm². Spectra were recorded over the frequency range 180 to 1500 cm^{-1} and a time interval of

Table II: Composition of thortveitite obtained by electron microprobe analysis.

Oxide	Wt% oxide	No of ions based on 14 oxygens	Detection limit (wt%)	Standard deviation
SiO_2	45.09	3.931	0.03	0.67
Al_2O_3	0.23	0.023	0.02	0.02
Sc_2O_3	52.90	4.019	0.05	0.26
Y_2O_3	0.10	0.005	0.07	0.04
Yb_2O_3	0.12	0.003	0.10	0.03
Fe_2O_3	0.63	0.046	0.06	0.06
Totals	**99.07**	**8.028**		

NB: Na, Mg, K, Ca, V, Ti, Mn, Sr, La, Ce, Dy, Ho, Er, Tm, Lu, Th and U were sought but below the limit of detection (<dt)

Thortveitite – a new gemstone

30 seconds. The system was calibrated using the single Raman peak positions of pure crystalline silicon and diamond at 521 and 1330 cm^{-1} respectively. Analyses were carried out in triplicate to ensure that random effects from cosmic rays or electrical surges could be discounted. All peak positions reported here are believed to be accurate to within ± 1 cm^{-1}.

The Raman spectrum *(Figure 7)* of the thortveitite crystal fragment shows a prominent peak at 441 cm^{-1} and a number of other well-defined and broader minor peaks in the range up to 945 cm^{-1} *(Table IV)*. As illustrated in *Table IV*, the peak positions are in very good agreement with those reported by Brethau-Raynal *et al.* (1979) for a pulverized single crystal of pure synthetic thortveitite ($Sc_2Si_2O_7$). Further Raman analysis of the faceted sample confirmed the results for thortveitite. The absence of peaks at 435 and 392 cm^{-1} in our spectra can be explained by crystal orientation effects whereas in pulverized samples a complete range of orientations of crystal faces are exposed to the laser beam compared with only specific orientations in single crystals; this was demonstrated by Brethau-Raynal *et al.* (1979) on orientated crystals of synthetic $Yb_2Si_2O_7$ which also possesses the thortveitite structure. The Raman spectra for this thortveitite specimen are significantly different to those reported by Ross (1971), probably due to the use of impure material in these earlier studies as discussed by Brethau-Raynal *et al.* (1979). The Raman spectrum reported in the Renishaw Mineral Library Database is also markedly different, probably due to sample misidentification.

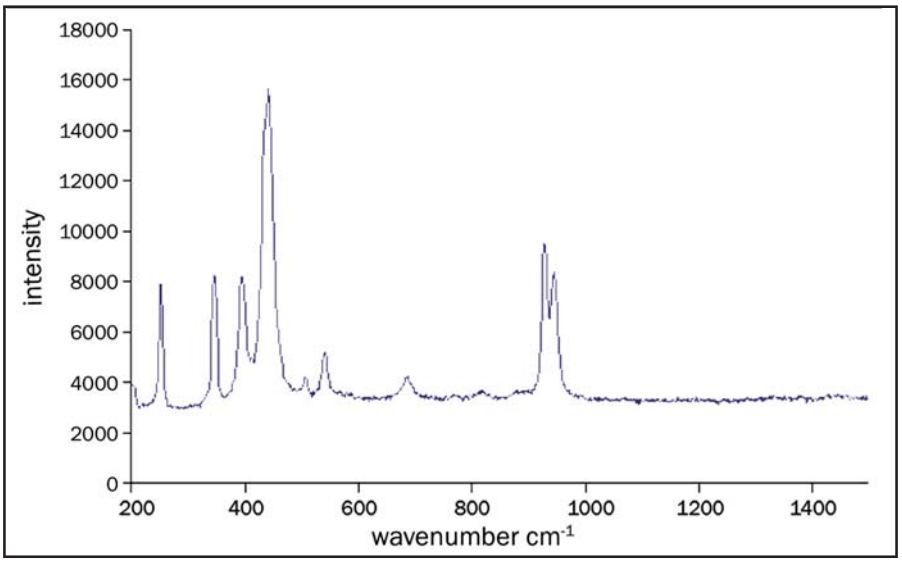

Figure 7: Raman spectrum of thortveitite.

The very small inclusions in the feather in the faceted stone (see *Figures 8* to *11*) contain three-phase (L+V+S) hydrothermal-type inclusions with a gas bubble, brine and probable halite (cubic NaCl) daughter mineral. The NaCl could not be confirmed as this mineral is Raman inactive and the H_2O band at *c.* 3500 cm^{-1} is obscured by strong fluorescence above *c.* 2800 cm^{-1}. With their high relative relief, these small inclusions are likely to be

Table III: Selected major element contents of thortveitite from various localities compared with the gem thortveitite.

Locality	Norway[1]				Madagascar[1]	USA[2]	USSR[3]	Italy[4]		This study
	Iveland 1	Setesdalen 2	Evje 3	Evje 4	Benfanamo? 5	Montana 6	Kola 7	Baveno 8	Cuasso al Monte 9	Locality unknown 10
SiO_2	37.59	40.44	41.29	41.9	44.63	44.6	46.2	44.4	45.19	45.09
Al_2O_3	0.61	0.90	0.88	0.96	1.05	0.81	n.d	1.1	0.07	0.23
Sc_2O_3	25.01	32.83	37.13	40.41	47.81	44.60	48.9	43.4	44.01	52.90
Y_2O_3	17.73	8.67	8.41	5.79	2.31	2.28	1.9	1.9	2.59	0.10
Yb_2O_3	7.01	2.58	4.52	3.33	0.18	0.41	0.7	0.1	0.74	0.12
Fe_2O_3	2.06	3.11	1.68	1.39	1.39	1.48	1.6	1.5	2.89	0.63

1. Bianchi *et al.*, 1988
2. Foord *et al.*, 1993
3. Vloshin *et al.*, 1991 (cited in Gramaccioli, 2000)
4. Gramaccioli *et al.*, 2000

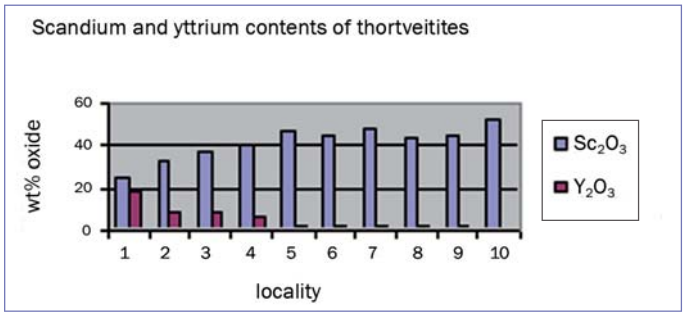

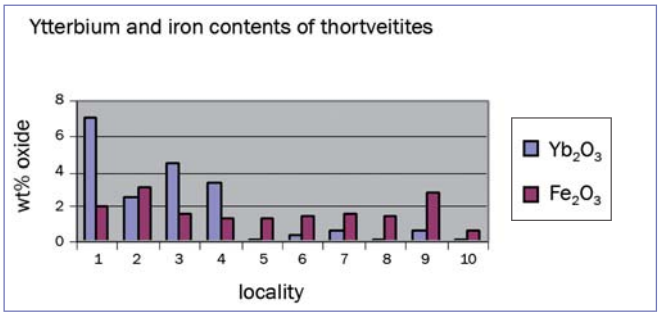

hydrothermal rather than quenched flux or melt inclusions. They are similar to those commonly observed in beryl and topaz crystals from granitic environments. There are possible decrepitation haloes around the rounded inclusions (one is outlined in *Figure 9*) due perhaps to subsequent heating, whether natural or during artificial heat treatment. The indications are that the material has a natural origin grown from, or affected by, moderate temperature, high salinity hydrothermal fluids.

Discussion

These results indicate that the material is thortveitite. Natural thortveitite, a monoclinic scandium yttrium sorosilicate with the chemical formula $(Sc,Y)_2Si_2O_7$, occurs in granitic pegmatites and is named after the Norwegian engineer Olaus Thortveit. It is a primary source of commercial scandium.

However, the low Fe, Y and REE content and very high scandium content of the studied sample could indicate that this is a laboratory-grown rather than a naturally-occurring specimen. Brethau-Raynal *et al.* (1979) have reviewed the various techniques previously used for the laboratory synthesis of thortveitite structure silicates (including the pure thortveitite end-member $Sc_2Si_2O_7$). Although most previous methods produced only small or impure samples, however, the 'floating zone' technique employed by these authors, involving heating of the starting materials in a platinum crucible to ~ 1800°C, produced clear single crystals up to 2–3 cm long and 5 mm in diameter.

Table IV: Major and minor Raman peak positions and intensities of the studied thortveitite crystal compared with peak positions reported by Brethau-Raynal et al. *(1979) for a pulverized sample of a pure synthetic crystal of thortveitite ($Sc_2Si_2O_7$)*

Peak position (cm^{-1}) This study	Peak position (cm^{-1}) Synthetic thortveitite*	Relative intensity This study	Shape This study
956	949	medium	sharp
929	932	medium	sharp
687	688	weak	broad
545	543	weak to medium	sharp
507	510	weak	broad
441	445 and 435**	strong	sharp
395	397 and 392**	medium	sharp
346	347	medium	sharp
251	253	medium	sharp
203	203	weak	sharp
192	194	weak	broad

* Brethau-Raynal *et al.* (1979)

** Not apparent from spectra recorded in the present study

Relevant factors in considering the origin of the studied stone may be summarized thus:

- This gemstone was originally purchased as a water-worn pebble. Of course, this could be simulated in a tumbler but, given the lack of a developed gemstone market for this material, could this be a chance appearance?
- If material of this size, colour and clarity is indeed synthetic, then more may have entered the market. If it has in fact been manufactured specifically for the gem market, it could be expected that further synthetic specimens are likely to have come to light during the past four years or more.
- The chemistry reveals a fairly pure scandium end-member material, which suggests possible synthesis.
- The inclusions are not particularly characteristic of synthetic material but they do indicate a likely hydrothermal origin. Published information on synthesis of thortveitite is currently confined to non-hydrothermal methods.
- Recent geological fieldwork results suggests that scandium minerals are more widespread than has hitherto been inferred (Gramaccioli *et al.,* 2000).

Figure 8: Plane of fluid inclusions within the cut stone.

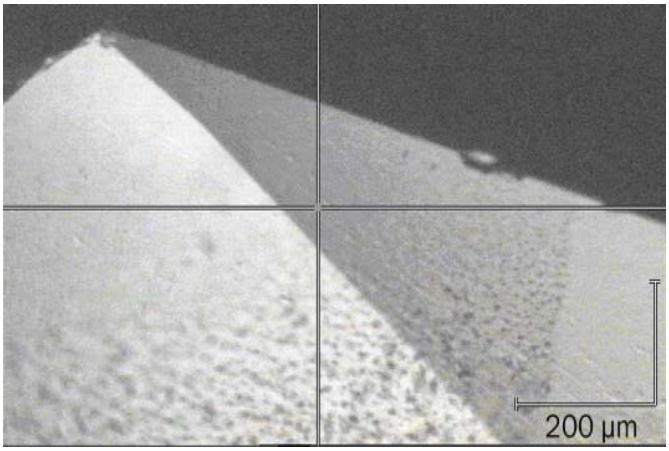

Figure 9: Rounded three-phase fluid inclusions surrounded by possible decrepitation aureoles of smaller inclusions (one is outlined).

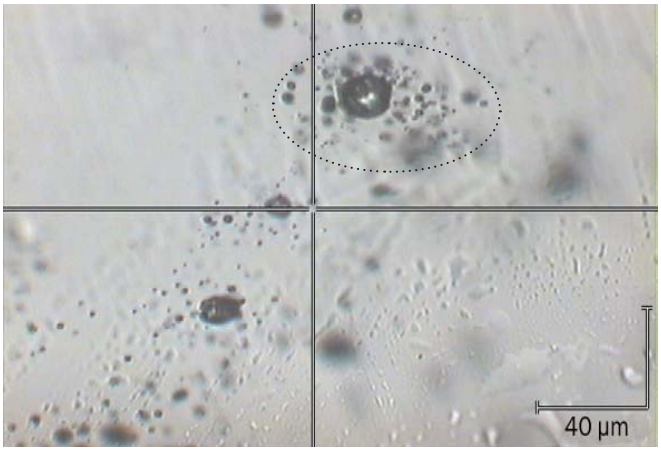

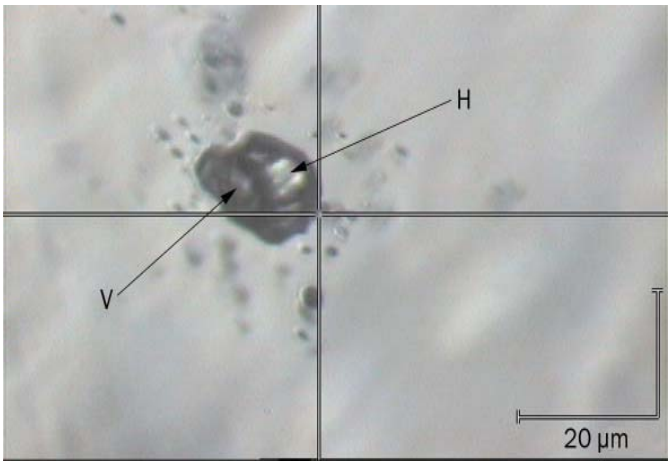

Figure 10: Close-up of rounded three-phase fluid inclusion with vapour bubble (V) and cubic daughter mineral believed to be halite (H).

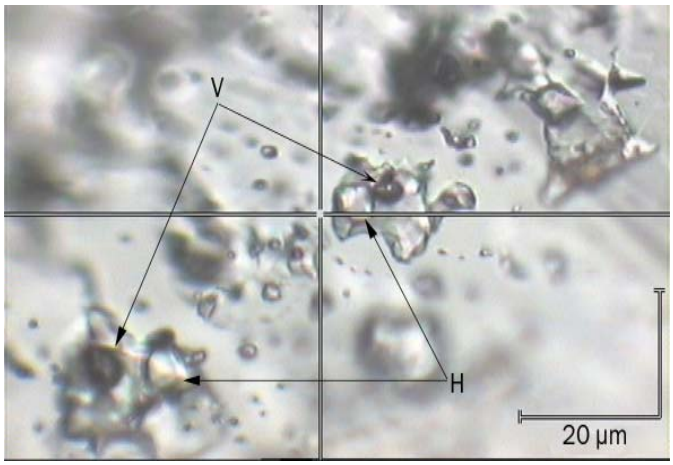

Figure 11: Group of irregular three-phase fluid inclusions with vapour bubbles (V), halite cubes (H) and an aqueous brine.

Conclusion

As the original pebble from which the test specimens derive was relatively large, reasonably clean and of unknown occurrence, initially it was considered that it may be an artificial, synthetic gemstone product. Chemical analysis which revealed a high scandium and low yttrium content appeared to substantiate this. Further observation, however, suggests the possibility that it is of natural mineral origin. Either way, the material appears to have been subjected to moderate heating, either by natural or by human agency. Given the size and clarity of the original rough specimen of thortveitite, it is suspected that more of this material may be in circulation but that specimens remain as yet unidentified. We hope that this article will prompt a search for more rough or cut specimens of gem-quality thortveitite which would enable observation and analysis to establish further useful data and maybe its origin.

Acknowledgements

The assistance of the late Grahame Brown, a leading Australian gemmologist and great supporter of international gem education, has been much appreciated. We also thank Peter Tandy of the Department of Mineralogy, Natural History Museum, London, for his assistance.

References

Bianchi, R., Pilati, T., Diella, V., Gramaccioli, C.M., and Mannucci, G., 1988. A re-examination of thortveitite. *Am. Mineral.,* **73**, 601-7

Brethau-Raynal F., Dalbiez, J.P. Drifford, M., and Blanzat B., 1979. Raman spectroscopic study of thortveitite structure silicates. *Journal of Raman Spectroscopy,* **8**(1), 39-42

Foord, E.E., Birmingham, S.D., Demartin, F., Pilati, T ., Gramaccioli, C.M., and Lichte, F.E., 1993. Thortveitite and associated Sc-bearing minerals from Ravalli County, Montana. *Can. Mineral.*, **31,** 337-46

Gramaccioli, C.M., Diella, V., Demartin, F., Orlandi, P., and Campostrini, I., 2000. Cesian bazzaite and thortveitite from Cuasso al Monte, Varese, Italy: a comparison with the material from Baveno, and inferred origin. *Can. Mineral.,* **38**, 1409–18

Ross, S.D., 1971. The vibrational spectrum of thortveitite. *Spectrochimica Acta,* **27A,** 1837-43

Further reading

Mathiesen, Carl, O., 1969. An occurrence of unusual minerals at Bidjovagge, Northern Norway, Norges Geologiske Undersokelse. Nr.266, 86-104 Universitetsforlaget Oslo

Pezzotta, F., Diella, V ., and Guastoni, A., 2005. Scandium silicates from Baveno and Cuasso al Monte NYF-granites, Southern Alps (Italy): Mineralogy and genetic inferences. *Am. Mineral.,* **90**, 1442-52
mindat.org (www.mindat.org) http://www.webmineral.com/data/Thortveitite.shtml

The Authors

R. Chapman
Carseldine, Queensland, Australia. email: ross@gemsofaus.com.au

I.F. Mercer
The Gemmological Association of Great Britain, 27 Greville Street, London EC1N 8TN. email: ian.mercer@gem-a.com

A.H. Rankin
CEESR, School of Earth Sciences and Geography, Kingston University, Kingston-upon-Thames, Surrey KT1 2EE. email: A.Rankin@kingston.ac.uk

J. Spratt
Department of Mineralogy, Natural History Museum, London SW7 5BD.
email: J.Spratt@nhm.ac.uk

Surface treatment of gemstones, especially topaz – an update of recent patent literature

Dr Karl Schmetzer

Abstract: This review provides an overview of numerous patent documents that have been published recently and describe various coating technologies for gem materials. Parts of the documents focus on the deposition of one single or several specifically structured or composed layers in order to obtain the desired colour and the desired optical effects or wear resistance. Contact heat treatment of faceted stones with solid transition metal-bearing plates as well as heat treatment of layers deposited on the surfaces of the gemstones, are also reported. Chemical data of one sample of iron-coated topaz provide a first insight into the reaction mechanism within the outer diffusion layer.

Introduction

The quantity of surface-treated gem materials, especially topaz, seen in the market *(Figure 1)* is increasing. This is, at least partly, due to problems in the United States of America related to the Nuclear Regulatory Commission (NRC) rules regarding the import and distribution of irradiated blue topaz by non-licensed companies. Surface-coated topaz of various colours might, at least partly, fill the enormous demand for this relatively cheap product. Much more valuable are various other surface-treated gemstones such as coated pink diamonds; because of their value, there is a greater need to identify any treatment of such stones.

Numerous patents dealing with different types of surface treatment or surface enhancement of gemstones, especially topaz, have been reviewed and summarized by Schmetzer (2006). Four different basic technologies were reported: (a) coating with differently coloured dyes; (b) coating by chemical vapour deposition, physical vapour deposition or sputtering without specific heat treatment;
(c) contact heat treatment with transition metal-bearing powder;
(d) deposition of a coating to the faceted stone and subsequent heat treatment.

While methods (a) and (b) produce surface coatings which are easily (at least partly) removable or scratched by normal wear of the faceted stones, techniques (c) and (d) claim a more permanent surface coating. Although 'diffusion into the outer surface' and 'chemical bonding to

Figure 1 (above and below): Surface-coated topaz specimens treated by various techniques to obtain different colours are available nowadays from various producers. The red cushion-cut stone above weighs 1.08 ct and measures 6.1 × 6.1 × 3.9 mm; the blue square-cut stone in the upper row below weighs 5.39 ct and measures 6.1 × 6.0 mm. Photos by L. Kiefert, AGTA Gemological Testing Center, New York, USA.

the surface' are described as a reaction mechanism occurring in techniques (c) and (d) which are related to heat treatment, the exact reaction mechanism or mechanisms are not known in detail. This is due to the lack of experimental data describing the chemical and/or physical properties of the surface coating layer or layers. First results have been obtained by Befi *et al.* (2006) and Kiefert *et al.* (2007), who mainly examined the chemical composition of the layer or layers nearest to the surface by X-ray fluorescence analysis (EDXRF).

Since publication of the review by Schmetzer (2006) which covered the period from about 1996 to 2005, new patent documents have been obtained and a general overview is given in *Table I*.

Detailed knowledge of possible treatment processes is essential for the recognition of treated gemstones in the laboratory, a task which becomes more and more complex for the gemmologist (see, for example, Shen *et al.*, 2007). It is a matter of speculation as to how relevant some of the matters discussed in the patents will be in the future to gemmologists, but to have outlines of such topics and to have points of reference for possible future work is, I believe, important. In addition, it should be mentioned that *Table I* summarizes only patents which are specifically related to and applied for the enhancement of gem materials and not to general surface treatments of various substances.

Some light is also shed on the importance of patents dealing with surface enhancement of gem materials if we consider the numerous law suits that occurred in the United States due to patent infringement of US patent 5,853,826 by Starcke *et al.,* issued 29 December 1998 and assigned to Azotic Coating Technology (document 3). Following the reactions of some of the companies involved, a re-examination of this patent was initiated and carried out by the United States Patent and Trademark Office (see the related re-examination communication, issued 7 May 2007). This process led to amended claims (especially to an amended claim 1) which were published in the related 'Ex Parte Re-examination Certificate' (document 4).

A. Deposition of a coating without specific heat treatment

Deposition of a coating including a wear-resistant material

A technique for the increase of wear resistance of a coloured coating is described by Neogi and Neogi (documents 17 and 18). In general, an integrated coating consisting of a colour-imparting agent and an abrasion-resistant agent is deposited on the surface of a faceted gemstone. Precursors of this technique have already been described by Nassau *et al.* (documents 1 and 2), who mentioned a diamond coating to improve and provide a harder surface on faceted moissanite that resists scratching and abrasion and by Wright (document 8), who described the coating of various gemstones by diamond-like-carbon.

In the patent applications of Neogi and Neogi (documents 17 and 18), two major embodiments are described. In one variant, the colour-imparting agent and the abrasion resistant agent are deposited in a single step within one layer. In an alternative embodiment, the colour-imparting agent is deposited in a first layer and the abrasion-resistant agent is deposited subsequently in a second layer. The colour-imparting agent may provide the perception of colour via interference phenomena or via absorption phenomena in the visible range. As examples, metals or semiconductors such as Au, Pt, Cr, Fe, Si, Ge, Bi, Ni, Co, Ta, Er, Mn, Mg, Al, Zr, Ti, Se and Be are mentioned. Furthermore, various coatings consisting of oxides, nitrides and alloys are applied. Abrasion wear resistance may be provided by integrating any of the materials such as diamond-like carbon, chemical-vapour-deposited diamond, alumina, polymer-based materials, nitrides or carbonitrides. The main example given of coated gemstones is topaz, but ruby, sapphire and emerald are also discussed.

Sub-surface implantation methods are also described by Neogi and Neogi in documents 17 and 18 as additional possible methods to improve the appearances of gemstones. Colour can be imparted to diamonds and other gemstones via implantation of impurities using a gas cluster ion beam apparatus. Subsequent to this first step of treatment, an abrasion-resistant layer with or without an additional colour component can then be deposited on the surface of the faceted stone.

Deposition of a coating causing optical phenomena

A special dichroic effect is produced by a coating consisting of alternating transparent layers containing metallic and/or ceramic particles. This method is described by Gaillard Allemand in documents 15 and 16 and uses various reflection and interference phenomena. The layers are made from, for example silica, titania or magnesium fluoride and metallic chromium. A final reflecting metallic layer is deposited on these alternating layers, which may consist of titanium or chromium.

Deposition of a coating and formation of a diffractive optical element

Another method for the enhancement of the optical appearance of gem materials, especially for the enhancement of fire, is described by Maltezos *et al.* (documents 20 and 21). For this purpose a diffractive optical element comprising a diffraction grating is formed on one or more facets of the stone. The formation of these diffractive optical structures to enhance dispersion or fire of a gemstone, for example diamond, is performed by the deposition of that particular structure on the surface or by etching the optical structure into the surface of the gemstone. One particular technique for the formation of distinct patterns of diffractive elements is the deposition of subsequent mask and resist layers in combination with lithographic techniques involving various etching steps. In addition to diamond, cubic zirconia, zircon, moissanite, topaz, rutile, strontium titanate, spinel, yttrium aluminium garnet and gadolinium gallium garnet are mentioned as examples.

B. Deposition of a coating with specific heat treatment

Contact heat treatment with transition metal-bearing solids

Another group of patent publications by Rauch and Würtenberger (documents 5 to 7) describes the contact heat treatment of faceted gem materials with transition metal-bearing solids. In contrast to previous descriptions, the gem materials are not heated in transition metal-bearing powders, but in contact with a solid plate of metal or metal oxide, where, for example cobalt oxide, iron oxide or vanadium oxide form a substantial constituent of the plate. The plate has recesses in the shapes of the pavilions of the stones. The faceted gemstones, for example, corundum or topaz, are simply placed on the plate and heated for several hours in oxidizing or reducing atmospheres. The process is designed to avoid damage to the gemstones during the heat treatment process.

Deposition of a coating to the faceted stone and subsequent heat treatment

Two groups of patent documents describe the coloration of gem materials by the deposition of colour-causing coating on the facets of the gemstones consisting of one or two layers or thin films and subsequent heat treatment.

Documents 9 to 14 by Starcke *et al.* contain descriptions of methods where heat treatment is performed preferably at temperatures below that at which substantial diffusion occurs from the coating into the gemstone. Examples are quartz, topaz and beryl. The coating applied preferably consists of two components, a carrier and a colour-causing dopant. The carrier may be any dielectric material, for example, any metal oxide, metal nitride, metal carbide, metal sulphide or metal boride, but not a pure metal or alloy. The dopant may be a metal, alloy, oxide, nitride, boride, or another compound which is highly absorptive in the visible range. To obtain homogeneous and uniform body colours, annealing temperatures between 300 and 1150°C are given. For example, topaz can be heated at a temperature of 450°C for about one hour. It is also mentioned that the coating on the pavilion is of maximum thickness adjacent to the culet and becomes thinner with increasing distance from the culet. This type of variable layer thickness is said to improve the coloration of the gemstone.

In a recently published patent application, Yelon *et al.* (document 19) have described how to obtain a uniform colour using a coating and subsequent heat treatment technology. The coating is applied in a reactor by means of a precursor consisting of an organometallic compound, especially a metal carbonyl, or another metallic source, for example an oxide of Al, Mg or Si doped with a metal. After the deposition step the coating is typically black or metallic. If necessary, a change of colour is performed by heating in a temperature range of about 250 to 550°C in an oxidizing atmosphere. A colour change is accomplished due to the change of the valence state of the metal in the coating. Topaz, quartz, ruby, emerald, and sapphire are given as examples. Adhesion of the coating is strengthened because part of the coating material forms a diffusive layer with the gemstone substrate; topaz is given as an example.

Analytical data from this type of reaction or diffusion zone are presented by Yelon *et al.* (see again document 19). The compositional details were obtained by Auger electron spectroscopy and are given with topaz as core or substrate and iron carbonyl, $Fe(CO)_5$, as precursor compound. The surface-related reaction or diffusion zone *(Figure 2)* consists of two sublayers. The outer sublayer with a thickness of about 50 nm contains distinct but relatively low amounts of Al and Si (from the topaz), as well as high concentrations of iron but no fluorine. In a subsequent area, between 50 and 100 nm, the iron content decreases and the silica and alumina contents increase. It is not disclosed whether the 0–100 nm zone is in a crystalline or amorphous state. More than 100 nm from the surface, the analyses indicate that the topaz is unaffected by any diffusion. These interesting analytical results indicate that a diffusion or solid state reaction zone is formed by the heat treatment process. Its two sublayers both consist of the elements of the topaz (from the core) and iron (from the deposited metallic layer).

It is assumed that the indicated content of Fe of between 2 and 5 wt.% at 100–400 nm from the surface are iron background values attributable to the analytical technique. This is because diffusion of iron into the topaz structure to produce an almost flat profile for 300 nm is very unlikely. The data from this example therefore indicate some content of iron in the 50 nm-thick outer layer and decreasing iron contents in the 50 nm-thick inner diffusion layer, but do not support the presence of any diffused iron deeper in the crystal.

Discussion

The patent documents reviewed in this paper and summarized in *Table I* reflect two different basic technologies.

The first group of documents contains methods for the deposition of various thin layers or films on the surfaces of faceted stones without additional heat treatment. In documents 3 and 4 by Starcke *et al.,* 15 and 16 by Gaillard Allemend, and 20 and 21 by Maltezos *et al.,* various optical reflection and interference phenomena are used to improve the optical properties (fire) of the gemstones or to create a specific visual impression. Documents 1 and 2 by Nassau *et al.* as well as documents 8 by Wright, and 17 and 18 by Neogi and Neogi, describe the improvement of hardness and wear resistance of the gem material itself or of the colour-causing coating or layer deposited on the surface of the gemstones. An example of this kind of material is diamond-coated synthetic moissanite which has already appeared on the gem market (Hammer and Schmetzer, 2000), and can provide misleading readings on moissanite testers.

A second group of patent publications describes techniques for the deposition of a coating accompanied by a specific heat treatment process. Documents 5 to 7 by Rauch and Würtenberger describe a

*Table I: Patent documents describing surface treatment of gem materials, especially topaz**

Document/patent family**	No.	Issued	Inventor/applicant	Type of surface treatment	Coating/diffusion material	Colours (examples)	Remarks
WO 98/21386 A1 US 5,882,786	1 2	22.5.1998 16.3.1999	Nassau *et al.*/ C3, Morrisville, NC, USA	Chemical vapour deposition or physical vapour deposition	Diamond	Colours according to the dopant of the core	Coating of moissanite
US 5,853,826 US 5,853,826 C1	3 4	26.12.1998 11.9.2007	Starcke *et al.*/ Azotic Coating Technology, Rochester, MN, USA	Sputtering or chemical vapour deposition or others	Thin coating of the pavilion of a stone with one or several thin layers, especially Ti, TiO_2, Zr, ZrO_2, also other metals, metal oxides, nitrides, sulphides and carbon	Green to violet (at different angles)	Various reflection and interference phenomena are observed when viewed at different angles of observation
US 2003/0124299 A1 AT 411 464 B US 7,033,640 B2	5 6 7	3.7.2003 26.1.2004 25.4.2006	Rauch and Würtenberger/ D. Swarovski & Co., Wattens, Austria	Contact heat treatment with a solid plate	Metals or metal oxides	Blue (cobalt oxide); yellow (vanadium oxide)	Diffusion directly from the solid plate or through an additional diffusion layer between the gemstone and the solid plate
US 2003/0224167 A1	8	4.12.2003	Wright, Kirkland, WA, USA	Conventional DLC application process	Diamond-like-carbon		Improvement of optical properties and wear resistance
US 2004/0083759 A1 US 6,997,014 B2 US 2006/0068106 A1 US 2006/0065016 A1 US 7,137,275 B2 US 2007/0157666 A1	9 10 11 12 13 14	6.5.2004 14.2.2006 30.3.2006 30.3.2006 21.11.2006 12.7.2007	Starcke *et al.*/ Azotic Coating Technology, Rochester, MN, USA	Sputtering or chemical vapour deposition or others	Thin coating of the pavilion of a stone with one or several thin layers of any dielectric material, e.g. oxide, nitride, carbide, sulphide, which consists of or contains a dopant that is highly absorptive in part of the visible area	Yellow (titania and vanadium oxide); blue (silica and cobalt oxide)	Additional heat treatment after coating is possible or necessary, but below a temperature at which diffusion from the coating into the gemstone occurs; different thickness of the coating on the pavilion with varying distance from the culet
EP 1 674 431 A1 WO 2006/070137 A1	15 16	28.6.2006 6.7.2006	Gaillard Allemand/ Baccarat, Glonville, France	Various known sputtering techniques	Successive transparent layers containing metallic and/ or ceramic particles with a final reflecting opaque metal layer		A decorative dichroic visual effect is produced

	US 2006/0182883 A1 WO 2006/089080 A2	17 18	17.8.2006 24.8.2006	Neogi and Neogi/ Temecula, CA, USA	Deposition of a colour-causing material and a wear-resistant material concurrently or in two steps	Integrated coating consisting of a colour imparting agent (metal, semiconductor, oxide, nitride, alloy) and an abrasion wear-resistant agent (diamond-like carbon, CVD diamond, alumina, polymer-based materials, nitrides, carbonitrides)	Amber with secondary green effects (an integrated layer of a diamond film with chromium oxide on topaz); yellow (a diamond-like-carbon layer with Si on topaz); light green, gold and amber shades (varying levels of gold with diamond-like carbon)	The colour may be caused by bulk absorption or via interference; colour improvement by sub-surface implantation techniques and other methods are also mentioned
	US 2007/0110924 A1	19	17.5.2007	Yelon *et al.*, Columbia, MO, USA	Chemical vapour deposition or physical vapour deposition	Organometallic compound or a metal-bearing compound as precursor for the deposition of a metallic layer	Different colours are obtainable by various precursors such as amber [$Fe(CO)_5$]; dark blue or green blue [$Co_2(CO)_8$]; orange [$Mn_2(CO)10$]; violet [$Ti(C_3H_7O)_4$]; red [Al_2O_3 doped with Cr)	If necessary, heat treatment of the stone with the deposited metallic layer, formation of an intermediate layer consisting of Al and Si (from the topaz core) and the metal, e.g. iron, of the precursor layer
	WO 2007/067696 A1 US 2007/0157667 A1	20 21	14.6. 2007 12.7.2007	Maltezos *et al.*, Fort Salonga, NY, USA	Formation of a diffractive optical element on the surface of the gemstone by deposition of a mask layer and a resist layer, lithography of the resist layer and subsequent etching	The mask layer may consist of titanium, aluminium, platinum, chromium, silicon dioxide or silicon nitride; the resist layer will depend on the lithography process and may consist of polymethylmethacrylate		The natural fire of the gemstone is increased

Deposition of a coating including a wear-resistant material without specific heat treatment

Deposition of a coating causing optical phenomena without specific heat treatment

Contact heat treatment with transition metal-bearing solids

Deposition of a coating and subsequent heat treatment

* patent documents are sorted in patent families (i.e. groups of patent documents with similar contents related to the same inventor or applicant, frequently based on the same priority application); patent families are presented chronologically according to the first member of a patent family published

** Abbreviations: AT Austria; EP Europe; US United States of America; WO World Intellectual Property Organization

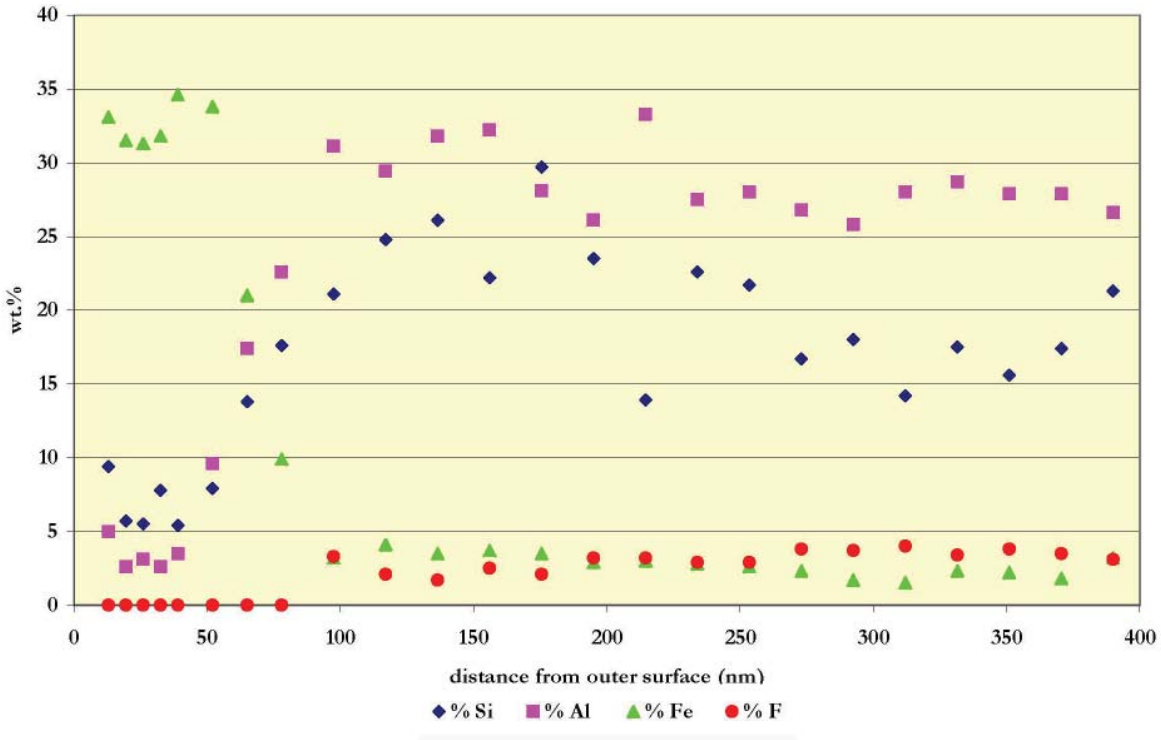

Figure 2: Chemical zoning within the reaction and/or diffusion layer of surface-coated and subsequently heat-treated topaz. The chemical data (obtained by Auger electron spectroscopy) were taken from the patent application of Yelon et al. (US 2007/0110924 A1, document 19); the two outer analysis points closest to the surface were omitted because they contained artefacts of sample preparation. The diagram reveals an outer reaction zone with high iron contents (from the coating) and small but distinct aluminium and silicon values (originating from the topaz core); within an intermediate zone between this outer layer and the topaz core, an intermediate layer is observed in which the iron contents gradually decrease and the aluminium and silicon contents gradually increase.

new variant of the contact heat treatment technology using a solid transition metal-bearing plate as source for the colour-causing agent. For this technology previously only transition metal-bearing powders were used. Another group of patent publications consisting of documents 9 to 14 by Starcke *et al.* and of document 19 by Yelon *et al.* describes improvements of the known two-step technology consisting of a deposition of a metal-containing layer on the surface of the gem material and subsequent heat treatment to improve or change the stability as well as the visual appearance to the coating.

Apart from surface-coated moissanite and diamond, the author is unaware of which, if any, of these various technologies has already been implemented and is in commercial production for release of such treated materials on to the market. From the descriptions given in the documents reviewed, it is very difficult to give any evaluation about the optical quality and wear resistance of the various coatings described for a number of gem materials. But it is most probable that at least some of the technologies referred to in this paper will be applied to gem materials in the future. Consequently the recognition of these various types of treatments will be a significant focus of research for gemmological laboratories in the future.

Most interestingly, the analytical data from the margin of a topaz specimen coated with iron carbonyl (Yelon *et al.*, document 19) provides a first insight into its chemical composition and formation as a reaction to heat treatment.

References

Befi, R., Kiefert, L., and Htut, M., 2006. Coated topaz. *Gems & Gemology,* **42**(3), 128-9

Hammer, V.M.F., and Schmetzer, K., 2000. Synthetischer Moissanit. *Goldschmiede Zeitung,* **98**(12), 108-9

Kiefert, L., Befi, R., and Harlow, G.E., 2007. Surface coating of topaz. 30th International Gemmological Conference, Moscow, Russia; The collection of expanded abstracts and some articles, p. 53

Schmetzer, K., 2006. Surface coating of gemstones, especially topaz — a review of recent patent literature. *Journal of Gemmology,* **30**(1/2), 83-90

Shen, A.H., Wang, W., Hall, M.S., Novak, S., McClure, S.F., Shigley, J.E., and Moses, T.M., 2007. Serenity coated colored diamonds: detection and durability. *Gems & Gemology,* **43**(1), 16-34

United States Patent and Trademark Office, 2007. Ex parte reexamination communication transmittal form, Patent No. 5,853,826. 7 pages; May 7, 2007

Patent documents

1. Nassau, K., Coleman, T.G., Hunter, C.E. (1998): Gemstones formed of silicon carbide with diamond coating. WO 98/21386 A1
2. Nassau, K., Coleman, T.G., Hunter, C.E. (1999): Gemstones formed of silicon carbide with diamond coating. US 5,882,786
3. Starcke, S.F., Kearnes, R.H., Bennet, K.E., Edmonson, D.A. (1998): Method of improving the color of transparent materials. US 5,853,826
4. Starcke, S.F., Kearnes, R.H., Bennet, K.E., Edmonson, D.A. (2007): Method of improving the color of transparent materials. US 5,853,826 C1 (ex parte re-examination certificate)
5. Rauch, T.W., Wurtenberger, M. (2003): Method of coloring cut gemstones. US 2003/0124299 A1
6. D. Swarovski & Co. (2004): Verfahren zur Färbung geschliffener Schmucksteine. AT 411 464 B
7. Rauch, T.W., Würtenberger, M. (2003): Method of coloring cut gemstones. US 7,033,640 B2
8. Wright, L.P. (2003): Hybrid gem system. US 2003/0224167 A1
9. Starcke, S.F., Kearnes, R.H., Bennet, K.E. (2004): Coatings for gemstones and other decorative objects. US 2004/0083759 A1
10. Starcke, S.F., Kearnes, R.H., Bennet, K.E. (2006): Coatings for gemstones and other decorative objects. US 6,997,014 B2
11. Starcke, S.F., Kearnes, R.H., Bennet, K.E. (2006): Methods for coating gemstones and other decorative objects. US 2006/0068106 A1
12. Starcke, S.F., Kearnes, R.H., Bennet, K.E. (2006): Coatings for gemstones and other decorative objects. US 2006/0065016 A1
13. Starcke, S.F., Kearnes, R.H., Bennet, K.E. (2006): Coatings for gemstones and other decorative objects. US 7,137,275 B2
14. Starcke, S.F., Kearnes, R.H., Bennet, K.E. (2007): Coatings for gemstones. US 2007/0157666 A1
15. Gaillard Allemand, B. (2006): Volume de cristal présentant un effect visual décorative de nature dichroïque. EP 1 674 431 A1
16. Gaillard Allemand, B. (2006): Volume de cristal présentant un effect visual décorative de nature dichroïque. WO 2006/070137 A1
17. Neogi, S., Neogi, J. (2006): Abrasion resistant coatings with color component for gemstones and such. WO 2006/089080 A2
18. Neogi, S., Neogi, J. (2006): Abrasion resistant coatings with color component for gemstones and such. US 2006/0182883 A1
19. Yelon, W.B., Yang, J., James, W.J. (2007) Process for improving the color of gemstones and gemstone minerals obtained thereby. US 2007/0110924 A1
20. Maltezos, G., Scherer, A., Witzens, J. (2007): Enhancing the optical characteristics of a gemstone. WO 2007/067696 A1
21. Maltezos, G., Scherer, A., Witzens, J. (2007): Enhancing the optical characteristics of a gemstone. US 2007/0157667 A1

The Author

Dr Karl Schmetzer
Taubenweg 16, D-85238 Petershausen, Germany. email: SchmetzerKarl@hotmail.com

Gem-A Centenary Conference and The 2nd European Gemmological Symposium

Saturday 25 — Sunday 26 October 2008

The Hilton London Kensington

Gem-A is proud to be hosting this year's European Gemmological Symposium in conjunction with our centenary celebrations. This dynamic two-day conference will highlight both the history of gemmology and the jewellery trade, and will discuss tips and new technologies that are relevant to today's gemmologists. Our gathering of international speakers and members promises to make this an historic event.

Day 1: The Foundations of Gemmology

There will be a range of papers reviewing the history of gemmology from many perspectives, including the history of diamonds, Portuguese gems, the history of inclusions, the life of George Frederick Kunz and the gems in the Swedish Crown Jewels. *Speakers:* Sandra Brauns, Rui Galopim de Carvalho, Al Gilbertson, John Koivula, Yvonne Markowitz and Jack Ogden.

Day 2: Practical Gemmology in the Modern World

Papers will discuss the practical use of gemmological instruments which are significant to gemmologists today and the analysis of certain gem materials, as well as new developments and discoveries. *Speakers:* Emmanuel Fritsch, Henry Hänni, Ulrich Henn, Alan Hodgkinson, Michael Krzemnicki, Duncan Parker and Brad Wilson.

Conference Dinner/Dance

A Conference Dinner/Dance will be held at the Hilton London Kensington on the Saturday evening.

Conference Events

Monday, 27 October

8:45 to 10:00	Private viewing of The William and Judith Bollinger Jewellery Gallery at the Victoria and Albert Museum, South Kensington, with an introduction by Richard Edgecumbe. £15.00 + VAT.
14:00 to 16:30	New Approach to the Teaching and the Use of the Refractometer. A practical session with demonstrations by Darko Sturman and Duncan Parker. £20.00 + VAT.
18:30 to 21:00	Graduation Ceremony at Goldsmiths' Hall in the City of London. The ceremony wil be followed by a reception. £10.00 + VAT.

Tuesday 28 October

10:00 to 16:30	Precious Metal Clay Workshop with Helen O'Neill of the PMC Studio. £40.00 + VAT.
16:45 to 18:00	Private viewing of the Crown Jewels with a guided tour by David Thomas. £40.00 + VAT.

Fees and booking details

The fee for the Conference, to include lunch, is £135.00 plus VAT for one day, or £255.00 plus VAT for two days. An early-bird discount of £10.00 per day may be deducted by those booking by 31 August. Tickets for the Dinner/Dance are £35.00 plus VAT.

For full details of the event, how to register and how book a room at the Hilton, visit our website at www.gem-a.com or contact Olga Gonzalez at Olga.Gonzalez@gem-a.com or tel: +44 (0)20 7404 3334. Details of sponsorship are available on request.

Photo: Kunzite and spodumene crystals © L Kuehn

Visualization of the internal structures of cultured pearls by computerized X-ray microtomography

U. Wehrmeister, H. Goetz, D.E. Jacob, A. Soldati, W. Xu, H. Duschner and W. Hofmeister

Abstract: Computerized three-dimensional X-ray microtomography is capable of revealing the internal structure and some of the material properties of pearls at high resolution, and is thus a more useful tool in pearl testing than conventional X-ray radiography. Differences in transparency to X-rays (radiodensities) can be detected and speed up the process of locating different $CaCO_3$-polymorphs in the pearl. When combined with micro-Raman spectroscopy, vaterite-containing areas can be identified.

Keywords: aragonite, cultured pearls, microtomography, pearl testing, Raman spectroscopy, vaterite

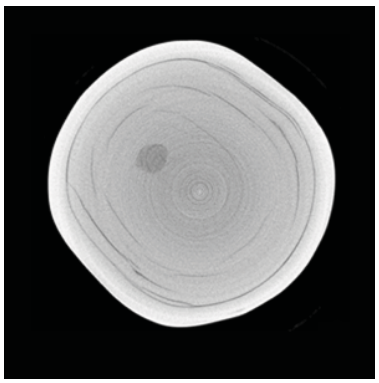

Introduction

Pearls are produced in nature by a number of mollusc species and man has taken advantage of this ability to develop cultured pearls. These can be divided into two groups: beaded (containing a bead nucleus manufactured from shell material) and non-beaded cultured pearls, both from marine and freshwater environments. The inner part of marine pearls commonly consists of prismatic crystals of calcite and the outer layer, the nacre layer, is made up of aragonite platelets (e.g. Watabe, 1965; Gutmannsbauer and Hänni, 1994; Song *et al.*, 2003; Snow *et al.*, 2004). Freshwater cultured pearls, however, have been shown to consist mainly of aragonite, whereas calcite has been reported only rarely. Instead, vaterite, a metastable $CaCO_3$ polymorph can be found in these pearls (Ma and Dai, 2001; Wehrmeister *et al.*, 2007; Qiao *et al.*, 2006). All $CaCO_3$ polymorphs are embedded in an organic matrix in a structure that is often referred to as a 'bricks and mortar' structure (e.g. Huang *et al.*, 2004; Snow *et al.*, 2004).

The differentiation of keshi cultured pearls (saltwater beadless cultured pearls) and natural seawater pearls as well as the distinction of natural freshwater pearls from beadless freshwater cultured pearls has become increasingly difficult since some of their characteristic radiographic features overlap (Lorenz and Schmetzer, 1986; Schlüter *et al.*, 2005; Hänni, 2006). In general, natural pearls show well-defined concentric growth patterns (Wada, 1998), while most beadless cultured pearls reveal less regular growth structures often accompanied by central cavities (in the case of keshi pearls, see Hänni (2006)) and central growth irregularities (in the case of beadless freshwater pearls, see Akamatsu *et al.* (2001)). However, in some cases, these differences are not well enough developed to differentiate between cultured and natural pearls on the basis of conventional X-ray radiography.

Here, we present computerized three-dimensional (3D) X-ray microtomograms combined with Raman spectra of beadless freshwater cultured pearls from Japan and China. Compared to conventional radiograms 3D-computerized X-ray microtomography reveals the internal structure of pearl at high resolution (less than 100 µm).

The occurrence of the metastable $CaCO_3$ polymorph vaterite in freshwater cultured pearls has been reported earlier in freshwater cultured pearls of low quality (Ma and Dai, 2001; Qiao *et al.*, 2007). However, by combining computerized X-ray microtomography and Raman spectroscopy, it has been shown that the occurrence of vaterite is not confined to so-called lacklustre pearls, but can also be detected in the inner parts of high quality cultured pearls, often closely associated with the remains of the tissue graft (Wehrmeister *et al.*, 2007).

Materials and experimental methods

Table I gives a summary of the pearls used in this study: two non-beaded freshwater cultured pearls, one from China (A) and one from Lake Biwa (B), and two cultured pearls with beads (one freshwater cultured pearl from Lake Biwa (C) and a marine South Sea cultured pearl (D)). The Chinese sample and the South Sea cultured pearl were bought from different pearl-dealers whereas the Japanese pearls were obtained directly from the farmers. Only sample D was drilled. Samples A and B were cut in half with a diamond-plated saw and polished with diamond paste on a copper plate. Raman maps were obtained from both cross-sections to identify vaterite and aragonite. Tomograms of the two pearl halves (A and B) and of the whole samples C and D were acquired directly by computerized X-ray microtomography without further pre-treatment.

X-ray micro computer tomography

All computerized X-ray microtomography measurements were carried out by a SCANCO µCT-40 instrument (Scanco Medical AG, Bassersdorf CH) at the Medical Faculty, Johannes Gutenberg-University of Mainz. The cone-beam computerized micro tomograph scanner is equipped with a microfocus X-ray source of 5 or 7 µm spot size and 30-70 kV (160 µA) acceleration voltages. Depending on the sample size, a nominal isotropic resolution of 6–72 µm is achievable.

Most of the samples were mechanically fixed in a special sample holder for the measurements. To get the highest possible contrast between the pearl's soft tissue and the intrinsic different inorganic phases, 2000 per 360° X-ray transmission images (2048 × 2048 pixel) were taken by averaging each 10 single X-ray radiographs at the same position x, y, z with an acquisition time of 300 ms. To minimize artefacts when calculating the tomograms, the charge coupled device (CCD) detector geometry (2048 × 256) limits the amount of slices per rotation to 2 mm in height. So, for example, pearls with a diameter of 16 mm require more than 16,000 X-ray radiographs to reconstruct the 2000 slices of 8 µm thickness with the cone-beam method which leads to total acquisition time of 13.7 hrs per sample. All measurements and reconstructions were carried out in real time by the computer system fitted with 4 RISC processors (2 × 24 GB RAM) of the new HP Itanium type controlled by a 64-bit VMS operating system.

The physical CT image contains the values for the Linear Attenuation Coefficients µ [1/cm] at each voxel (volume pixel) which depend on the energies of the incoming X-ray photons and the material properties. The calculated µ-values are converted into a 2-byte number (-32768 to 32767) internally and visualized as 12-bit greyscale pictures.

Computerized microtomography is particularly optimized for application in the field of medicine. In this connection it is of great interest to correlate the Linear Attenuation Coefficient with definite tissue or bone density in order to detect deviations from healthy biomaterial. Sir G.N. Hounsfield invented a scale, which is a linear transformation of the measurement of the Linear Attenuation Coefficient in a new scale. This scale is denoted in Hounsfield units (HU). The radiodensity of water (at standard pressure and temperature) is determined with zero HU, whereas bones have a numerical value of 400 HU and up. For an average bone density a value of 500HU is given.

Raman spectra

The Raman spectra were recorded at room temperature using an Horiba Jobin Yvon LabRAM HR 800 spectrometer equipped with a Si-based CCD-detector (Peltier-cooled) and an integrated Olympus BX41 optical microscope. A 50x objective (numerical aperture 0.55) was used. The Rayleigh radiation was blocked using notch filters. The scattered light was diffracted by a grating with 1800 grooves/mm. The 514.5 nm line of an Ar^+-ion laser and the 632.8 nm Helium-Neon laser line were used for excitation, and laser power was 10mW. Data acquisition and spectra treatment were carried out with the commercially available program LabSpec v4.02 (Jobin Yvon Horiba). For single point measurements, spectra were recorded twice.

By using the Raman mapping technique the spatial distribution of different $CaCO_3$ polymorphs could be identified. For the Raman mapping of a pearl cross section a certain area was defined (for example 8.15 x 8.15 mm in the maps presented in *Figures 4F* and *5F*) and every 40 µm in x and y directions a spectrum was recorded twice for two seconds using a motorized and software-controlled x-y stage. The 40 µm step was selected to optimize the time acquisition for the resolution of the Raman maps. The resulting intensity of every peak was converted to a colour code. The Raman maps in *Figures 4F* and *5F* show the intensity variations at 1090 ± 1 cm^{-1} – the most intense band of vaterite. Thus, every pixel in these maps represents a single spectrum and every shade of grey a certain intensity.

Modern data acquisition software for Raman spectroscopy allows the necessary calculations for further data evaluation. In this project the analysis was performed with an Origin-lab® 7.5G professional software package. After background subtraction, a calculation of the full width at half maximum as well as a calculation of the position and intensity of the maxima are done by fitting a calculated curve to the measured spectrum. The peaks were fitted as the composition of either single or overlapping Lorentz curves.

Table I: Details of cultured pearls examined in this study.

Sample	Pearl description	Presence or absence of bead	Provenance
A	freshwater cultured pearl *c.* 8 mm diameter cut in halves	beadless	China
B	freshwater cultured pearl *c.* 8.55 mm diameter cut in halves	beadless	Japan – Lake Biwa
C	freshwater cultured pearl *c.* 11 mm max. diameter	drilled bead nucleus	Japan – Lake Biwa
D	saltwater cultured pearl, drilled *c.* 12 mm max. diameter	bead nucleus	South Sea

Analytical methods for pearl investigation

Because the determination of the nature of a pearl these days can be increasingly difficult, in some specimens it is only the combination of different methods that can lead to a successful identification. Pearls from a freshwater environment, for example, typically contain orders of magnitude higher contents of Mn than those from a marine environment (Gutmannsbauer and Hänni, 1994; Habermann *et al.*, 2001). These high Mn-concentrations can be detected by trace element analysis (e.g. by Laser Ablation ICP-MS, Jacob *et al.*, 2006a, b) or by X-ray luminescence methods (Banerjee and Habermann, 2000; Banerjee and Rager, 2001) and can be used to clearly differentiate between freshwater and marine pearls. In a pearl where the determination of its provenance is in question, good results can be achieved by quasi-non-destructive trace element measurements by Laser Ablation ICP-MS (Jacob *et al.*, 2006a,b), whereas spectroscopic methods (IR and Raman spectroscopy) are used to identify the modifications of $CaCO_3$ in pearls (e.g. Barnard and de Waal, 2006; Urmos *et al.*, 1991; Hedegaard *et al.*, 2005; Wehrmeister *et al.*, 2007) and have been found to be useful in identifying the origin of pearl colour (e.g. Li and Chen, 2001; Karampelas *et al.*, 2006). Lastly, both naturally coloured Tahiti cultured pearls and naturally coloured freshwater cultured pearls can be distinguished from their artificially dyed counterparts by Raman spectroscopy (e.g. Li and Chen, 2001; Karampelas *et al.*, 2006).

For the differentiation of natural from cultured pearls the best methods are different radiographic investigations (Lorenz and Schmetzer, 1986). These are often carried out with radiograms (X-ray shadow pictures; see *Figure 1*) that enable one to visualize the internal structures of a pearl and can show the presence of a manufactured nucleus. The recorded images are two-dimensional, while the structures occur at varying depths within the pearl. Therefore several radiograms are normally taken to get sufficient information about the internal growth structures. However, the identification is not always easy, because some radiographic features are common to both beadless cultured and natural pearls (Akamatsu *et al.*; 2001; Hänni, 2006; Lorenz and Schmetzer, 1986; Schlüter *et al.*, 2005). The development and availability of tabletop X-ray tomograms offers a rather new and improved method for pearl testing, because of their much higher resolution and three-dimensional capacities compared to conventional radiograms.

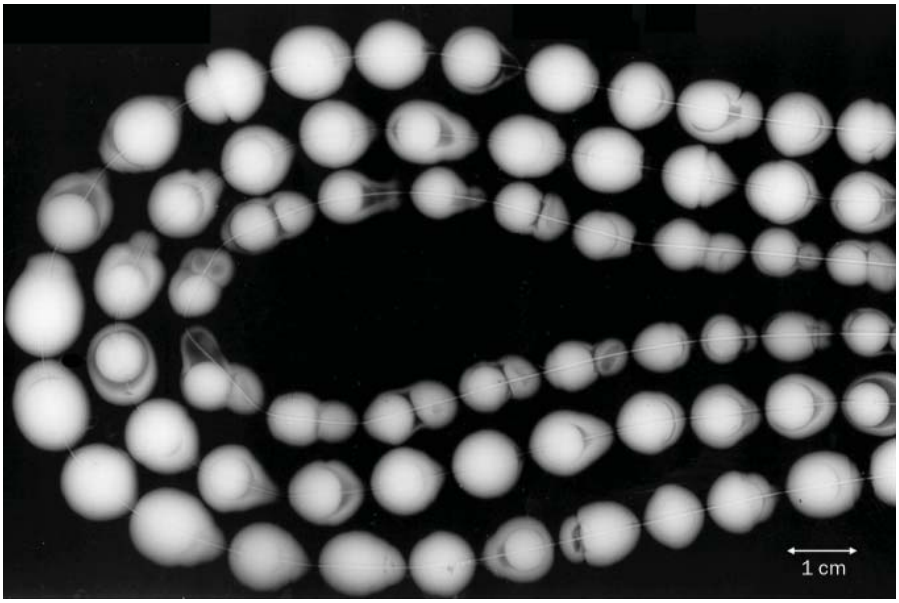

Figure 1: X-ray shadow image (radiogram) of South Sea cultured pearls. The internal structures and the bead nuclei are visible in most pearls, albeit with little structural detail.

Results and discussion

Pearls are composite materials, consisting of $CaCO_3$ platelets with an organic interlayer. These two substances differ in radiodensity (i.e. the transparency towards X-rays) which is the basis of a good visualization by microtomograms. The identification of different mineral phases and organic material is achieved by different grey values in the tomogram.

Structures easily visualized by micro-tomograms are the beads in pearl C (Lake Biwa, Japan) and in pearl D (South Sea), both in two-dimensional sections *(Figures 2 c-f* and *Figure 3 c-f)* and in 3D visualizations *(Figures 2a, b* and *Figure 3 a, b)*. The bead nucleus in pearl C *(Figure 2)* is drilled, whereas the whole pearl is not drilled. Because of their special

Visualization of the internal structures of cultured pearls by computerized X-ray microtomography

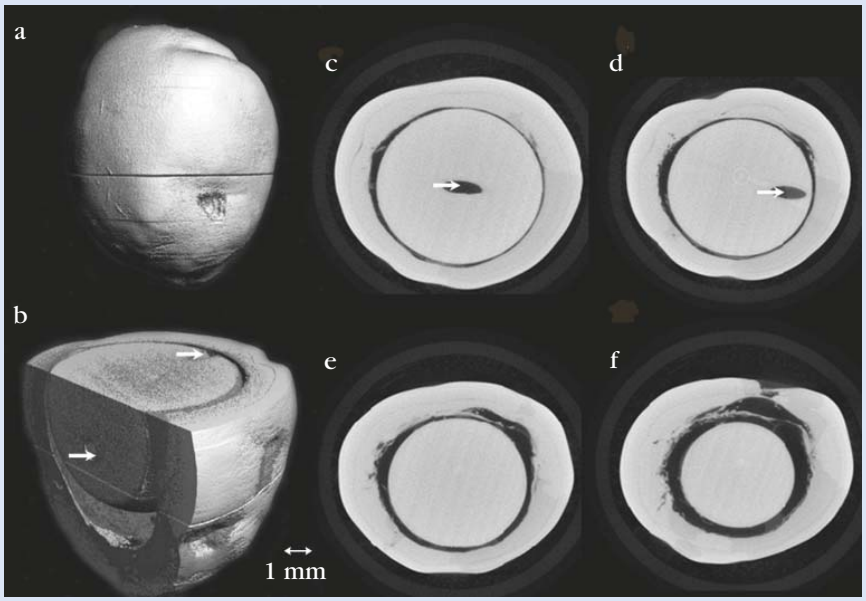

Figure 2: Radiograms of a freshwater beaded cultured pearl from Lake Biwa (pearl C). Images a and b show the 3D shape of the pearl and sections through the bead. In b the drill hole through the bead (the pearl is not drilled) is marked with white arrows as it is in the two-dimensional sections c and d. Drilled beads are part of the special implanting procedure used by the pearl farmers at Lake Biwa and Lake Kasumigaura. Contrast in the tomograms is optimized to detect any variation in the carbonate phases, so detail is lost in the area between the bead and the nacre layers that is rich in organic material and thus appears black.

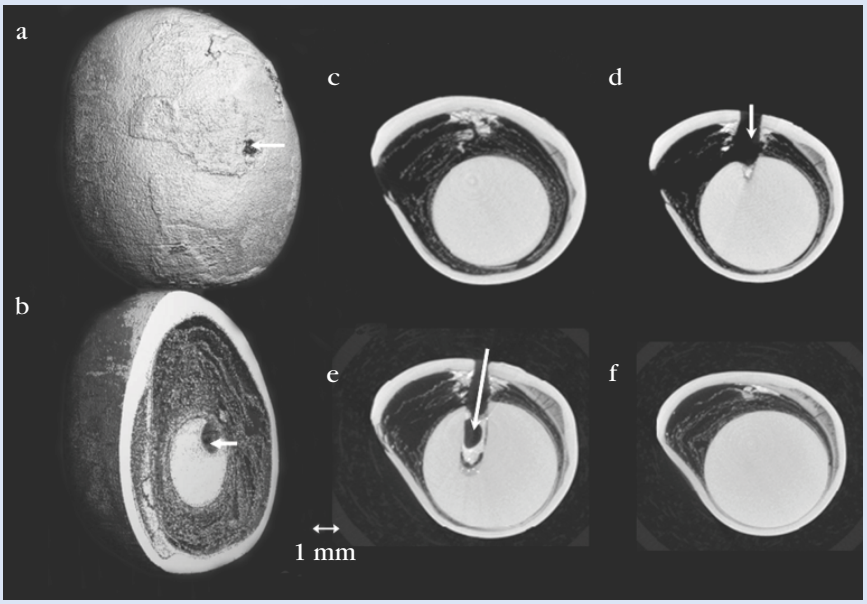

Figure 3: Three- (a and b) and two-dimensional (c–f) images of a drilled South Sea cultured pearl (pearl D).
The drill hole is marked with white arrows. In the two-dimensional, as well as in the 3D section and tomograms c-f, the bead and the cavity between it and the nacre coating are clearly visible. The organic material (darker shades of grey) has grown in a distinct layer around the bead, whereas between these organic layers no material can be detected (black). Any faint concentric rings in c-f are artefacts of the tomography.

implanting method, the pearl farmers K. Yanase (Lake Kasumigaura) and M. Sakai (Lake Biwa) use these drilled nuclei. The drilling of the nuclei is also often (but not always) detectable in X-ray radiograms that have much lower resolution than the tomograms. Freshwater cultured pearls from China contain either no bead or one made of freshwater shell-material that has not been drilled. Thus, beaded cultured pearls can be differentiated on the basis of presence or absence of a drill hole in their X-ray image and attributed to a Japanese source or otherwise. However, development of new implantation methods in China may very well require drilled nuclei in the future, requiring different or additional methods (e.g. Jacob *et al.*; 2006a,b).

Tomograms of a South Sea cultured pearl (pearl D) (see *Table I* and *Figure 3*) show the nucleus and the outer nacreous layer in great detail, as well as the gap between both. The dimensions of the gap are very variable, which can easily be seen in *Figures 3b–f*. The organic material has grown in a distinct layer around the nucleus. The empty space between the layers of organic material can be clearly discerned. Before this pearl was drilled, the gap could have been filled with a liquid. It is also clear that the thickness of the nacre layer can vary considerably.

The sizes of South Sea cultured pearls are in the range of 7 mm to 25 mm and their nacre thicknesses range from *c.* 1.5 mm to 4 mm, whereas baroque or oval shaped pearls can reach lengths of up to 40 mm (Strack, 2006). An X-ray shadow picture of South Sea cultured pearls of both baroque and round shapes is shown in *Figure 1*. The round bead nucleus and the nacre layer can be seen clearly in most of the pearls, but the X-ray radiograph fails to show any difference between the deposits of organic material and cavities.

None of the known X-ray radiographic methods is able to show any differences between the carbonate polymorphs, vaterite, calcite and aragonite areas and thereby indicate where they may be present. For example, in a radiograph only organic material, cavities, fissures and drill holes can be visualized in a calcium

Visualization of the internal structures of cultured pearls by computerized X-ray microtomography

carbonate matrix, and the X-rays cannot 'see' which polymorph might be present. The different shades of grey shown by the pearls in *Figure 1,* which can be identified as bead and nacre, both consist of aragonite and their intensities depend on the thicknesses of carbonate traversed by the X-rays. In the radiographs shown in *Figures 2* and *3* no difference in the shade of grey between bead and nacre (both identified as aragonite by Raman spectroscopy) is visible.

In order to test the potential of the microtomography method to distinguish between the polymorphs vaterite and aragonite, two sectioned freshwater cultured pearls (pearl A, *Figure 4* and pearl B, *Figure 5*) with vaterite sectors were analyzed. The two-dimensional X-ray microtomograms at various levels (*a, b, c and d* in *Figures 4* and *5*) within the pearls clearly indicate the internal structure. Irregular organic layers show the heterogeneity of the growth structure and are clearly unlike those of natural pearls (Gutmannsbauer and Hänni, 1994; Wada, 1998; Strack, 2006). The surfaces of the polished cross sections *(Figures 4e* and *5e)* show small cavities close to the centres of the pearls and to the vaterite regions — these cavities are also typical of beadless cultured freshwater pearls. The Raman spectral peak at 1090 ± 1 cm^{-1} is indicative of vaterite (Wehrmeister *et al.*, 2007) and mapping the incidence of this peak across a surface indicates the spatial distribution of vaterite. Raman intensity maps of cross sections of pearls A and B are presented in *Figures 4f* and *5f*. Raman spectra outside the vaterite areas have different intensities of the Raman shift at 1085 cm^{-1} and peaks at 701 and 705 cm^{-1}, showing that the vaterite is surrounded by aragonite (Urmos *et al.*, 1991). The boundaries between aragonite and vaterite areas are sharp and clearly visible in the Raman maps. *Figures 4a* and *5d* are two-dimensional microtomograms taken slightly below the surfaces depicted in *4e* and *5e* and show small but significant contrasts in grey-values which indicate the different polymorphs; these may be compared with the Raman maps. The difference in density between

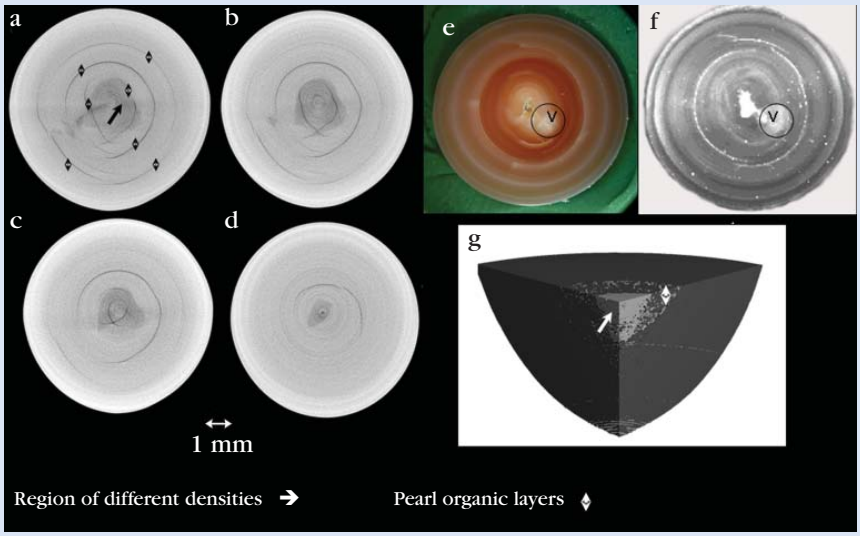

Figure 4: a-d show two-dimensional X-ray microtomograms of a sectioned freshwater cultured pearl (pearl A). These tomograms at various levels within the pearl (with a showing the highest level – 0.5 mm under the sectioned surface and d the lowest level) clearly reveal the internal structure. In 4a the darker coloured region of lower density within the pearl is marked with an arrow, whereas the organic layers are denoted with double arrows. Faintly visible concentric rings in a-d are artefacts of the tomography. In the sectioned pearl 3D image, g, the area of different density is lighter grey and marked with a white arrow; the organic layers are marked with white double arrows.
4e is a photograph of the polished cross-section of pearl A, and next to it (f) is a Raman intensity map of this surface at 1090 ± 1 cm^{-1}, a characteristic band for vaterite. Thus, using Raman spectroscopy, vaterite could be identified in the light grey area close to the centre of the pearl (denoted with V).

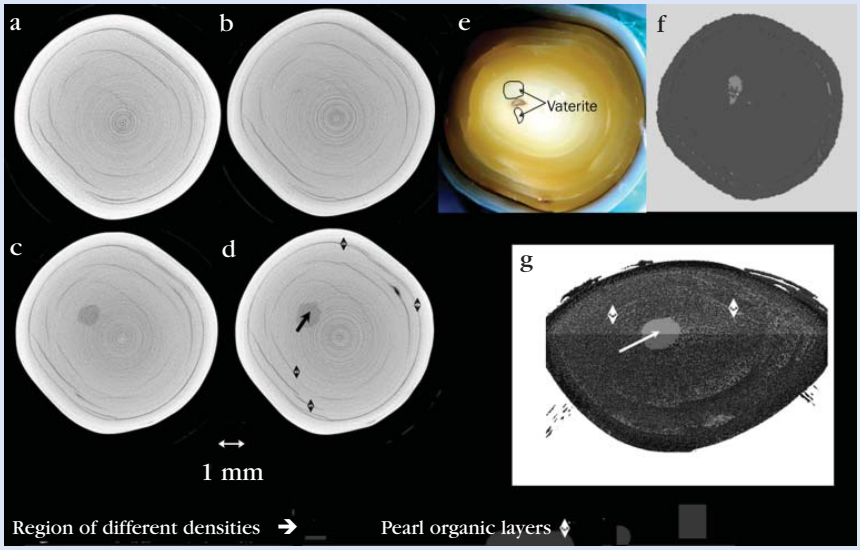

Figure 5: a–d show two-dimensional tomograms at various levels (a is the lowest and d is the level 0.5 mm under the surface) within freshwater cultured pearl B (Table I*). Symbols as in* Figure 4.
In the 3D image of the sectioned pearl, g, the areas of different densities are visible as different grey levels. Photograph e is a polished section of pearl B and two areas of vaterite are indicated. The Raman intensity map f at 1090 ± 1 cm^{-1} clearly indicates vaterite regions (pale grey) near the centre of the pearl.

inorganic aragonite and vaterite (0.39 gcm^{-3}) is sufficient to allow a distinction between these two phases based on their characteristic radiodensities. However, in pearls, these carbonate phases are both intimately mixed with organic material (e.g. Addadi *et al.*, 2006) thus changing their densities. It has often been argued that vaterite in biominerals is stabilized by organic material (e.g. Hasse *et al.*, 2000; Jacob *et al.* 2007) and in vitro studies indeed show higher concentrations of organic molecules in vaterite than in aragonite (Falini *et al.* 1998, 2000). Because organic molecules are low in density, a higher content of organics in vaterite will therefore preferentially reduce the vaterite density (2.54 gcm^{-3}) compared to that of the heavier aragonite (2.93 gcm^{-3}). A higher content of organic material in vaterite will therefore enhance the density difference between aragonite and vaterite and, in turn, the difference in radiodensity and contrast of the microtomograms.

However, this correlation may not be so straightforward and a detailed examination of the areas in the microtomograms indicates that they do not perfectly coincide with those identified as vaterite by Raman mapping. The vaterite areas identified by Raman mapping are smaller than the areas of different radiodensity resolved by the microtomograms. Furthermore, Raman spectroscopy shows that the transition between vaterite and aragonite occurs abruptly (within 2 µm, Wehrmeister *et al.*, 2007), indicating that the differences between the tomograms and the Raman maps are not likely to have been caused by variable mixtures of vaterite and aragonite. Instead, it is possible that a higher content of organic material in the general vaterite-containing region could be the cause of the different outlines.

This then suggests that the microtomography method is capable of identifying areas of higher organic to carbonate ratios, whereas the presence of vaterite has to be ascertained by Raman spectroscopy.

Conclusions

The identification of pearls is increasingly difficult and in some cases only the combination of different methods leads to a successful identification. Computerized X-ray microtomography enables resolution of structures on the micrometre scale, one or two orders of magnitude better than traditional X-ray radiograms. The inner structure and organic growth lines of pearls can be observed; cavities and hollows can be clearly differentiated from deposits of organic material due to their different grey scale in the tomograms, and features of bead nuclei distinguished. In addition, vaterite-containing areas within aragonite in two pearls have been identified on the basis of different intensities of grey in two- and three-dimensional tomograms. This contrast in the grey levels may, in part, be caused (and thereby emphasized) by higher concentrations of organic molecules in the vaterite-containing area rather than being solely due to the difference between the densities of aragonite and vaterite. The method is a fast and non-destructive method to identify the location of any vaterite in a pearl before Raman spectroscopy is used to map its exact distribution. However, microtomography is a most useful tool for scientific purposes and in testing highly valuable pearls, it can yield definitive structural information.

Acknowledgements

Support from the Johannes Gutenberg-University Research Fund for Young Scientists, the Institute of Gem Stone Research and the Geocycles Cluster, both at the University of Mainz, have made this study possible. The authors are grateful for support and fruitful discussions with Dr T. Häger, B. Dillenburger, Y. Demia, K. Yanase, M. Sakai, K. Kawabata and the brothers Ibuki. K.-P. Jochum is thanked for making pearl D available for study. This is Geocycles Cluster contribution No. 316.

References

Addadi, L., Joester, D., Nudelman, F., and Weiner, S., 2006. Mollusk shell formation: A source of new concepts for understanding biomineralization processes. *Chem. Eur. J.,* **12**, 980-7

Akamatsu, S., Zansheng, I.T., Moses, T.M., and Scarratt, K., 2001. The Current Status of Chinese Cultured Pearls. *Gems & Gemology,* (2), 96-113

Banerjee, A., and Habermann, D., 2000. Identification of Chinese freshwater pearls using Mn^{2+} activated cathodoluminescence. *Carbonates and Evaporites,* **15,** 138-48

Banerjee, A., and Rager, H., 2001. Discrimination between sea-water and freshwater tissuegraft cultured pearls by EPR. *Canadian Gemmologist,* **22**(3), 82-7

Barnard, W., and de Waal, D., 2006. Raman investigation of pigmentary molecules in the molluscan biogenic matrix. *J. Raman Spectrosc.,* **37**, 342-52

Falini, G., Fermani, S., Gazzano, M., and Ripamonti, A., 1998. Oriented crystallization of vaterite in collagenous matrices. *Chem. Eur. J.,* **4**(6), 1048-52

Falini, G., Fermani, S., Gazzano, M., and Ripamonti, A., 2000. Polymorphism and architectural crystal assembly of calcium carbonate in biologically inspired polymeric matrices. *J. Chem. Soc., Dalton Trans.,* 2000, 3983-7

Gutmannsbauer, W., and Hänni, H., 1994. Structural and chemical investigations on shells and pearls of nacre forming salt- and fresh-water bivalve molluscs. *The Journal of Gemmology,* **24**(4), 241-52

Habermann, D., Banerjee, A., Meijer, J. and Stephan, A., 2001. Investigation of manganese in salt- and freshwater pearls. *Nucl. Instr. and Meth. in Phys. Res. B,* **181,** 739-43

Hänni, H., 2006. A short review of the use of ´keshi´as a term to describe pearls. *The Journal of Gemmology,* **30**(1/2), 52-8

Hasse, B., Ehrenberg, H., Marxen, J.C., Becker, W., and Epple, M., 2000. Calcium carbonate modifications in the mineralized shell of the freshwater snail *Biomphalaria glabrata*. *Chem. Eur. J.,* **6**(20), 3679-85

Hedegaard, C., Bardeau, J.-F., and Chateigner, D., 2005. Molluscan Shell Pigments: An in Situ Resonance Raman Study. *Journal of Molluscan Studies,* **72,** 157-62

Huang, F., Chen, Z., Tong, H., Zhou, Y., Zhang, Z., and Yang, M., 2004. The microstructure of the shell and cultured blister pearls of *Pteria penguin* from Sanya, Hainan, China. *The Journal of Gemmology,* **29**(1), 25-36

Jacob, D. E., Wehrmeister, U., Häger, T., and Hofmeister, W., 2006a. Provenance determination of freshwater cultured pearls by Laser Ablation ICP-MS. *Asia-oceania conference, Singapore. Abstract book,* 59-SE-A0828

Jacob, D. E., Wehrmeister, U., Häger, T., and Hofmeister, W., 2006b. Identifying Japanese Freshwater cultured pearls from Lake Kasumiga. *The Australian Gemmologist,* **22**(12), 539-41

Jacob, D. E., Soldati, A.L., Wirth, R., Huth, J., Wehrmeister, U., and Hofmeister, W., 2008. Nanostructure, chemical composition and mechanisms of bivalve shell growth. *Geochimica et Cosmochimica Acta,* in press

Karampelas, S., Fritsch, E., Mevellec, E.-Y., Gauthier, J.-P., Sklavounos, S., and Soldatos, T., 2006. Determination by Raman scattering of the nature of pigments in cultured freshwater pearls from the mollusk *Hyriopsis cumingii*. *J. Raman Spectrosc.,* **38**, 217-30

Li, L., and Chen, Z., 2001. Cultured pearls and colour-changed cultured pearls: Raman spectra. *The Journal of Gemmology,* **27**(8), 449-55

Lorenz, I., and Schmetzer, K., 1986. Möglichkeiten und Grenzen der röntgenographischen Untersuchungen von Perlen. *Z. Dt. Gemmol. Ges.,* **34**(1/2), 57-68

Ma, H.Y., and Dai, T.G., 2001. The first discovery of vaterite in lusterless fresh water pearls of Leidan, Zhejiang. *Acta Mineral. Sin.,* 21, 153-7

Qiao, L., Feng, Q.L., and Li, Z., 2007. Special vaterite found in freshwater lacklustre pearls. *Crystal Growth and Design,* **7**(2), 275-79

Schlüter, J., Lohmann, M., Metge, J., and Reime, B., 2005. Diffraction Enhanced Imaging: a new X-ray method for detecting internal pearl structures. *The Journal of Gemmology,* **29**(7/8), 401-6

Snow , M. R., Pring, A., Self, P., Losnic, D., and Shapter, J., 2004. The origin of color of pearls in iridescence from nano- composite structure of the nacre. *American Mineralogist,* **89**, 1353-8

Song, F., Soh, A.K., and Bai, Y.L., 2003. Structural and mechanical properties of the organic matrix layers of nacre. *Biomaterials,* **24**, 3623-31

Strack, E., 2006. *Pearls.* Rühle-Diebener-Verlag, Stuttgart, Germany. 707 pp

Urmos, J., Sharma, S.K., and MacKenzie, S.T., 1991. Characterization of some biogenic carbonates with Raman spectroscopy. *American Mineralogist,* **76**, 641-6

Wada, K., 1998. Formation and quality of pearls. *Journ. Gemmol. Soc. Japan,* **20**, 47-56

Watabe, N., 1965. Studies on shell formation XI. Crystal-matrix relationships in the inner layers of mollusk shells. *J. Ultrastracture Research,* **12**, 351-70

Wehrmeister, U., Jacob, D., Soldati, A., Häger, T., and Hofmeister, W., 2007. Vaterite in freshwater cultured pearls from China and Japan. *The Journal of Gemmology,* **30**(7/8), 399-412

The Authors

U. Wehrmeister and W. Hofmeister

Centre of Gemstone Research, Johannes Gutenberg-Universität Mainz, D-55099 Mainz, FRG

Corresponding author, email address: wehrmeis@uni-mainz.de

H. Goetz and H. Duschner

Applied Structure- and Microanalysis, Faculty of Medicine, Johannes Gutenberg-Universität Mainz, D-55131 Mainz, FRG

D.E. Jacob, A. Soldati and W. Xu

Department of Geosciences, Johannes Gutenberg-Universität, D-55099 Mainz, FRG

One hundred years of Gemmological Education

This year Gem-A will be celebrating One Hundred Years of Gemmological Education. To ensure that we remain the provider of the highest status gem education through our second century, we have ambitious plans for the expansion and increased accessibility of Gem-A courses worldwide.

This can only be achieved with the support of our Fellows and Members. Our target is one hundred donations of a minimum of £1000 (US$2000) by September 2008.

As a member of the 100 Club, you will play an important role in helping us to achieve our charitable aims. As a patron, you will be honoured with:

- a 100 Club certificate
- your name on a plaque in the London Headquarters of Gem-A, in our Centenary publication and on our website.

Your contribution will help us to:

- Develop our gem courses and make them more widely available
- Upgrade our in-house facilities for students
- Establish our website as a primary focus for gemmological education and gem information
- Establish a scholarship fund
- Encourage the study of gemmology worldwide through articles and the media
- Make gem education more accessible in developing countries
- Improve ethical and environmental awareness in the gem trade
- Reinstate the Research Diploma for Fellows
- Support for continuous gemmological learning in the gem trade.

Payments may be spread over one year (minimum £83.33 or US$167 per month). Companies and those wishing to make larger contributions or to support specific initiatives, should go to www.gem-a.com/information/noticeBoard.php or contact Olga Gonzalez on +44 (0)20 7404 3334, email olga@gem-a.com.

One hundred years 1908 2008
OF GEMMOLOGICAL EDUCATION

Specular reflectance infrared spectroscopy – a review and update of a little exploited method for gem identification

Thomas Hainschwang and Franck Notari

Abstract: Specular reflectance FTIR (Fourier Transform Infrared) spectroscopy is a relatively little-exploited but very efficient technique to identify minerals and other materials that possess a somewhat reflective surface. In the past years the Gemlab and GemTechLab laboratories have used and refined the method for gemmological purposes and developed an extensive database of specular reflectance infrared spectra of minerals, gemstone imitations, organic materials and synthetic gem materials. This paper explains the method, introduces the spectrometer and accessories used and highlights the practical applications and advantages of specular reflectance FTIR spectroscopy in gemmology.
Keywords: intrinsic absorptions, spectral database, specular reflectance FTIR spectroscopy, vibrational spectroscopy

Introduction

Vibrational spectroscopy is very important for gemmological analysis and has been increasingly used in laboratories over the last few decades. The two methods included in the term vibrational spectroscopy are Raman and infrared spectroscopy (Schrader, 1995). Both are based on the interaction of light waves with vibrating molecules or crystal lattices. Raman spectroscopy detects bands due to inelastic scattering of laser light (thus monochromatic light) by vibrating molecules and crystal structure. Upon scattering, Raman bands are detected slightly shifted towards wavelengths of lower energy (higher wavelength, lower wavenumber) (Stokes shift) and with much weaker intensity to higher energy (lower wavelength, higher wavenumber) (Anti-Stokes shift). In infrared spectroscopy the vibrational energy of molecules changes upon absorption of infrared radiation, thus vibrational transitions are detected; in order to be infrared active, a molecule needs to possess a permanent dipole moment (Schrader, 1995).

Infrared and Raman spectroscopy are methods very commonly employed in analytical laboratories (Kiefert *et al.*, 1999). The best-known method of analysing samples with an infrared spectrometer is transmitting the infrared beam directly through the sample and observing the resulting absorption bands (King *et al.*, 2004). The intrinsic absorption bands of most materials (found in the mid infrared from ~ 2000–400, rarely to 200 cm^{-1}) however, are very intense, and cannot be resolved unless samples are thin enough (by polishing into thin films), or powdered and mixed with potassium bromide (KBr) and then pressed into pellets for analysis (Martin *et al.*, 1989). When investigating the infrared spectra of gemstones, however, sectioning or powdering are generally not possible and transmission spectra are performed without special preparation. Although the nature, shape and volume of a gem may allow some latitude, one can generally only observe the near to mid-infrared domain from around 7500 to about 2000 cm^{-1} with a standard Fourier Transform Infrared (FTIR) spectrometer. The features in this domain practically all relate to trace contents or impurities in samples, such as water in beryl (see for example Adamo *et al.*, 2005), and are only of limited use for identifying materials.

A very effective solution for this problem is to use specular reflectance

Materials and methods

For building the Gemlab–Gemtechlab specular reflectance FTIR spectral database and for the research conducted for this paper, a PerkinElmer Spectrum BXII FTIR spectrometer and a Nicolet Nexus FTIR spectrometer, each one equipped with a DTGS (Deuteriated Triglycin Sulphate) detector, were used. One to 100 scans were carried out at room temperature and spectra recorded with a resolution of 4 cm^{-1}. Higher resolutions up to 1 cm^{-1} were also investigated, but found not to be worth the extra time involved since all reflectance bands are far larger than 4 cm^{-1}; the narrowest reflectance band found was 8 cm^{-1} at full width half maximum (FWHM). A PerkinElmer fixed angle specular reflectance accessory and a modified Spectra Tech diffuse reflectance accessory were used to record the specular reflectance infrared spectra *(Figure 1)*. In the PerkinElmer fixed angle accessory the sample is placed with any smooth or near-smooth face on a disc with a central hole to hold the stone which fits into the sample stage *(Figure 1a)*. Small samples need to be fixed with Blu Tack in the centre of the disc. In the Spectra Tech accessory the mirror usually used as 'sample stage' needs to be removed and the stone placed with Blu Tack on the pedestal instead of the mirror; thus the selected sample surface is used instead of the mirror to reflect the infrared beam *(Figure 1b)*. Since both accessories have their advantages and disadvantages, for practical purposes it is good to have both on hand. The fixed angle specular reflectance accessory is low in cost and extremely simple to use; large objects can be analyzed and the time of sample preparation and spectral analysis is very short, since no adjustments whatsoever are necessary. For curved faces, matte surfaces and extremely small facets the accessory is not ideal, although in most instances an interpretable result can be obtained. The best results are obtained from faceted gemstones of 0.10 ct and larger, the larger the reflecting facet the better.

The modified diffuse reflectance accessory is ideal for the analysis of samples with curved and or matte surfaces, but its disadvantages are: the analysis of large stones is not possible due to limited space in the sample chamber, the time of sample preparation is longer, they have to be fixed with Blu Tack, and spectral analysis is more time consuming since the signal strength must be adjusted manually. Therefore the only applications where this more expensive accessory is useful are those rare cases where no acceptable result can be obtained from the fixed angle specular reflectance accessory. Due to the geometry of the diffuse reflectance accessory, very small surfaces and surfaces with little reflectivity can be effectively analyzed.

In order to identify materials automatically, a search database consisting of the spectra of more than 600 mineral species has been built by the Gemlab and Gemtechlab laboratories. The samples used to record the spectra for this database were all selected from the Gemtechlab and Gemlab laboratory reference collections; the stones in these collections have all been precisely identified by various techniques such as chemical analysis, X-ray diffraction, Raman spectrometry, etc. All spectra were recorded in reflectance mode in a range of 4000–400 cm^{-1} with a resolution of 4 cm^{-1} and normalized to 100% at the wavelength of the most intense reflectance peak. The automatic search database was set up using the Omnic software by Thermo Nicolet, with which recorded spectra can be identified automatically, indicating the match in percent of the sample spectrum with reference spectra.

Due to the intensities of the reflectance bands, atmospheric artefacts can in practice be ignored and thus background spectra do not need to be repeated for gem identification purposes. Another advantage of these band intensities is that for most samples, only a few scans are sufficient to achieve a good signal-to-noise ratio; when a stone has flat facets, then no more than one sample scan is necessary.

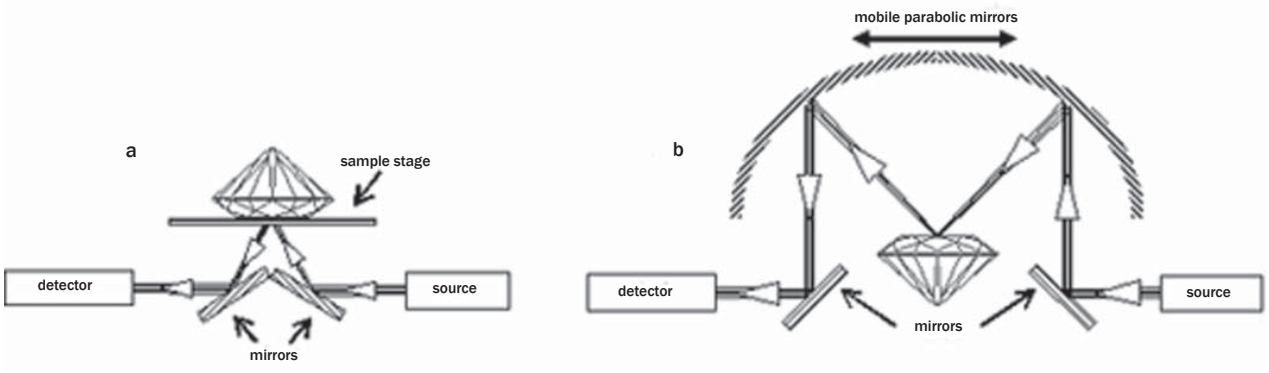

Figure 1: The design and function of the two accessories used to record specular reflectance infrared spectra: (a) fixed angle specular reflectance accessory, (b) modified diffuse reflectance accessory.

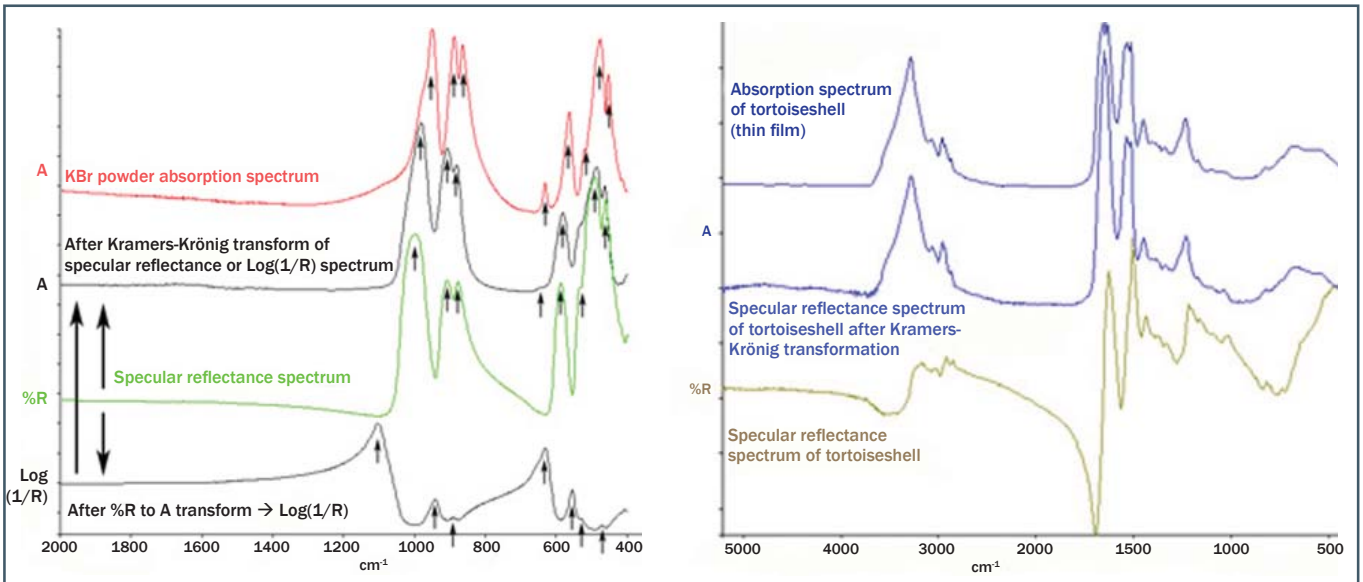

Figure 2: Comparison of specular reflectance versus true absorption spectra for an almandine garnet (left) and for tortoise shell (right, from Hainschwang and Leggio, 2006). The two examples are used to demonstrate the effect of the Kramers-Krönig transform: in the case of tortoiseshell the result is a perfect match with the true absorption spectrum, while in the almandine garnet the transform only had a slight effect on the reflectance spectrum; after the transformation the spectrum still was not a perfect match with the true absorption spectrum. In the garnet graph the bottom trace shows what happens upon %R to A transformation and consequent indexation of the 'absorptions'. Such transformation does not make much sense when determining a mineral from a reflectance spectrum since the unmodified reflectance peaks are much closer to a real absorption spectrum; upon application of the Kramers-Krönig transform to this Log(1/R) spectrum, the resulting spectrum will be the same as the one resulting from the application of the Kramers-Krönig transform to the specular reflectance spectrum. The examples garnet and organic material were chosen for demonstration because of their isotropy.

FTIR spectroscopy: this is a powerful vibrational analysis method to determine intrinsic structural vibrations of materials without destructive sample preparation; the beam is not transmitted through a sample, but reflected off the surface (White, 1974; Martin *et al.*, 1989; Coates, 2000; King *et al.*, 2004). With a comprehensive collection of reference spectra this method allows one to identify all minerals and imitations, most organics, and, in certain cases, even synthetics after only a few seconds analysis time (Martin *et al.*, 1989). The spectral information alone allows identification of the mineralogical group in most instances. Additionally, complexity of a crystal structure and presence of structural OH groups can be determined.

The Gemlab and Gemtechlab gemmological laboratories have refined this method for gemmological applications and have created an extensive database of reference specular reflectance FTIR spectra since 2001.

Characteristics and interpretation of specular reflectance spectra

Specular reflectance spectra resemble true absorption spectra to different degrees. In some gemstones, reflectance bands correspond closely to absorption bands, but in other cases, especially in organic materials, they appear strongly distorted due to abnormal dispersion *(Figure 2)*. This distortion can in most cases be corrected by the application of the Kramers-Krönig transform, which is used to transform specular reflectance spectra into true absorption spectra *(Figure 2)*. However, the applicability of this transform needs to be verified for each material because although the modified spectra of some stones are perfect matches with their true absorption spectra, for others the results are not an improvement on the original reflectance trace *(Figure 2)*. For identification purposes it is thus best to keep the spectra unmodified. So, for most minerals (and consequently for gemstones) the reflectance spectra can practically be regarded and interpreted in the same way as absorption spectra; the most prominent exception is diamond, because diamond is purely covalent and thus does not exhibit distinct FTIR reflectance peaks. For the general case of gemstones, where only infrared light reflected from a mirror-like surface reaches the detector, only structural peaks can be detected. In those minerals where the infrared beam can also be reflected from internal surfaces (such as in foliated minerals like mica), absorptions due to impurities may also be seen in the spectra. These features will then appear as they do in transmittance spectra, that is, they will appear in the opposite direction to that of reflectance peaks caused by structural vibrations. It has been noted in some recent publications that authors have recorded specular reflectance spectra of polished gemstones and shown them upside down, with a Y-scale indexed with 'Log(1/R)'; this happens when a spectrum recorded in reflectance mode is

Specular reflectance infrared spectroscopy – A review and update of a little exploited method for gem identification

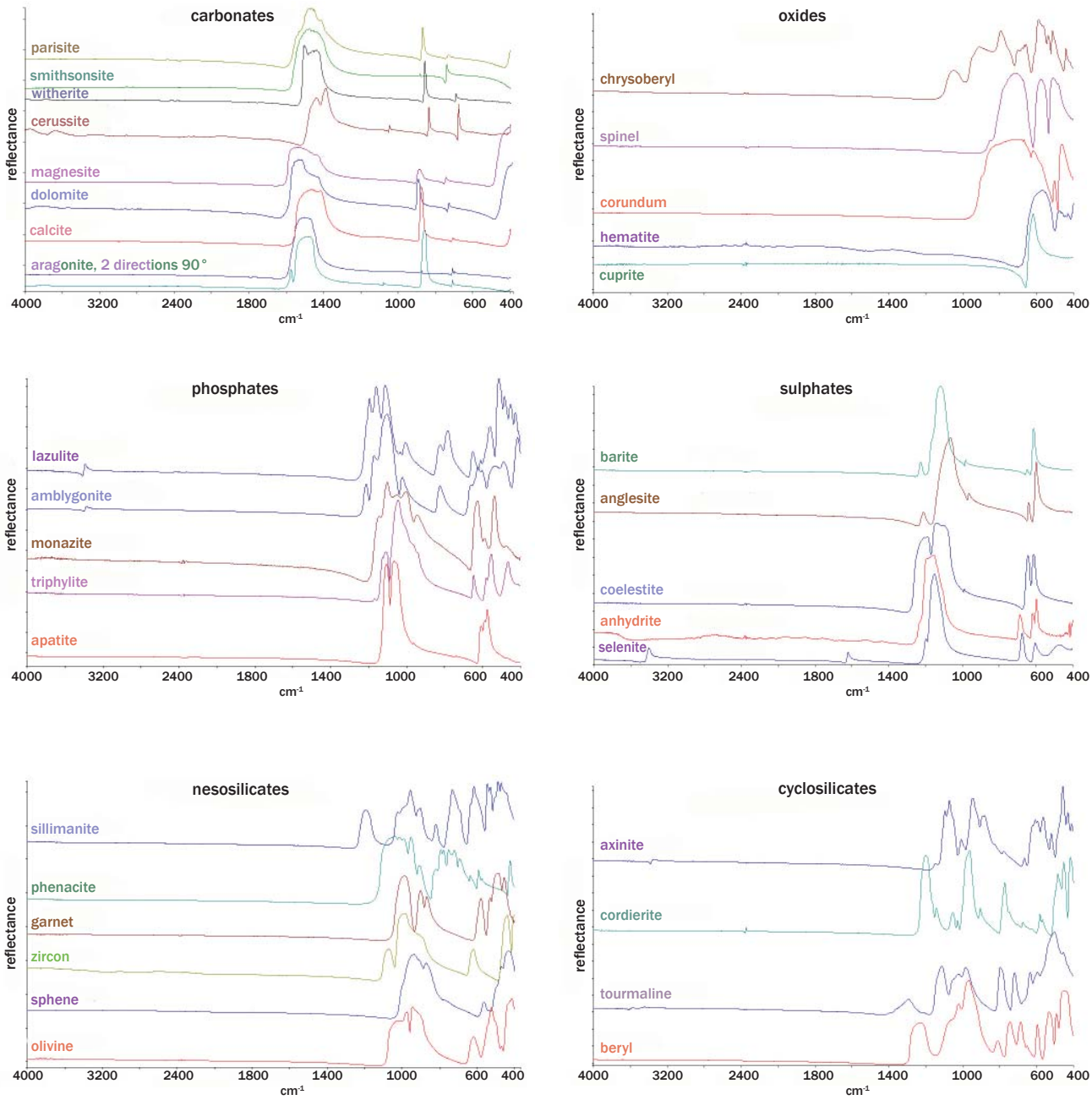

Figure 3: A selection of specular reflectance FTIR spectra of various arbitrarily oriented gemstones and minerals arranged according to their mineralogical groups.

transformed by a spectrometer program into absorbance, without using the Kramers-Krönig transform. The unusual shape of such transformed spectra and indexing the apparent 'absorption peaks' leads to much confusion and appears not to make much sense for the purpose of gem identification, since the unmodified reflectance spectra are much closer to a real absorption spectrum (*Figure 2,* left graph).

The bands detected in specular reflectance FTIR spectroscopy are very intense and only the peaks due to major compositional components of a material are detected, i.e. vibrations directly associated with the chemical formula of a substance. Because of this sensitivity to chemical composition and to the molecular coordination such a spectrum can be regarded as the fingerprint of a material. From the particular shape of a curve and the presence or absence of certain vibrations, a specular reflectance FTIR spectrum can usually be attributed to a mineralogical group. In *Figure 3* the spectra of gem minerals belonging to some of the more important mineralogical groups are shown and the differences between the groups are quite evident.

In gemstones with a simple structure, such as many of the carbonate and the sulphate minerals, the main vibrations

Box A: Notes on spectroscopic terms

- %**Transmittance (%T)**: the ratio, expressed in percent, of the intensity of the light transmitted through a sample to the intensity of light striking a sample, i.e. intensity of emerging light divided by intensity of incident light, × 100.
- **Absorbance**: inversely and logarithmically related to transmittance by the formula A = log(100/%T).
- %**Reflectance (%R)**: the ratio, expressed in percent, of the amount of radiation reflected from a sample surface to the amount of radiation reflected from a standard surface, usually an infrared mirror.
- **Kramers-Krönig transform (KKT)**: transform used to transform specular reflectance spectra into absorption spectra; it is based on the relations between refraction and absorption of electromagnetic waves in a substance.
- **Vibrations in molecules or ions**:
  External vibrations (lattice vibrations/lattice modes) [~600 to 80 cm^{-1}]:
  Translations (T_x, T_y, T_z) and Rotations (R_x, R_y, R_z)
  Internal vibrations (Internal modes) [~ 3800 to 400 cm^{-1}]:
  ν_1 = symmetric stretch (Raman) ν_2 = out of plane bend (b) (IR)
  ν_3 = asymmetric stretch (s) (IR+Raman) ν_4 = in plane bend (IR+Raman)
  Number of vibrations in a non-linear molecule or ion with n atoms = 3n-6 internal vibrations;
  Number of vibrations in a linear molecule or ion with n atoms = 3n-5 internal vibrations.
  Both linear and non-linear molecules or ions possess 6 external vibrations, 3 rotary and 3 translatory.
  Detailed explanations and definitions of terms for vibrational spectroscopy can be found in the Glossary of Terms used in Vibrational Spectroscopy (Bertie, 2002).

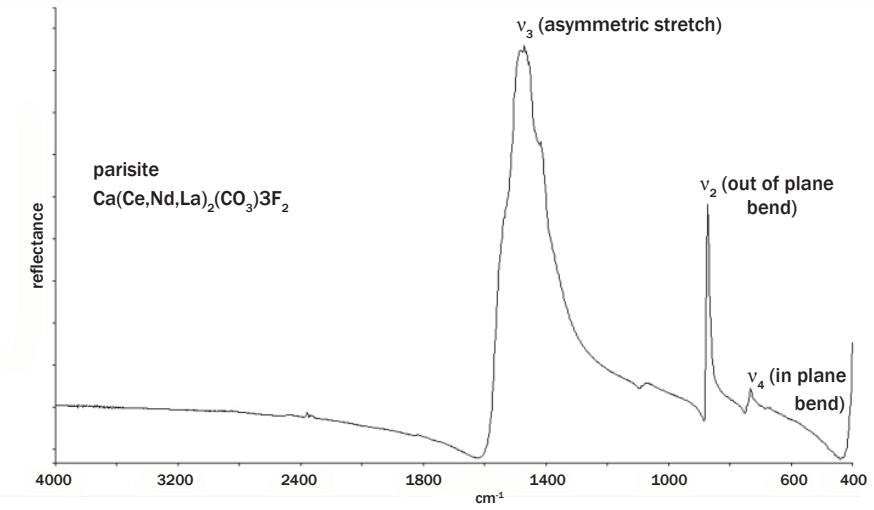

Figure 4: The attributions of the principal reflectance peaks to the corresponding molecular vibrations of the carbonate ion CO_3^{-2} in the specular reflectance spectrum of the rare carbonate parisite.

(ν_2, ν_3, ν_4) of the molecular group can be directly attributed. For example the carbonate ion CO_3^{-2} in different carbonate minerals (for example calcite, aragonite and dolomite) has its main vibrations at the following positions: ν_2 → 850 – 900 cm^{-1} – ν_3 → 1400 – 1600 cm^{-1} – ν_4 → 680 – 770 cm^{-1} *(Figure 4)* (see, for example, White 1974). For more complex minerals like many of the silicates attribution is more complex and is beyond the scope of this paper.

In anisotropic gem materials (i.e. in all minerals except the ones belonging to the cubic crystal system plus aggregates [for example jadeite, chalcedony, nephrite] 'Mineraloids' [for example obsidian, tektites, opal] and organic materials [for example tortoiseshell, amber, bone]) the orientation of the samples in the specular reflectance accessory can have visible effects on the reflectance spectra due to the anisotropy. Anisotropic materials not only show distinct orientation-dependent variations in the UV and visible part of the electromagnetic spectrum, but also in the infrared region. The spectra of the α, β and γ rays of tanzanite recorded using an infrared polarizer between the infrared beam and the specular reflectance accessory are shown in *Figure 5;* the distinct differences between the individual rays are evident. The effects of this anisotropy are far less distinct without use of a polarizer. Although sample orientation alone will cause certain variations, only in a few materials will they be significant enough to potentially affect the efficiency of the automatic search function. Such minerals with different spectra in different directions therefore need to be recorded in various orientations and several reference spectra saved. In the great majority of gem materials the variations due to anisotropy do not affect the efficiency of the automatic search function, since it is usually only the intensities of the individual peaks that vary, not their positions or wavenumbers.

Practical applications of specular reflectance FTIR spectroscopy

This method has some major applications in gem identification. The specular reflectance spectra are generally characteristic for one single gem species. Therefore, when the matching reference spectra are in a database, any material can be rapidly identified by a technician or gemmologist trained to use the FTIR instrument and the spectrometer software; this is also true for diamond, since all diamond-imitations show reflectance peaks while diamond does not.

Also, even in the absence of a matching reference spectrum, an experienced

spectroscopist can obtain extensive clues towards identifying a material by relating the major peaks of a spectrum to a mineralogical group and assessing its complexity. Since the method is very sensitive to compositional changes, synthetic gemstones can be differentiated from their natural counterparts when they are not a perfect structural match; so substances like synthetic turquoise, flame fusion synthetic spinel and most synthetic alexandrite can be identified rapidly. The sensitivity to compositional changes even permits in most cases the determination of gems in complex solid solution series such as the garnet group. If properly identified end-member garnets are in the database, at least the major components in a gem garnet under test can be identified *(Figure 6)*.

In many items submitted to laboratories for identification, gemstones are mounted in jewellery and identification by standard gemmological methods or even by many advanced methods like UV-Vis-NIR can be very challenging, time consuming or even impossible. The method described here is the ideal solution for identifying all materials used as gems, and even very small stones in heavy mountings can be identified. Additionally the specular reflectance data can be saved and, together with other gemmological data, used as formal proof in the event of any dispute.

Another application is the identification of very small surface-reaching inclusions in gemstones and grains within rocks; surfaces with a diameter as small as 0.5 mm were sufficient to yield critical data using the modified diffuse reflectance accessory, even when they were curved or matte. Using the fixed angle accessory approximately double the surface diameter was necessary to get good data and surfaces had to be more or less flat and smooth. To avoid interference from the surrounding material on the spot being analysed, Blu Tack was used as a screen because it does not produce artefacts in this analytical method, in contrast to transmittance spectroscopic analysis.

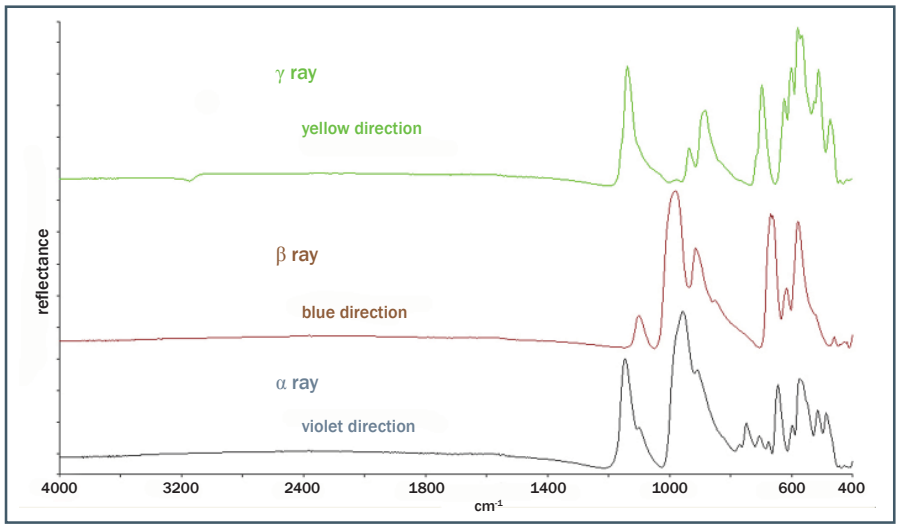

Figure 5: The polarized specular reflectance spectra of the α, β and γ rays of tanzanite. The spectra show very distinct differences due to extreme anisotropy. Arbitrarily oriented tanzanite would result in a spectrum of a combination of the three traces, showing most peaks and varying intensities. The spectra are cut off at 450 cm^{-1} since the infrared polarizing filter used did not transmit below this wavenumber. The colour annotations were added to each trace to show how each ray relates to the pleochroic colours of tanzanite.

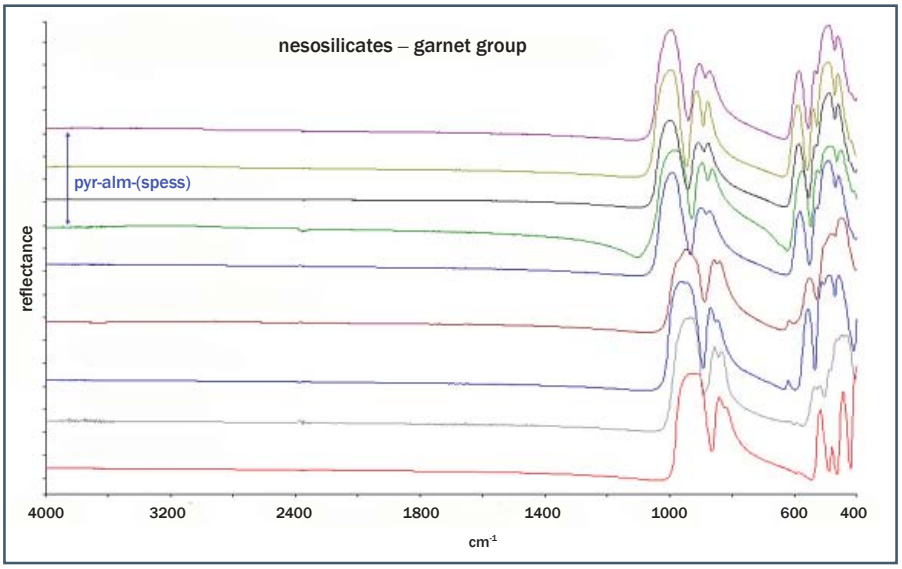

Figure 6: The garnet group shows extensive isomorphous replacement between molecules of almost all of its species. The major components of non-end member garnets can be identified by specular reflectance infrared spectroscopy.

Although all these tasks can also be achieved by Raman spectroscopy, the Raman systems used in gemmological laboratories are generally very costly compared to an infrared spectrometer and to maintain their financial viability, they are normally occupied by tasks other than gem identification. Due to the high intensities of reflectance bands and due to the large FWHM of all bands it is not necessary to use a research-grade FTIR spectrometer for gem identification – a low cost FTIR system with a maximum resolution of 4 cm^{-1} is more than sufficient.

A very important point in day-by-day work is that the time needed for gem identification with this spectroscopic method can be short. Assuming the spectroscopy software is open and the

search database ready, by using the fixed angle accessory an experienced operator can take approximately one minute to identify a stone conclusively; this includes sample preparation and data storage. Of course, one should not forget that rapid microscopic observation is always necessary in order to avoid misidentifications of, for example, assembled stones such as doublets or triplets.

Concluding remarks

The advantages of the spectroscopic method of specular reflectance FTIR analysis for gem identification purpose have been presented in this paper. These include high accuracy of gem identification and very short analysis time. Even though the specular reflectance spectra vary somewhat in appearance from true absorption spectra, they are similar enough to obtain most of the information that can be obtained from KBr powder absorption spectra. Compared to the only other spectroscopic method capable of very rapid and precise gem determination — Raman spectroscopy — the instruments necessary for specular reflectance FTIR spectroscopy are relatively low-cost and robust. While the method presented in this paper is limited to the identification of gem materials, the spectrometer used with other accessories has many more applications such as diamond type and treatment determination, determination of foreign substances such as glass, resin and oil in gemstones and is thus an important tool for gemmological laboratories.

References

Adamo, I., Pavese, A., Prosperi, L., Diella, V., Merlini, M., Gemmi, M., and Ajo, D., 2005. Characterization of the new malossi hydrothermal synthetic emerald. *Gems & Gemology,* **41**(4), 328–38

Bertie, J.E., 2002. Glossary of terms used in vibrational spectroscopy. In: *Handbook of Vibrational Spectroscopy,* J.M. Chalmers and P.R. Griffiths (Eds). John Wiley & Sons Ltd., Chichester, 1–49

Coates, J., 2000. Interpretation of infrared spectra, a practical approach. In: *Encyclopedia of Analytical Chemistry,* R.A. Meyers (Ed.). John Wiley & Sons Ltd, Chichester

Hainschwang, T., and Leggio, L., 2006. The characterization of tortoise shell and its imitations. *Gems & Gemology,* **42**(1), 36-52

Kiefert, L., Hänni, H.A., Chalain, J.P., and Weber, W., 1999. Identification of filler substances in emeralds by infrared and Raman spectroscopy. *The Journal of Gemmology,* **26**(8), 501–20

King, P.L., Ramsey, M.S., McMillan, P.F., and Swayze, G., 2004. Laboratory fourier transform infrared spectroscopy methods for geologic samples. In: *Infrared Spectroscopy in Geochemistry, Exploration, and Remote Sensing,* P. King, M. Ramsey, G. Swayze (Eds), Mineral. Assoc. of Canada, ON, **33,** 57– 91

Martin, F., Mérigoux, H., and Zecchini, P., 1989. Reflectance infrared spectroscopy in gemology. *Gems & Gemology,* **25**(4), 226–31

Schrader, B. (Ed.), 1995. *Infrared and Raman Spectroscopy*. VCH Publishers Inc, New York. Chapter 4

White, W.B., 1974. The carbonate minerals. In: *The Infrared Spectra of Minerals,* V.C. Farmer (Ed.), Chapter 12. Mineralogical Society, London, 232

The Authors

Thomas Hainschwang

GEMLAB Gemological Laboratory, Gewerbestrasse 3, FL-9496 Balzers, Liechtenstein. email: thomas.hainschwang@gemlab.net

Franck Notari

GemTechLab, 2 rue de Chantepoulet, CH-1201 Geneva, Switzerland

HONG KONG GRADUATION AND AWARDS DINNER

In Celebration of One Hundred Years of Gemmological Education

To be held at the Royal Palace Chinese Restaurant

1/F, China Hong Kong City, 33 Canton Road, Tsimshatsui, Kowloon

on Tuesday 16 September 2008

Organized by Gem-A in conjunction with its training centres:
The Asian Gemmological Institute and Laboratory Limited (AGIL ATC)
The Hong Kong Institute of Gemmology (HKIG ATC)

A special Dinner is to be held in Hong Kong this year to celebrate
One Hundred Years of Gemmological Education.
Following the dinner, Gem-A awards will be presented to successful graduates of Gem-A teaching centres in Hong Kong, Taiwan, Mainland China and elsewhere in the Far East and Pacific area.

Perfectly timed for those visiting the Hong Kong Jewellery and Watch Fair (see below), the Hong Kong Graduation and Awards Dinner is a great opportunity for members and students to meet. Join Gem-A and its Asian teaching centres for this special centenary dinner.

Tickets: Non-member/non-student £36.00 each

Gem-A members, students and their guests £32.00 each

Table Bookings: £336.00 for a table of twelve

Sponsorship opportunities: Gem-A is inviting sponsorship of this important event. As a non-profit-making educational charity, Gem-A ploughs back any profits into the continued development of gem education, so your support would be very much welcomed.

To book tickets or for sponsorship information, contact Kehan Li on +44 (0)20 7404 3334
email kehan.li@gem-a.com or visit **www.gem-a.com**

HONG KONG JEWELLERY AND WATCH FAIR

Hong Kong Convention and Exhibition Centre — Wednesday 17 to Sunday 21 September 2008

Visit Gem-A at booth 2M49 where the newly developed Gemmology Foundation course can be viewed.

Gem-A Seminar

Gem-A is pleased to announce that it will be holding a seminar during the Fair in

Room 604, Level 6, at theHong Kong Convention and Exhibition Centre

on Friday 19 September 2008 from 11:00 am to 1:00 pm

Afghan beryl varieties

Lucyna Natkaniec-Nowak

Abstract: Colour varieties of Afghan beryls from pegmatites at Ghursalak in Konar Province (aquamarine, morganite) and from the Panjshir Valley (emerald) have been investigated. The aquamarine, composition with SiO_2 (65.75 wt.%), Al_2O_3 (17.87 wt.%) and BeO (12.29 wt.%) is similar to that of many other aquamarines, and the low concentration of alkalis as well as relatively high amounts of Li_2O (0.34 wt.%) all indicate the gemstone to be normal beryl with limited isomorphous substitution in octahedral and tetrahedral sites. The calculated unit cell parameters (i.e. a = 9.2221 Å, c = 9.1990 Å, c/a = 0.9975), optical characteristics (i.e. ω = 1.576, ε = 1.571; Δ = 0.005) and the IR spectra of aquamarine with characteristic bands at 1206 and 963 cm^{-1} are typical of normal beryl. Emerald with contents of SiO_2 (64.50 wt.%), Al_2O_3 (15.19 wt.%) and BeO (12.73 wt.%) and significant amounts of alkalis (i.e. $Na_2O+K_2O+Li_2O$ = 2.1 wt.%) is alkali-rich octahedral beryl. This attribution is also indicated by the unit-cell parameters (i.e. a = 9.2399 Å, c = 9.1984 Å, c/a = 0.9955) and optical characterization (i.e. ω = 1.580, ε = 1.574; Δ = 0.006). Morganite with SiO_2 (64.16 wt.%), Al_2O_3 (17.91 wt.%) and BeO (11.81 wt.%) has the highest total alkali content ($Na_2O+K_2O+Li_2O$ = 3.51 wt.%) and is assigned to alkali-rich (Na-K-Li) tetrahedral beryl. The IR spectra of morganite (additional band at ***c.*** 1060 cm^{-1}, no shifts of 1215, 970 cm^{-1} towards lower wave numbers) together with calculated unit-cell parameters (i.e. a = 9.2198 Å, c = 9.2314 Å, c/a = 1.0012) and optical characteristics (i.e. ω = 1.580, ε = 1.574; Δ = 0.006) are all typical for a tetrahedral beryl. The Afghan beryls formed within granitic, beryl-muscovite pegmatites in hydrothermal conditions.

Keywords: aquamarine, emerald, morganite, NE Afghanistan

Introduction

The mountainous country of Afghanistan has been known for ages as a source of valuable mineral resources: gold, silver, lead, zinc, iron, antimony, copper, manganese, nickel, tin, sulphur, gypsum, salt, coal, oil as well as various precious stones, among which two of the most prominent are colour varieties of beryl, emerald and aquamarine. Exceptionally beautiful gem-quality beryls provide the slowly developing Afghan market with foreign currency.

Among the many papers dealing with Afghan beryls, especially emeralds and aquamarines, of special interest are those by Bariand and Poullen, 1978; Bowersox, 1985; Aurisicchio *et al.*, 1988; Bowersox *et al.*, 1991; Jones, 1991; Seal *et al.*, 1991; Bowersox and Chamberlin, 1995; Forestier and Piat, 1998; Bowersox *et al.*, 2000; Sachanbinski and Sobczak, 2001; Vapnik and Moroz, 2001; Hänni and Krzemnicki, 2003; Sachanbinski *et al.*, 2003; Fijał *et al.*, 2004.

The occurrence of beryls in Afghanistan

Beryl-bearing pegmatites occur in the NE part of Afghanistan, mainly in the provinces of Badakhshan, Laghman, Konar, Kapisa and Nangarhar (Chmyriov *et al.*, 1973; Rossovskiy *et al.*, 1976; Bowersox and Chamberlin, 1995; Hausel, 2006). The top quality aquamarines and morganites are mined in the Nilaw, Mawi and Kurghal regions of Laghman Province from cavities in pegmatite veins *(Figure 1)*.

Materials and methods

Beryl samples from pegmatites of Ghursalak (Konar Province) and Panjshir Valley in NE Afghanistan were provided by Mr Jacek Szczerba. Investigations of nine colour varieties of beryl were carried out at the laboratories of the Department of Mineralogy, Petrography and Geochemistry, Faculty of Geology, Geophysics and Environment Protection, AGH University of Science and Technology in Cracow, Poland. They included hand specimen observations, optical investigation with a standard polarizing microscope in transmitted light, chemical, X-ray (XRD) and infrared spectroscopic (IR) analyses as well as special gemmological determinations.

Standard optical examinations were carried out with an Olympus BX 51 polarizing microscope. XRD analyses were done with a Philips X-Pert PW 1729 diffractometer in the range 5-75° 2Θ, applying CuKα radiation, a graphite monochromator, voltage 35 kV, lamp current 30 mA. Unit-cell parameters were calculated using the least squares method applying the DHN-PDF programme. A pure Si powder was used as an internal standard. IR spectra for selected beryl powdered samples were recorded with a BIO-RAD model FTS 1665 spectrometer in the range 400-4000 cm^{-1}. Determinations of chemical elements in three samples (aquamarine, emerald and morganite) were made. Main components, i.e. SiO_2, BeO, Al_2O_3, CaO, Li_2O, V_2O_3, were determined by inductively coupled plasma-atomic emission spectrometry (ICP-AES). The analyses were made using a PLASMA 40 Perkin Elmer spectrometer. Rb_2O and Cr_2O_3 were measured by inductively coupled plasma mass spectrometry (ICP-MS), using an Elan 6100 Perkin Elmer spectrometer. Other components, i.e. Fe_2O_3, MgO, CuO, MnO, K_2O, Na_2O, were determined by instrumental neutron activation analysis (INAA). The investigations were carried out with a 2 MW Pool Type reactor and a CANBERRA detector. The gemmological determinations of internal features, optical characteristics and luminescence were carried out using Schneider equipment.

The famous deposits of emerald occur in the Panjshir Valley (Kapisa Province).

The Nilaw-Kolum Pegmatite Field (35°12' N and 70°21' E) is one of the major regions producing gems in Afghanistan (Bariand and Poullen, 1978; Wolfart and Wittekindt, 1980; Orris and Bliss, 2002). Besides gem-quality beryl crystals, the pegmatites also contain albitized microcline, black tourmaline, lepidolite, multicolour tourmaline, kunzite (pink spodumene), columbite, manganotantalite, tantalite, cassiterite and others. According to Fuchs *et al.* (1974), beryl reserves of the pegmatites were estimated in the hundreds of tons.

The Mawi pegmatite (35°12' N and 70°20' E), occurring east of Nilaw near the Kolum river, hosts morganite accompanied mainly by kunzite and tourmaline and rarely by gem-quality aquamarine (Hausel, 2006). These morganites enriched in Cs are pink, pinkish-orange or orange (Hänni and Krzemnicki, 2003). They are usually up to 6 cm in length, prismatic and non-transparent.

South of Nilaw and Mawi, in the Kurghal deposit (35°04' N and 70°18' E), near the Alingar river, rare beryl crystals are accompanied by oligoclase, microcline, black tourmaline and muscovite, but it is most famous for extraordinary transparent green tourmalines.

The Ghursalak (Gursalak) Pegmatite Field in Konar Province (about 34°57' N and 70°43' to 70°44' E) has yielded beryl but it remains less well known than Mawi and Kurghal (Schumann, 1997; Hausel, 2006).

The emerald mines in the Panjshir Valley, located on the eastern side of the

Table I: Characteristics of aquamarine from the Ghursalak Pegmatite, Konar Province, NE Afghanistan.

Sample No.	Linear dimensions [length × width × height] (cm)	Weight (g)	Specific gravity SG	RI and birefringence	Characteristics of the crystal	Remarks
A1	2.5 × 2.0 × 2.7	22.02	2.68	ω = 1.576 ε = 1.571 Δ = 0.005	Pale blue with weak growth-zoning, translucent (many flaws and cracks)	Selected for detailed investigations
A2	2.2 × 1.6 × 2.2	14.80	2.80	ω = 1.575 ε = 1.571 Δ = 0.004	Blue with a green hue, translucent, numerous internal flaws and cracks filled with brown material	SEM and Raman investigations indicate brown material is probably clay minerals + Fe-compounds or bituminous substance
A3	1.7 × 1.5 × 2.6	9.62	2.72	ω = 1.578 ε = 1.573 Δ = 0.005	Euhedral crystal, pale blue, growth zones and tiny, 2-phase gas-liquid inclusions, transparent, locally translucent	Gem of high quality, *Figure 3.*

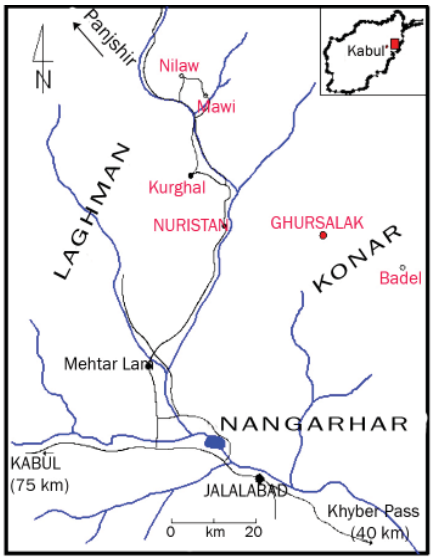

Figure 1: Locality map of beryl deposits in the NE provinces of Afghanistan (after Bariand and Poullen, 1978).

river at altitudes between 2690 and 3800 m, cover an area of 16 km^2 (Neilson and Cannon, 1977; Bowersox, 1985; Bowersox *et al.*, 1991; Orris and Bliss, 2002; Schwarz and Giuliani, 2002). The beryls occur sporadically in quartz-ankerite-pyrite veins. The pyrite can be used as an indication of the emerald mineralization. In general, the Panjshir Valley emeralds are dark green *(Figure 2)*, similar in colour to the fine emeralds found at the Muzo mine in Colombia (Kazmi and Snee, 1989; Sabot *et al.*, 2001) and sporadically over 15 mm in length. They are larger and cleaner than those found in the Swat and Gilgit regions of Pakistan (Gübelin, 1982; Kazmi *et al.*, 1985).

Since the 1970s most Afghan emeralds have been mined in the Bismal area (35°28' N and 69°49' E; 2690 m above sea level) in Kapisa Province, i.e. Bismal — Rewat and Ringe i Mukeni — Zara Kel (www.fieldgemology.com). Other emerald mining areas of less economic significance are in Konar Province, i.e. the Badel mine (34°50' N and 70°56' E) and in the Sorobi District near the Jagdalak ruby mine, as well as in the Laghman Province (Various authors, 2002).

Mineralogical and gemmological characteristics of Afghan beryls

Aquamarine

Three gem-quality samples of aquamarine (A1, A2, A3) from the Ghursalak deposit were studied *(Table I)*. The crystals are a delicate pale blue or blue with a green tint and a weak vitreous lustre. Different parts of the crystals are transparent or translucent according to the absence or presence of growth zones densely distributed parallel to the crystallographic *c*-axis, fissures or other defects. No mineral inclusions were found. However, tiny, 2-phase (gas and liquid) inclusions are present and visible in the zoned beryl A3.

Aquamarine A1 was selected for detailed investigation *(Figure 3)*. It is a perfect hexagonal prism, and its unit cell parameters are: a = 9.2221 Å, c = 9.1990 Å, c/a = 0.9975, which are consistent with published values (Aurisicchio *et al.*, 1988; Andersson, 2006). According to Gaines *et al.* (1997), the measured values of the RIs (ω = 1.576, ε = 1.571) and birefringence Δ = 0.005 are characteristic of low-alkali aquamarines. This aquamarine is inert under short- and long-wave ultraviolet (SW and LW UV) light.

The composition of aquamarine A1 is given in *Table II,* and on this basis, its structural formula is:

Figure 2: Emerald crystals from the Panjshir Valley, NE Afghanistan; collection J. Szczerba; Photo: S. Konopacki.

Afghan beryl varieties

$(Be_{2.65}Li_{0.12})(Al_{1.79}Fe^{3+}_{0.03}Ca_{0.03}Mg_{0.02})$
$(Si_{5.90}Al_{0.10})O_{18}$ $(Na_{0.06}K_{0.01})\cdot 0.52(H_2O)$

The relatively high contents of Al_2O_3 (17.87 wt.%) and BeO (12.29 wt.%) show that the aquamarine is a normal beryl with limited isomorphic replacements in both octahedral and tetrahedral sites. Here, the octahedral sites are occupied mainly by Al, Fe^{3+}, Ca and Mg. According to Aurisicchio *et al.* (1988), if Na + K > Mg then the total Li substitutes for Be in the tetrahedral sites, while Na and K are located in structural channels. Since Na_2O + K_2O < 0.5 wt.%, this aquamarine can be considered a low-alkali beryl (Černy, 1975). The Rb/K ratio is 0.08 and such a low value is also characteristic of beryls with low contents of alkali ions. Minor amounts of Mn, Rb, V and Cr are present as trace components.

A concentration of 0.37 wt.% Fe_2O_3 indicates that this element is responsible for aquamarine colour. In comparison to beryls from other localities in the world, the Fe-content is rather low, which is consistent with a pegmatitic origin (Chukhrov, 1963).

Table II: Chemical compositions of three Afghan beryls.

Oxide (wt.%)	A1 Aquamarine	E1 Emerald	M1 Morganite
SiO_2	65.75	64.50	64.16
Al_2O_3	17.87	15.19	17.91
Fe_2O_3	0.37	0.70	0.26
CaO	0.31	0.89	0.25
MgO	0.18	1.37	0.015
MnO	0.02	0.045	0.02
K_2O	0.11	0.27	0.44
Na_2O	0.34	1.15	1.61
Li_2O	0.34	0.68	1.46
Rb_2O	0.019	0.065	0.031
BeO	12.29	12.73	11.81
V_2O_3	0.013	0.093	0.004
Cr_2O_3	0.028	0.219	0.028
CuO	0.022	0.10	0.021
H_2O^+ (at 900°C)	1.75	2.08	1.89
Total	**99.412**	**100.082**	**99.909**
number of oxygens	18	18	18
Si	5.900	5.786	5.771
Al [IV]	0.100	0.214	0.229
Al [VI]	1.790	1.392	1.670
Fe^{3+}	0.025	0.047	0.017
Ca	0.030	0.086	0.024
Mg	0.024	0.183	0.002
Mn	0.002	0.003	0.002
K	0.013	0.031	0.051
Na	0.059	0.201	0.281
Li	0.123	0.246	0.529
Rb	0.001	0.003	0.002
Be	2.649	2.744	2.552
V	0.001	0.006	–
Cr	0.002	0.015	0.002
Cu	0.002	0.007	0.002

Emerald

Three gem-quality emeralds from the Panjshir Valley were selected for study *(Table III)*. They are from light to dark green with yellow or blue tints and a weak vitreous lustre. They contain numerous inclusions of different kinds, and some cracks and fissures are filled with a brown substance, probably containing bituminous matter.

Selected for detailed investigation, emerald E1 is a prismatic crystal *(Figure 4)*. The crystal is dichroic in blue-green for the extraordinary ray and yellow-green for the ordinary ray. It is inert in both LW and SW UV light which is probably a result of its iron content, a feature in Afghan emeralds reported for example by Fijał *et al.* (2004). It is known that even small amounts of this element annihilate fluorescence of emeralds (Gaines, 1976).Its unit-cell parameters are: a = 9.2399 Å, c = 9.1984 Å, c/a = 0.9955, and the X-ray diffraction reflections are: 8.04(100); 4.62(35); 4.00(30); 3.27(96); 2.88 (91); 2.53 (20) Å.

The composition of emerald E1 is given in *Table II,* and on this basis, its structural formula is:

$(Be_{2.74}Li_{0.25}\ Na_{0.01})$
$(Al_{1.39}Fe^{3+}_{0.05}Ca_{0.09}Mg_{0.18}Cr_{0.02}V_{0.01}Cu_{0.01})$
$(Si_{5.79}Al_{0.21}O_{18}(Na_{0.19}K_{0.03})\cdot 0.62(H_2O)$

In comparison to the other investigated beryls, the emerald has the lowest content of Al, but has higher Fe, Ca, and Mg. The BeO content of 12.73 wt.%, is lower than the 'ideal' content 13.96 wt.%, but this is characteristic of emeralds from granitic beryl-muscovite, Ta-Be or Li-Be pegmatites (Zasiedatielev, 1970). This also indicates some substitution of Be in the tetrahedral (BeO_4) sites: firstly because Na + K > Mg, Li could substitute for Be, and secondly because the ratio H_2O/Na_2O < 2, Na could also substitute for Be. The remaining Na together with K occurs in structural channel sites. Rb_2O and MnO are present in traces only. The minor content of CuO probably indicates Cu compounds occurring as inclusions in the emerald crystal.

Figure 3: Aquamarine (A3) from the Ghursalak Pegmatite, Konar Province, NE Afghanistan; collection J. Szczerba; Photo: S. Konopacki.

Cr, V and subordinately Fe are, generally, chromophores responsible for the colour of emeralds (Nassau and Jackson, 1970; Taylor, 1977; Sinkankas, 1981; Spiesser and Fritsch, 1998; Various authors, 2005). In comparison with emeralds from other world occurrences, the Afghan emeralds show relatively high Cr_2O_3 content (0.219 wt.%), but are below the majority of Colombian stones (Muzo emeralds have around 0.29 wt.% Cr_2O_3 and 0.21 wt.% V_2O_3, vide Fijał *et al.*, 2004).

Noticeably high in the emerald E1 is the MgO concentration (1.37 wt.%), which is characteristic of beryls from pegmatites intruding ultrabasic and basic rocks. This is consistent also with the presence of significant amounts of CaO (0.89 wt.%).

According to Černy (1975), the emerald analysed can be classified as alkali-rich beryl with contents of Na_2O (1.15 wt.%), Li_2O (0.68 wt.%) and K_2O (0.27 wt.%); $Na_2O + K_2O$ = 1.42 wt.% makes up 67% of total alkalis with Na and Li noticeably prevailing over K (Ginsburg, 1955; Černy, 1975; Seal *et al.*, 1991).

Morganite

The details of investigations on three morganites from the Ghursalak mines are given in *Table IV*. The crystals are pale to dark pink and have a weak vitreous lustre. Due to their numerous internal defects the gems are translucent and non-transparent. Additionally, gas-filled cavities and 2-phase liquid-gas inclusions lie in zones parallel to the crystallographic *c*-axis, and fine, dark, solid inclusions – probably biotite flakes are also present. Under SW and LW UV light the crystals are pale violet.

The unit-cell parameters of morganite M1 are: a = 9.2198 Å, c = 9.2314 Å; c/a = 1.0012.

The results of chemical analysis of the morganite *(Table II)* were used to calculate its structural formula:

$$(Be_{2.55}Li_{0.45})(Al_{1.67}Fe^{3+}_{0.02}Ca_{0.02})(Si_{5.77}Al_{0.23})O_{18}(Na_{0.28}K_{0.05}Li_{0.08})\cdot 0.57(H_2O)$$

Morganite M1 has the lowest Be and highest Li contents of the three analyses and one may conclude that some Li has substituted for Be in the tetrahedral sites, which is typical of tetrahedral beryls *(t-beryls)* (Kurazkovskaya *et al.*, 1987). The channel sites are occupied by Na, K and the remaining amounts of Li. Trace elements include Mg, Mn, Rb, V, Cr and Cu. The low content of MnO (0.02 wt.%) and the Fe/Mn ratio of 8.5 could indicate a significant role for Fe as a colouring agent in this crystal.

Infrared spectroscopic investigations

IR spectra of the three beryls, i.e. aquamarine A1, emerald E1 and morganite M1, are presented in *Figure 5*. Bands in the range 1400-400 cm^{-1} can be attributed to Si-O, Be-O and Al-O stretching and bending vibrations. The Si-O asymmetric stretching vibrations appear at

Figure 4: Emerald (E1) from the Panjshir Valley, NE Afghanistan; collection J. Szczerba; Photo: S. Konopacki.

1200-900 cm^{-1} (Wood and Nassau, 1968; Aurisicchio *et al.*, 1994; Moroz *et al.*, 1999). Absorption maxima in this region were recorded at 1206, 1087, 1019, 963 cm^{-1} (aquamarine), 1163, 1060, 957 cm^{-1} (morganite), 1198, 1061, 1017 and 957 cm^{-1} (emerald). In the standard infrared absorption spectrum of beryl without any isomorphous substitution, the absorption maxima appear about 1215 and 970 cm^{-1} (Pliusnina, 1964; Sitarz *et al.*, 1997). Hence, for the coloured beryls in this study, the positions of these bands are at lower wave numbers. In detail, the band at 960 cm^{-1} is split into two maxima at 963 and 957 cm^{-1} and this can be explained by deformation of the silicate ring. The band at 1019/1017 cm^{-1} occurring in aquamarine and emerald, was not recorded for the morganite crystal.

The bands at 809-807, 747-744 and 682-680 cm^{-1} result from the Be-O stretching vibrations. In the absorption spectra of all beryl varieties there are bands at 653-649 and 593-590 cm^{-1}, characteristic of ring structures. The bands at 443-439 cm^{-1} are associated with the O-Si-O bending vibrations, whereas the bands at 525-519 and 499-493 cm^{-1} correspond to the Al-O vibrations in octahedral coordination.

The presence of the H_2O molecules of type II, i.e. those coordinated by the alkali cations (mainly Na and Li) and O-H groups, is indicated by the bands at 3596-3595 cm^{-1} (stretching vibrations) and 1637-1624 cm^{-1} (bending vibrations) (Sinkankas and Read, 1986; Wood and Nassau, 1967, 1968).

In the spectra of aquamarine and emerald there are two bands in the range 2900-2800 cm^{-1} attributed to the ν(C-H) stretching vibrations. This indicates the presence of organic matter, probably bituminous within structural channels of the beryls.

Summary and conclusions

Three beryl varieties of different colours, i.e. aquamarine, emerald and morganite have been investigated applying mineralogical and gemmological methods. Numerous internal and external defects negatively affect the

Table III: Characteristics of emeralds from the Panjshir Valley, Kapisa Province, NE Afghanistan.

Sample No.	Linear dimensions [length × width × height] (mm)	Weight (g)	SG	RI and birefringence	Characteristics of the crystal	Remarks
E1	9 × 4.5× 4	0.24	2.67	ω = 1.582 ε = 1.576 Δ = 0.006	Prismatic crystal, dark green, zoned, weak vitreous lustre, transparent to translucent (visible small cracks); high-quality gem	Selected for detailed investigations *Figure 4*
E2	10 × 3 × 2.5	0.19	2.68	ω = 1.585 ε = 1.576 Δ = 0.009	Prismatic crystal, dark green with a light yellow shade, weak vitreous lustre, transparent to translucent; small external cracks; high-quality gem	
E3	10 × 4.5 × 6	0.40	2.70	ω = 1.588 ε = 1.580 Δ = 0.008	Hexagonal prism, zonal, green with a blue shade; weak vitreous lustre, translucent, numerous liquid and 2-phase (liquid-gaseous) inclusions observed in structural channels, tiny, elongated solid inclusions (?) and brownish substance, probably composed of bituminous matter, cracks	

Table IV: Characteristics of morganites from the Ghursalak Pegmatite, Konar Province, NE Afghanistan.

Sample No.	Linear dimensions [length × width × height] (cm)	Weight (g)	(SG)	RI and birefringence	Characteristics of the crystal	Remarks
M1	2.3 × 1.8 × 2.5	20.05	2.74	ω = 1.590 ε = 1.582 Δ = 0.008	Pale pink with weak vitreous lustre, translucent, many flaws and cracks	Selected for detailed investigations
M2	2.8 × 2.9 × 3.8	25.83	2.68	ω = 1.598 ε = 1.588 Δ = 0.010	Pink, translucent, numerous internal flaws and cracks	
M3	2.8 × 2.0 × 4.5	26.88	2.76	ω = 1.602 ε = 1.594 Δ = 0.008	Deep pink, translucent, numerous internal cracks and liquid-gas inclusions	Gem of low quality

degree of transparency of these gem-quality minerals. This is especially true for the emerald in which many cracks, growth lines, gaseous and 2-phase gas-liquid inclusions, solid inclusions (for example organic compounds) have been recognized.

The chemical analyses revealed that the beryl varieties differ in their contents of Al_2O_3 and BeO. In emerald, the low Al_2O_3 combined with a high Rb_2O/K_2O ratio (0.24) suggest that it can be classified as an octahedral beryl *(o-beryl)*. The lowest BeO content occurs in the morganite (11.81 wt.%) and is typical of tetrahedral beryls *(t-beryls)*. Its low concentration indicates a probable derivation from granitic, beryl-muscovite pegmatites (Zasiedatielev, 1970; Černy, 2002).

Aquamarine was classified as a normal beryl with limited replacements in octahedral and tetrahedral sites, since its Al_2O_3 (17.87 wt.%) and BeO (12.29 wt.%) contents correspond quite well with the literature data for normal beryls, for example 17.0–19.5 wt.% Al_2O_3 and 12.3–14.0 wt.% BeO (Bakakin *et al.*, 1970; Kurazkovskaya *et al.*, 1987).

On the basis of their total alkali contents, aquamarine is classified as a low-alkali beryl, while emerald is a Li-Na beryl (Li>Na>K). The highest concentration of alkalis was reported in morganite and this is a Li-Na-K beryl.

From the relatively high contents of Li and H_2O^+ in all the beryls as well as their lower concentrations of BeO and Fe_2O_3, it can be stated that Afghan beryls crystallized within beryl-muscovite pegmatites under conditions characteristic of pneumatolytic and hydrothermal stages. Moreover, the emerald-bearing pegmatites probably intruded basic or ultrabasic rocks, as the emerald shows considerable amounts of MgO (1.37 wt.%) and CaO (0.89 wt.%). The occurrence nearby of Eocene, basic and ultrabasic rocks is consistent with this suggestion (Fijał *et al.*, 2004). Afghan emeralds probably formed at temperatures between 220 and 350°C (see Cheilletz *et al.*, 1994). Such a temperature range indicates that the emeralds crystallized at a late or final stage of pegmatite formation (Chukhrov, 1963). Li as well as Rb, Mn, V and Cu occurring as traces in the beryls accumulate in residual magmatic melts under hydrothermal conditions (Hawthorne and Černy, 1977). Considerable amounts of H_2O^+ in structural sites are also typical of beryls derived from granitic, beryl-muscovite pegmatites (Taylor *et al.*, 1992).

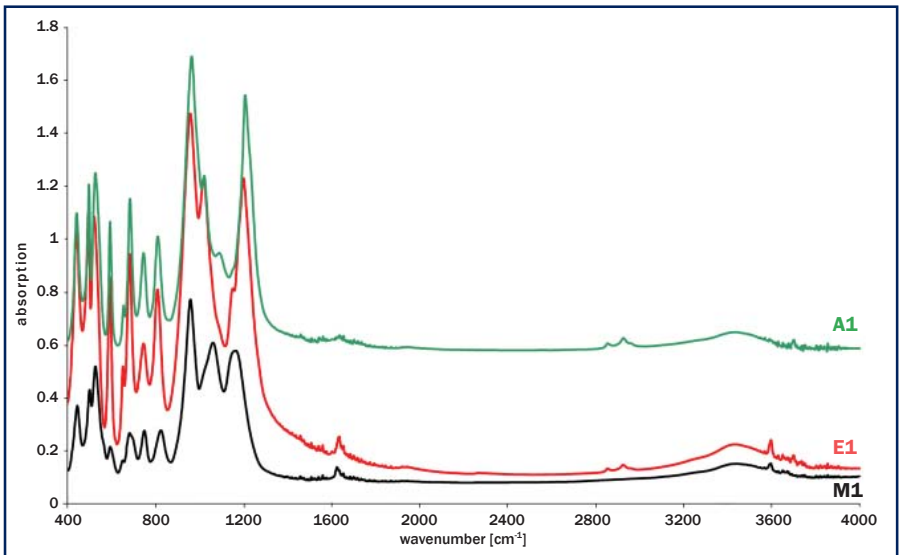

Figure 5: IR spectra of aquamarine A1, emerald E1 and morganite M1.

The chemical data are supported by the IR spectra *(Figure 5)*. Main bands in the range of 1200-950 cm^{-1} are diagnostic in distinguishing the three types of beryls according to the classification of Aurisicchio *et al.* (1994). The bands at 1206 and 963 cm^{-1}, recorded for aquamarine A1, occur at similar wave numbers as bands of standard beryl without isomorphous substitution, hence the mineral investigated belongs to the normal beryl group with limited substitution in tetrahedral and octahedral sites. In the spectrum of morganite M1 there is a band at 1060 cm^{-1} typical of tetrahedral beryls. The position of the band at 1017 cm^{-1} and the presence of an additional band at 1161 cm^{-1}, recorded for emerald E1 are characteristic of octahedral beryls. For both, morganite and emerald, the maxima at 1215 and 970 cm^{-1} were shifted towards lower wave numbers.

The unit-cell parameters, i.e. *a, c* and *c/a,* obtained in this investigation correspond well with published parameters. According to the lattice parameter classification of Andersson (2006), aquamarine has been assigned to the normal type, morganite to the tetrahedral type and emerald to the octahedral type beryls. The highest value for *a* is diagnostic for octahedral beryls, enriched in Fe^{3+}, Fe^{2+} and Mg^{2+}. Alkali-rich members of the beryl group, i.e. tetrahedral types, have the highest *c*, which is mainly caused by the presence of Li^+ in the tetrahedral sites.

Until recently Afghanistan has not been a major gem-mineral producer for the world market. However, gem-quality beryl, lapis lazuli, corundum, spodumene, garnet and tourmaline have been recorded from this country since Egyptian, Greek and Roman times. At present the production and supply of good-quality Afghan gemstones is growing, and many examples of superb material can be seen in gem markets worldwide. Gem mining plays an important role in the present-day economy of Afghanistan, and the search for new gemstone deposits continues in the mountainous regions of Afghanistan.

Acknowledgements

The author would like to thank Magdalena Dumanska-Slowik and Wieslaw Heflik for critical reading and translation of the manuscript into English. Jacek Szczerba is thanked for providing beryl samples for the investigation, Stanislaw Konopacki for

taking macrophotographs, Marta Gora and her team for chemical analyses, Adam Gawel for X-ray analyses and Stanislaw Olkiewicz for IRS investigations.

The investigation was supported by AGH University of Science and Technology, research grant no 11.11. 140.158.

References

Andersson, L.O., 2006. The positions of H^+, Li^+ and Na^+ impurities in beryl. *Physics and Chemistry of Minerals.* Springer Berlin/Heidelberg. **33**(6), 403-16

Aurisicchio, C., Fioravanti, G., Grubessi, O., and Zanazzi, P.F., 1988. Reappraisal of the crystal chemistry of beryl. *Am. Mineral.,* **73**, 826-37

Aurisicchio, C., Grubessi, O., and Zecchini, P., 1994. Infrared spectroscopy and crystalchemistry of beryl group. *Can. Mineral.,* **32,** 55-68

Bakakin, V.V., Rylov, G.M., and Bielov, N.V., 1970. X-ray diffraction data for identification of beryl isomorph. *Geokhimia,* **11,** 1302-11

Bariand, P., and Poullen, J.F., 1978. Famous mineral localities: the pegmatites of Laghman, Nuristan, Afghanistan. *The Mineral. Record,* **9**(5), 301-8

Bowersox, G.W., 1985. A status report on gemstones from Afghanistan. *Gems & Gemology,* **21**(4), 192–204

Bowersox, G.W., Snee, L.W, Foord, E., and Seal, R., 1991. Emeralds of the Panjshir Valley, Afghanistan. *Gems & Gemology,* **27**(1), 26-39

Bowersox, G.W., and Chamberlin, B.E., 1995. *Gemstones of Afghanistan.* Geoscience Press, Tucson, Arizona, 220 pp

Bowersox, G.W., Foord, E.E., Laurs, B.M., Shigley, J.E., and Smith, C.P., 2000. Ruby and sapphire from Jegdalek, Afghanistan. *Gems & Gemology,* **36**(2), 110-26

Černy, P., 1975. Alkali variations in pegmatitic beryls and their petrogenetic implications. *Neues Jahb. Mineral. Abh.,* **123,** 198-212

Černy, P., 2002. Mineralogy of beryllium in granitic pegmatites. In: E.S. Grew, *Beryllium: mineralogy, petrology and geochemistry,* Min. Soc. Of America, Washington. Rev. Mineral. and Geochem., 50, 405-44

Cheilletz, A., Feraud, G., Giuliani, G., and Rodriguez, C., 1994. Time-pressure and Temperature constraints on the formation of Colombian emeralds: An 40Ar/39Ar laser microprobe [40Ar/39Ar] and fluid inclusion study. *Econom. Geol.,* **89**, 361-80

Chmyriov, V.M., Stazhilo-Alekseev, K.F., Mirzad, S.H., Dronov, V.I., Kazikhani, A.R., Salah, A.S., and Teleshev, G.I., 1973. Mineral resources of Afghanistan. In: *Geology and Mineral Resources of Afghanistan.* Afghanistan Department of Geological Survey, Kabul, 44-85

Chukhrov, F.V., 1963. *[Minerals]* (in Russian). T. 3, part 2. Nauka, Moscow, 296 pp

Fijał, J., Heflik, W., Natkaniec-Nowak, L., and Szczepaniak, A., 2004. Emeralds from the Panjshir Valley (Afghanistan). *Z. Dt. Gemmol. Ges.,* **53**(4), 127-42

Forestier, F.H., and Piat, D.H., 1998. Emeraudes de Bactriane: mythe ou réalité, La vallée du Panjshir (Afghanistan). In: Giard, D., Giuliani, G., Cheilletz, A., Fritsch, E., and Gonthier, E. L'émeraude. Connaissances actuelles et prospectives (AFG, CNRS, ORSTOM, eds), Paris, 139-46

Fuchs, G., Matura, A., and Scherman, O., 1974. Vorbericht über geologische und lagerstättenkundliche Untersuchungen in Nurestan, Afghanistan. *Verhanglungen Geologische Bundesanstalt,* **1**, 9-23

Gaines, R.V., 1976. Beryl – a review. *The Mineral. Record,* 211-23

Gaines, R.V., Skinner, H.C.W., Foord, E.E., Mason, B., and Rosenzweig, A., 1997. *Dana's New Mineralogy. 8th edn.* John Wiley & Sons, New York, N.Y.

Ginsburg, A.I., 1955. Contribution to the question of chemical composition of beryl. *Tr. Min. Muz. AN SSSR,* **7**, 56-69

Gübelin, E.J., 1982. Gemstones of Pakistan: emerald, ruby, and spinel. *Gems & Gemology,* **18**(3), 123-9

Hänni, H.A., and Krzemnicki, M.S., 2003. Caesium-rich morganite from Afghanistan and Madagascar, *J. Gemmol.,* **28**(7), 417-29

Hausel, W.D., 2006. *Gemstones of the world. Geology, Occurrence & Exploration.* Soc. Min. Eng., 427 pp

Hawthorne, F.C., and Černy, P., 1977. The alkali-metal positions in Cs-Li beryl. *Can. Mineral.,* **15**, 414-21

Jones, B., 1991. The beryl suite of gems. *Rock & Gem.,* **21**(1), 60-3, 76-7

Kazmi, A.H., Peters, J.J., and Obodda, H.P., 1985. Gem pegmatites of the Shingus-Dusso area, Gilgit, Pakistan. *The Mineral. Record,* **16**(5), 393-411

Kazmi, A.H., and Snee, L.W., 1989. Geology of world emerald deposits: A brief review. In: Kazmi, A.H., and Snee, L.W. (Eds), *Emeralds of Pakistan; geology, gemology and genesis.* Van Nostrand Reinhold Company, New York, and Geological Survey of Pakistan, 165-228

Kurazkovskaya, W.S., Kuprianova, I.I., and Novikova, M.I., 1987. IK-spektry razlichnykh kristallokhimichieskikh tipov beryla. *Novyje Dannyje o Minieralakh,* **34**, 86-101

Moroz, I.I., Roth, M.I., and Diech, V.B., 1999. The visible absorption spectroscopy of emeralds from different deposits. *The Australian Gemmologist,* **20**, 315-20

Nassau, K., and Jackson, K., 1970. Trapiche emeralds from Chivor and Muzo, Colombia. *Am. Mineral.,* **55**, 416-27

Neilson, J.B., and Cannon, P.J., 1977. *Mineral evaluation project of Afghanistan:* vol. 2, United Nations Development Programme AF G/74/002, Toronto, Canada

Orris, G.J., and Bliss, J.D., 2002. *Mines and mineral occurrences of Afghanistan.* U.S. Geological Survey Open-File Report 02-110, Tucson, Arizona, 95 pp

Pliusnina, I., 1964. Infrared absorption spectra of beryls. *Geochemistry,* 13-21

Rossovskiy, L.N., Chmyrev, V.M., and Salakh, A.S, 1976. New fields and belts of rare-metal pegmatites in the Hindu Kush (Eastern Afghanistan). *International Geology Review,* **18**(11), 1339-42

Sabot, B., Cheilletz, A., de Donato, P., Banks, D., Levresse, G., and Barres, O.,

2001. Afghan emeralds face Colombian cousins. *Chronique de la Recherche Miniére,* **541**, 111-14

Sachanbinski M., and Sobczak T., 2001. [Oxygen isotopes as "fingerprints" of emeralds] (in Polish). *Polski Jubiler,* **2**(13), 35-6

Sachanbinski M., Weber-Weller, A., and Sobczak T., 2003. New data on emeralds from Panjshir Valley, Afghanistan. *Special Papers PTMin.,* **22**, 189-92

Schumann, W., 1997. *Gemstones of the world*. Sterling Pub. Co., New York, 272 pp

Schwarz, D., and Giuliani, G., 2002. Emeralds of the world. Panjshir Emerald Geology. *extraLapis English No 2,* 62

Seal, R R., Hammarstrom, J.M., Snee, L.W., and Kazmi, A.H., 1991. Geochemistry of the emerald deposits of Pakistan and Afghanistan. Program with Abstracts — Geological Association of Canada; Mineralogical Association of Canada; Canadian Geophysical Union; *Joint Annual Meeting*, **16**, 113

Sinkankas, J., 1981, *Emerald and other Beryls*. Van Nostrand, New York. 665 pp

Sinkankas, J., and Read, P., 1986. *Beryl*. Butterworth & Co Ltd, London. 225 pp

Sitarz, M., Mozgawa, W., and Handke, M., 1997. Vibrational spectra of complex ring silicate anions — methods of recognition. *J. Molecular Structure,* **404**, 193-7

Spiesser, M., and Fritsch, E., 1998. The discovery of chromium and beryllium in emerald by Nicolas Louis Vauquelin: 200th anniversary. In *L'émeraude*, ed. D. Giard, Paris, Association Francaise de Gemmologie, 46

Taylor, A.M, 1977. Emeralds and emeralds. *J. Gemmol.,* **15**(7), 372-6

Taylor, R.P., Fallick, A.E., and Breaks, F.W., 1992. Volatile evolution in Archean rare-element granitic pegmatites — evidence from the hydrogen isotopic composition of channel H_2O in beryl. *Can. Mineral.,* **30**, 877-93

Vapnik, YE., and Moroz, I., 2001. Fluid inclusions in Panjshir emerald (Afghanistan). In: XVI ECOROFI European Current Research on Fluid Inclusions, Porto, 2001. Abstracts (Eds Noronha, F., Doria, A., and Guedes, A.). Faculdade de Sciencias de Porto, Departamento de Geologia, *Memoria,* **7**, 451-4

Various authors, 2002. Emeralds of the world. *extraLapis English No 2*. Lapis International, East Hampton, CT, 24-35

Various authors, 2005. Beryl and its color varieties. *extraLapis English No. 7*. Lapis International, East Hampton, CT, 7

Wolfart, R., and Wittekindt, H., 1980. *Geologie von Afghanistan* (in German with summaries in English and Russian). Gebruder Borntraeger, Berlin. 500 pp

Wood, D.L., and Nassau, K., 1967. Infrared spectra of foreign molecules in beryl. *J. Chem. Phys.,* **47**(7), 2220-8

Wood, D.L., and Nassau, K., 1968. The characterization of beryl and emerald by visible and infrared absorption spectroscopy. *Am. Mineral.,* **53**(5-6), 777-800

Zasiedatielev, A.M.,1970. Osobiennosti akcesornykh berilov v razlichnykh tipakh pegmatitovykh zhil. *Mineral. Sborn.,* Lvov, **24**(2), 163-7

The Author

Lucyna Natkaniec-Nowak

AGH–University of Science and Technology, Faculty of Geology, Geophysics and Environment Protection, Department of Mineralogy, Petrography and Geochemistry; 30 Mickiewicz Av., 30-059 Cracow, Poland. e-mail: natkan@uci.agh.edu.pl

The positions of light spots on rose quartz star spheres

Harold Killingback

Abstract: An explanation is offered of the apparent difference between the positions of light spots on a star rose quartz sphere as seen in a photograph of the actual sphere, compared with a photo of a table tennis ball marked with the orientations of these spots.

Keywords: asterism, rose quartz

Introduction

Schmetzer and Krzemnicki (2006) describe various configurations of light spots which can be seen on some examples of star rose quartz spheres. These spots are mostly on the rays of light forming the asterism, but occasionally they can also be observed between the rays. The authors concluded that the cause is the reflection of light from minute plane surfaces orientated in accordance with the crystal structure of quartz. It could not be determined whether these plane surfaces were negative crystals or platelets but, for simplicity, I shall here refer to them as platelets. The important point is that the reflections are from plane surfaces, unlike the needle-like inclusions which give rise to the continuous arcs of asterism in quartz. The authors illustrated the geometrical positions of light spots and arcs by means of stereographic projections.

Figure 1: Rose quartz sphere showing two light spots on a ray of epiasterism.

Their paper encouraged me to look more closely at examples in my own collection which also show light spots, and to mark a table tennis ball with a three dimensional map based on the relevant stereographic projection.

Observations

An example of a rose quartz sphere having light spots is shown in *Figure 1*. This picture shows two of the 20 light spots which can be seen as the sphere is rotated. My preliminary measurements of the angles were sufficient to confirm that, when viewed normal to the surface of the sphere and with the light source behind one, the patches of light are in those angular positions in which the most strongly defined spots occurred in the examples described by Schmetzer and Krzemniki (2006). They are all on arcs of

asterism and comprise:-

- two at the centres of the six-ray stars, at each 'pole' (associated with the basal planes)
- 12 at 51.8° from the *c*-axis, there being six above and six below the 'equator', (associated with the rhombohedron faces)
- six at 90° from the *c*-axis, i.e. on the 'equator' (associated with the hexagonal prism)

I could not see any other light spots in my example.

I marked a table tennis ball *(Figure 2)* so as to show the rays and the light spots, as an alternative to, and based on, the stereographic projection. It was at once apparent that there was a material difference in appearance between the photo of the actual sphere and that of the model of the same object. In the photo of the real thing *(Figure 1),* two light spots are visible. One of them is related to a rhombohedral face angle and the other to a prism face. The sphere is orientated so that the spots are more or less equally spaced from the centre of the view. Measured on the photo, the distance between the spots is some 76% of the sphere's diameter.

In the picture of the model one can, in contrast, see nine light spots. The gap between the two spots corresponding to those in *(Figure 1)* is here only some 33% of the sphere's diameter.

Photographs of the Earth from space look, except for cloud cover, like the terrestrial globe in the schoolroom. So why do not my two photos look similar? I now propose an explanation of this apparent discrepancy.

Discussion

Figure 3 shows a cross section of the rose quartz sphere in the plane of one of the three circular azimuthal arcs of asterism. It is tilted so that RO, the normal to a rhombohedral face direction, and PO, the normal to a prism face direction, are equispaced about a horizontal line SO. This is the orientation of the sphere in *Figure 1*. CO is the *c*-axis. Angle COR is 51.8° and angle COP is 90°. So angle ROP is 38.2° and angle ROS is half this, i.e. 19.1°. Points C, R and P are some of those marked on the table tennis ball. The distance RP relative to the diameter of the sphere is sin 19.1, i.e. about 33%, as drawn on the model.

Throughout the sphere there are countless minute platelets, which act like two-sided mirrors. As, in this example, there are 20 spots, there must be ten orientations of platelets. Four of the orientations are perpendicular to the cross section in the illustration, as are the needle-shaped crystals which give rise to the great circle of asterism which corresponds to the circle drawn here. To avoid overcrowding the drawing, I have not included the radius vector at 51.8° from the 'south' pole, nor any details on the 'west' side. I have shown a representation of each of the other three families of platelets as short lines at right angles to CO, RO and PO, but of course there are platelets having the other orientations also.

Now consider the situation of an observer looking along SO, again with the light behind him. For simplicity, assume both source and observer are a long way from the sphere so that incident rays and reflected rays that reach the observer can be taken to be parallel to SO. Light rays along SO are normal to the surface of the sphere so will not be refracted, but they will not return to the observer from inside the sphere because none of the ten platelet face angles is normal to SO.

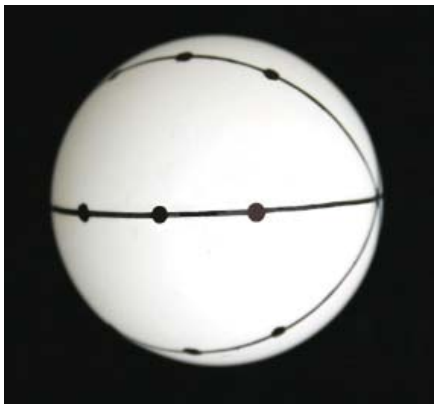

Figure 2: Table tennis ball marked with the positions of asterism and light spots.

Point P corresponds to the position of a light spot direction on the table tennis ball. A ray striking the sphere near P would meet the sphere obliquely so it would be refracted. It might meet a platelet orientated in any one of the ten directions, but none will result in light reaching the observer. As an example, one ray path showing reflection from a plate normal to PO is drawn on the diagram. By symmetry, the same is true for a ray reaching the sphere in the region of R, corresponding to another dot on the table tennis ball; it will not return to the observer either. So the appearance cannot be like that of the table tennis ball shown in *Figure 2*.

Now consider two incident rays of light which strike the sphere at Q and Q' respectively. Let the incident angle in each case be Θ. After refraction on entering

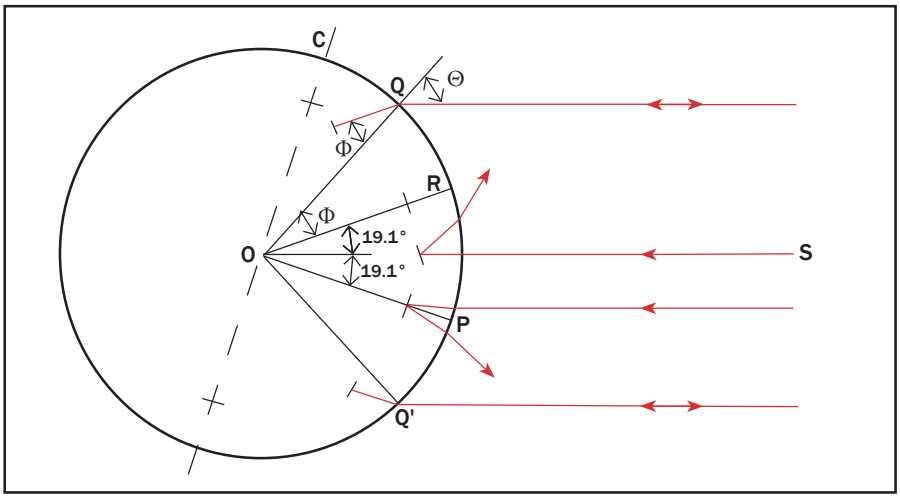

Figure 3: Ray diagram for the formation of light spots.

the sphere, the angle becomes Φ, say. Suppose I have so chosen the spacing of the rays at Q and Q' that the refracted rays are parallel to RO and PO respectively. Then there will be platelets on the paths of the rays which are at right angles to these paths. Light which meets such reflective surfaces will retrace its route and bright spots will be seen by the observer when looking at points Q and Q'. This resembles what we see when looking at the actual sphere, as shown in *Figure 1*.

We now can understand why the rose quartz sphere and the tennis ball look different, but we next need to calculate the positions of the points Q and Q'.

Because the refracted ray from Q is parallel to RO, angle QOR = Φ. Angle QOS is Θ, so

$$\Phi = \Theta - 19.1$$

and, taking a mean refractive index of 1.55,

$$\sin \Theta = 1.55 \sin \Phi.$$

From these two equations, it can be shown that Θ = 47.5°, and Φ = 28.4°.

With the derived value for Θ, the distance QQ' is 74% of the diameter of the sphere.

This is only in moderately good agreement with the value 76% observed in *Figure 1*. It should be noted, however, that although the light source, the sun, was far away, the camera was quite close.

The closeness of the camera, needed to get a good size of image, means that, for accuracy, we should take account of at least two of three factors in order to obtain better agreement. Firstly, in the photograph, the apparent diameter of the sphere will be smaller than the true diameter (by the cosine of the angle between the horizontal axis and the line from the camera tangential to the sphere). This has the effect of increasing Φ slightly. Secondly, the refracted ray will no longer be normal to the platelet, and although the amount is small the effect is doubled by reflection. Consequently, the angle of incidence at the quartz/air interface will be a few degrees greater, even if we ignore the third factor, namely that the point of exit of the ray will be a little lower on the sphere so the angle of the normal to the surface at the point of exit will have changed. If the platelet is close to the surface we may be justified in ignoring this effect. Working back from the observed spacing of 76% for QQ', I calculate that the emerging ray will be sloping down by some 3.6°. Such a ray meets the axis about 379 mm from the sphere. This is near enough where the camera was.

So we now know why we should expect to see light dots apart by about 76% of the sphere's diameter when the viewpoint is about 38 cm from the sphere.

Conclusions

The apparent discrepancy between the views in *Figures 1* and *2* is explained by noting that they are showing different things:

- In *Figure 1*, the photo shows reflection from those platelets which, although not being observed along a radius vector, are in positions which allow the reflected and twice refracted ray to reach an observer who has the light behind him.
- In *Figure 2*, the marked-up table tennis ball is a map of all the various positions of radius vectors along which an observer could see a light spot if the source of illumination were behind him and shining along the vector.

I was led into expecting the table tennis ball to look like the actual sphere, in the way that a schoolroom globe looks like the earth, by mistakenly thinking of light spots as things, in the way that physical features are things, whether they are distinctive inclusions in the quartz or features on the surface of the earth. Light spots, however, are effects, not things. You cannot take a piece home with you any more than you can capture a rainbow.

Coda

Is the marked-up table tennis ball useful? I believe it does give an accurate and helpful indication of the pattern of asterism and light spots, provided its message is properly understood. So, bearing in mind the difference between the representations in *Figures 1* and *2*, it is helpful to view the table tennis ball through a hole in a piece of card or plastic in contact with the ball, such a hole limiting the outlined area of the ball by being about 17 mm in diameter. In this way the viewer is not confused by parts of the pattern which would not be seen from the viewpoint in question. The ball can, of course, be rotated behind the card to display other aspects of the pattern. In *Figure 4,* the distance between the two light spots is the same in relation to the diameter of the hole as it is in *Figure 1* to the diameter of the sphere, so the impression given is reasonably accurate.

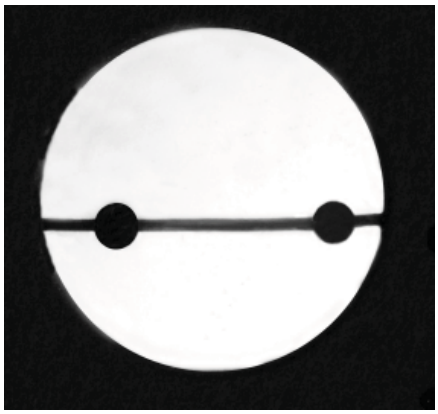

Figure 4: Table tennis ball with mask.

Acknowledgement

I am grateful to Dr Karl Schmetzer for the inspiration provided by his paper and for his helpful comments during the preparation of this note.

Reference

Schmetzer, K., and Krzemnicki, M., 2006. The orientation and symmetry of light spots and asterism in rose quartz spheres from Madagascar. *Journal of Gemmology,* **30**(3/4), 183-91

The Author

Harold Killingback FGA

Brooke, Oakham, Rutland

email: haroldkillingback@btinternet.com

Identification of taaffeite and musgravite using a non-destructive single-crystal X-ray diffraction technique with an EDXRF instrument

Ahmadjan Abduriyim, Taisuke Kobayashi and Chihiro Fukuda

Abstract: The rare gems taaffeite and musgravite have lately become more popular among collectors. Due to their similar chemical compositions and crystal structures, their main gemmological properties overlap and so sophisticated measurement techniques such as quantitative chemical analysis, Raman spectroscopy or X-ray powder or single crystal diffraction are needed for their identification. This study describes an EDXRF instrument used as single-crystal X-ray diffraction apparatus and the technique to identify taaffeite and musgravite in a relatively conclusive procedure. A special rotating and tilting stage has been constructed to non-destructively determine the differences in diffraction pattern based on the different symmetries (trigonal and hexagonal), unit cell dimensions and space groups of taaffeite and musgravite.

Keywords: EDXRF, musgravite, non-destructive gem test, rotating and tilting stage, single crystal XRD, taaffeite, Wulff net

Introduction

Taaffeite and musgravite from Sri Lanka, Myanmar and Tanzania are rare gemstones that are popular among collectors *(Figure 1)*. Gem-quality taaffeite and musgravite are both transparent, commonly with red, purple, blue, violet, grey or very dark colours. Taaffeite ($BeMg_3Al_8O_{16}$) shows a wider range of colours (which are due to high amounts of chromium and iron) than musgravite ($BeMg_2Al_6O_{12}$) which has only been found as purplish grey, greenish grey, greyish blue, and dark stones to date. These two mineral species, belonging to the same mineral group taaffeite, have very similar chemical compositions and crystal structures and their gemmological properties are so similar that they cannot be distinguished using standard gemmological identification tests. Several

Figure 1: Purple taaffeite (2.25 ct) and greyish-green musgravite (0.86 ct) from Sri Lanka are mounted in a pendant and ring respectively. These gems are popular among rare stone collectors. Courtesy of Midori Jewellery, Tokyo; Photo by Masaaki Kobayashi.

Identification of taaffeite and musgravite

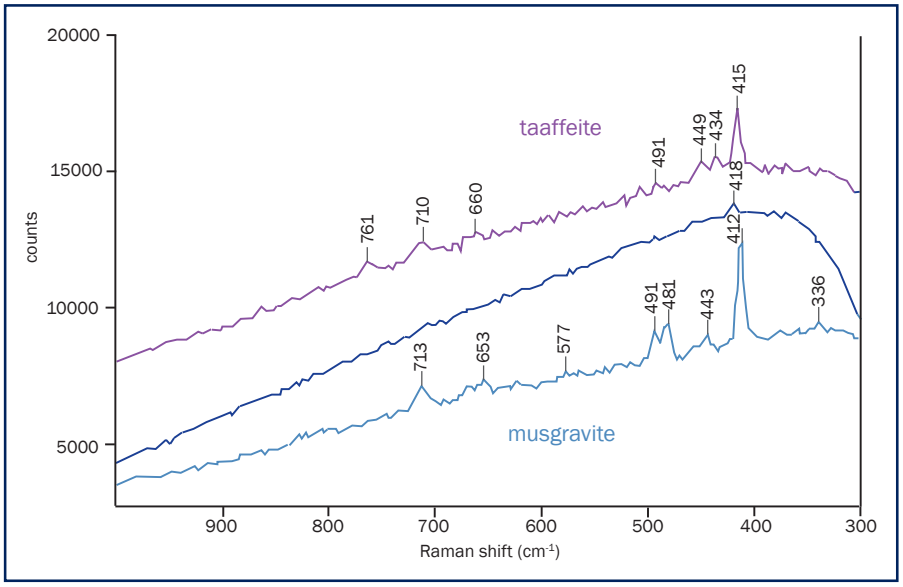

Figure 2: The Raman spectra of taaffeite and musgravite from Sri Lanka, obtained using 514 nm laser excitation. There is a strong Raman peak for taaffeite at 415 cm^{-1}, moderate peaks at 434 and 449 cm^{-1} and several weak peaks in the region of 600-800 cm^{-1} (660, 710 and 761 cm^{-1}). In the musgravite sample, the 412 cm^{-1} peak is the strongest, and several moderate and weak peaks were detected at 336, 443, 481, 491, 653 and 713 cm^{-1}. However, if a sample has an extremely high continuous background fluorescence (central spectrum) it may show only a very weak peak at 418 cm^{-1}, and peaks in the region 440-800 cm^{-1} may be indistinct and of little help in identification.

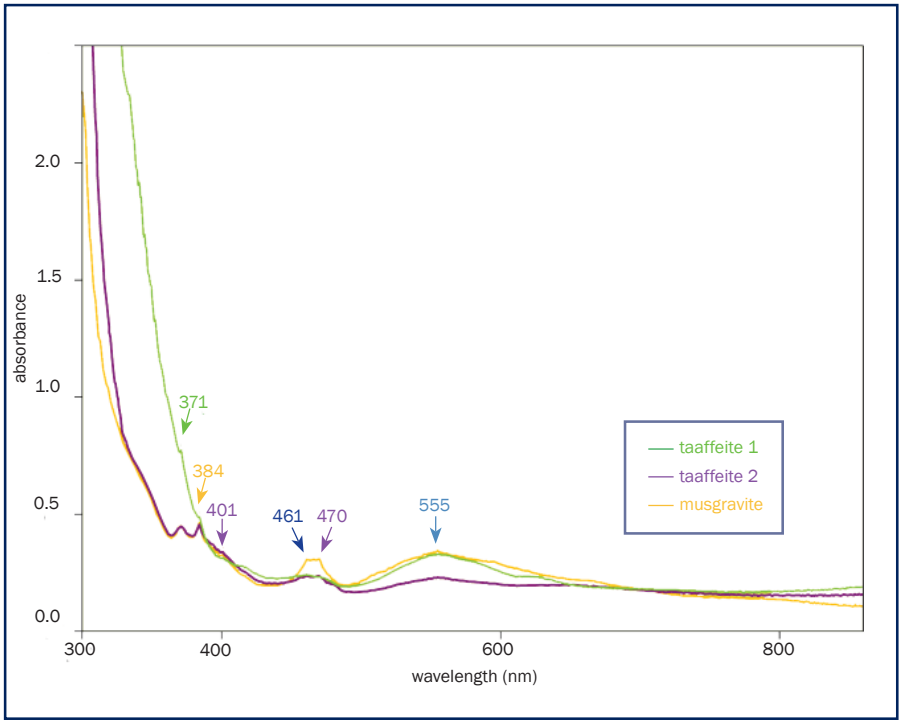

Figure 3: The UV-Vis-NIR spectral features of taaffeite are similar to those of musgravite. A broad absorption band centred at 555 nm and five other absorption peaks at 371, 384, 401, 461 and 470 nm are present. The intensity of the peak at 371 nm may be somewhat weaker in taaffeite than in musgravite, but in a few taaffeites this peak is strong, so it is not a reliable distinguishing feature.

techniques with high resolution and accuracy such as X-ray single crystal and powder diffraction, chemical quantitative analysis by electron probe microanalysis (EPMA) and Raman spectroscopy are effective in distinguishing these two minerals (Schmetzer *et al.*, 2000, 2005a,b, 2006, 2007; Kiefert and Schmetzer, 1998). In petrology and mineralogy the X-ray diffraction method is used as the most effective means to identify minerals. However, this involves taking small powder samples for testing which means losing some of the gem. Non-destructive Raman spectroscopy can be highly effective in distinguishing the two minerals, but some stones generate such a high continuous fluorescence background *(Figure 2)* that a useful Raman spectrum may not be detected. In the UV-visible absorption spectrum, absorption peaks at 371, 384, 401, 461, 470 and 555 nm are present in both minerals, and any differences are not consistent enough to be reliable distinguishing features *(Figure 3)*. Semi-quantitative analysis using an energy-dispersive X-ray fluorescence (EDXRF) spectrometer can yield the elemental ratios, and if one sums the trivalent elements (Al_2O_3+V_2O_3+Cr_2O_3+Ga_2O_3) and divalent elements (MgO+CaO+MnO+FeO+ZnO) *(Figure 4)* (Okano *et al.*, 2006), and assumes that the sum of molecular proportions (XO+X_2O_3=100%), the totals for a stone should either fall near 42.86% XO for taaffeite or 40% for musgravite. However, semi-quantitative EDXRF analysis resolution is not always of sufficiently high level to detect the light elements. A Si-semiconductor detector (SSD) should provide relative standard deviations (RSD) of light elements, especially Mg of less than 1.0 wt% and if it does not, further sophisticated measurements are required to obtain satisfactory data.

Consequently, in this study we tested the possibility of distinction between taaffeite and musgravite by analysing the distribution of their X-ray diffraction patterns obtained using an EDXRF analysis instrument. Many gemmological laboratories have such an instrument and

to adapt this for diffraction work would avoid having to obtain an X-ray generator and Laue back reflection camera.

The main use of an EDXRF instrument is to obtain compositions from X-ray fluorescence analysis, but when analyzing a single crystal, diffracted X-rays that meet the diffraction conditions for particular lattice planes and interplanar spacings are also produced and can be diagnostic for particular species. Therefore, to use this property and develop an easy method to separate taaffeite from musgravite relatively quickly, we have installed a special sample stage on the EDXRF instrument that can be used to rotate a sample through 360° under an incident X-ray beam and also tilt it ± 20 degrees. This enables one to obtain a suitable crystal orientation for diffraction by adjusting the stage holding the gem sample. (See also the report at the annual meeting of the Gemmological Society of Japan 2007 by Abduriyim *et al.* (2007a,b,c).)

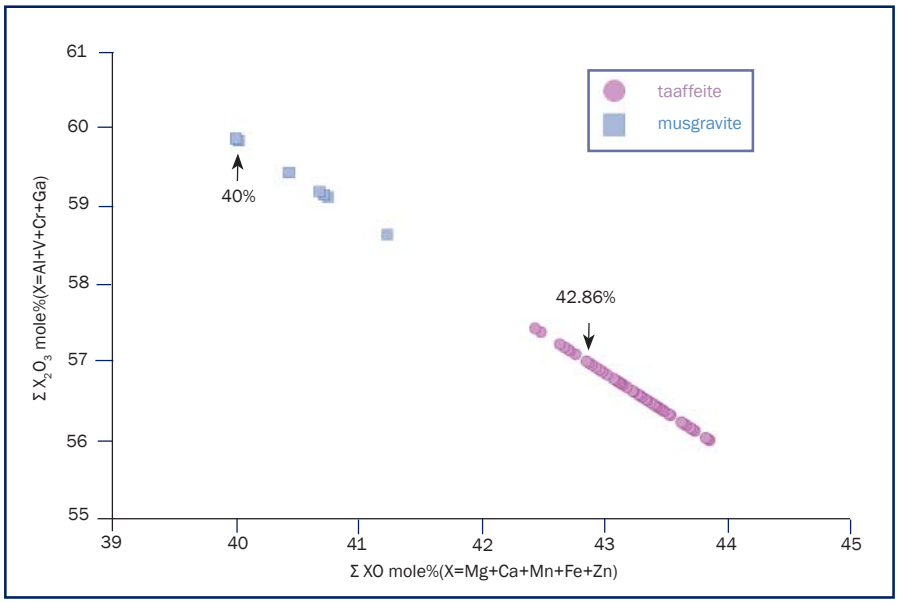

Figure 4: Comparison of the total molecular ratios of trivalent oxides X_2O_3 (Al_2O_3+V_2O_3+Cr_2O_3+Ga_2O_3) and divalent oxides XO (MgO+CaO+MnO+FeO+ZnO) in taaffeite and musgravite obtained using EDXRF analysis. The theoretical value of XO for taaffeite is 42.86% and for musgravite it is 40%. There is a clear separation of taaffeite and musgravite values with taaffeite showing the higher divalent values, and musgravite the higher totals of trivalent oxides.

Understanding the non-destructive single-crystal X-ray diffraction technique using an EDXRF instrument

Principle

This application of X-ray diffraction using an EDXRF instrument is based on the principle of Laue back-reflection. In the conventional Laue method which uses film, a 'symmetrical' image made by a group of X-rays diffracted by a crystal will be projected on the X-ray film when continuous X-rays enter the crystal which is in a fixed orientation. At this time, the lattice constants (unit cell parameters) and Miller indices of crystal lattice planes that correspond to each spot projected on the film cannot be estimated by collating information only from symmetry of the sample. In our method, this limitation or functional restriction of the Laue method can be dealt with by examining the energy dispersive X-ray spectrum of the sample. If orientation of a known sample crystal with known unit cell dimensions and space group can be precisely set, a relation between the crystal lattice planes and emitted X-rays that result from optimum diffraction conditions can be estimated by calculation.

In an EDXRF spectrum of a crystalline sample, diffracted X-rays originating from lattice planes of the crystal will be detected as well as characteristic X-rays resulting from its chemical constituents. The energy distribution of the diffracted X-ray peaks is not constant because they vary according to the orientation of the crystal. To determine whether any peaks in an X-ray fluorescence spectrum can be attributed to diffraction, several spectra obtained from random settings of the crystal should be compared. After removing the peaks that have common energy values and relative intensity ratios in the spectra, i.e. the peaks of the characteristic X-rays, any remaining peaks with different energy values and intensities are a result of diffraction by the crystal structure. Although both taaffeite and musgravite are optically uniaxial and have hexagonal lattices, they have different unit cell dimensions and different symmetries (hexagonal and trigonal) resulting from different space groups and crystal structures. In this study, we exploit the differences in spectra of diffracted X-rays from the crystal lattice planes, which result from the two minerals even though they are in the same crystallographic orientation, in order to distinguish between them. The quickest and most effective method is to compare the diffraction peaks of the {h0$\bar{h}$l} {0k$\bar{k}$l} lattice planes (see 'Analysis process' below and *Figure 9a,b*).

Firstly, assuming that the orientation of the stone is with its *c*-axis parallel to the X-ray beam and that the incident X-rays can be directed parallel to the *c*-axis, the position of diffraction peaks in the energy dispersive spectrum can be calculated. In the crystal systems of taaffeite and musgravite, the lattice constants and space groups are as follows:

Taaffeite:

a=5.684Å c=18.332Å space group: $P6_3mc$

Musgravite:

a=5.675 Å c=41.096 Å space group: $R\bar{3}m$

The spacing of lattice planes in hexagonal lattices can be calculated by the following formula using the Miller index (hkil) and appropriate lattice constants a and c:

Materials and methods

Figure 5: Nine taaffeites and three musgravites from Sri Lanka display a range of colours, with red, purple, violet, grey and black taaffeite on the left side (top, 0.20–0.64 ct, bottom, 0.74-2.83 ct), and purple, grey and black musgravite (a smaller colour range) on the right (0.34–4.50 ct). Courtesy of Magical Stone Lab; Photos by Masaaki Kobayashi.

To identify taaffeite and musgravite and to understand the new non-destructive X-ray diffraction analysis technique, a total of 85 faceted gems have been examined in this study. They were supplied by a merchant from the Magical Stone Lab, Tokyo, Japan, who informed us that these stones were purchased in Sri Lanka, but that their source(s) were unknown. The range of weights of the stones is 0.20 to 4.50 ct; the colour of the taaffeites ranges from red, dark red, purplish red, purple, intense or dark purplish violet, and dark greyish violet to dark grey, and in musgravite the colours are purple grey, greyish violet, bluish grey, greyish green, brownish grey and black (see *Figure 5*). The refractive indices of all samples were checked and then they were examined to obtain their compositions using EDXRF, their Raman spectra and finally their structure using destructive X-ray powder diffraction techniques. Only 11 of the 85 stones were musgravite.

To obtain diffracted X-rays that meet the diffraction conditions of certain lattice planes of taaffeite and musgravite, a new goniometric sample stage was developed and fitted to a JEOL EDXRF spectrometer JSX-3600 (see *Figure 6*). From the stones investigated, one representative sample of taaffeite (T-001) and one musgravite (M-10) were selected to explain how this new non-destructive single-crystal X-ray diffraction technique is used. For X-ray diffraction analysis, polychromatic white X-rays of molybdenum (Mo) wavelength 0.07 nm were used; the beam passed through a 100 μm φ collimator, 30 kV voltage was applied for acceleration, and 200–300 second periods were set for data collection. All X-ray fluorescence lines and numbers of Laue back-reflection peaks were detected in air and under vacuum at ~ 0.01 Pascal.

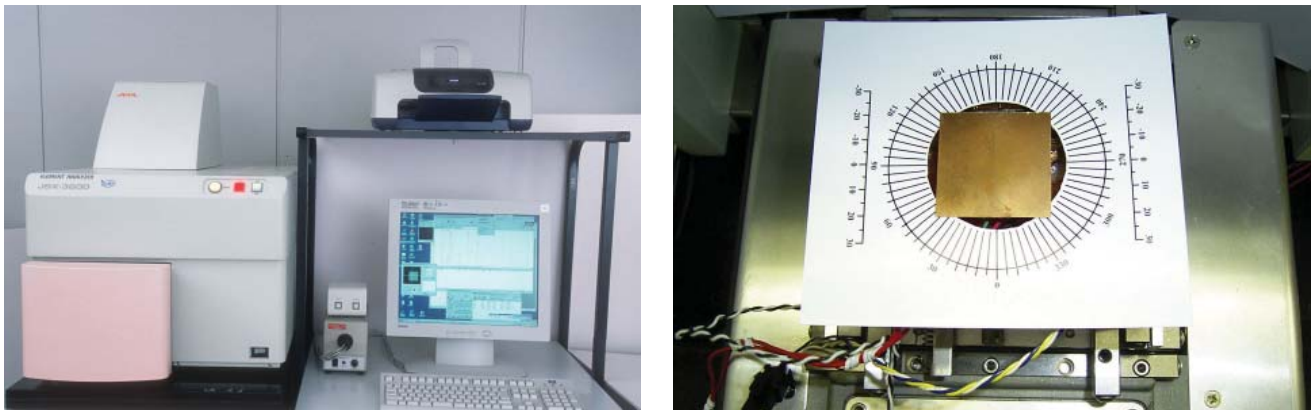

Figure 6: A JEOL energy dispersive X-ray fluorescence (EDXRF) spectrometer JSX-3600 used in this study is shown on the left. On the right is a close-up view of the newly developed goniometric sample stage for attachment to an EDXRF JSX-3600. A rotating stage with rotation angle (ω) is mounted on the X-Y scanning stage, and a tilting stage with tilting angle (τ) is placed on the rotation stage. The tilting stage can be inclined ± 20°. Each stage is labelled with a graduated scale underneath and is powered by a stepping motor. Photo by Masaaki Kobayashi (left) and A. Abduriyim (right).

Identification of taaffeite and musgravite

$$\frac{1}{d_{hkil}^2} = \left(\frac{4}{3} \times \frac{h^2+hk+k^2}{a^2}\right) + \frac{l^2}{c^2} \quad (1)$$

where d is the distance in Å between adjacent (hkil) planes. The wavelength of the X-rays that meet the diffraction conditions can be found by Bragg's law:

$$n\lambda = 2d_{hkil} \sin\theta \quad (2)$$

where λ is the wavelength of the X-rays, and θ is the Bragg angle. From the angular relationship between the incident X-rays and the fixed detector in the EDXRF instrument (45°, see *Figure 7*), the possibilities of obtaining diffracted X-rays are limited to a Bragg angle of:

$$\theta \approx (180°-45°)/2=67.5° \quad (3)$$

The energy values of diffracted X-ray peaks that are expected to be seen in an EDXRF spectrum can be directly obtained from the X-ray wavelength. The values of energy and wavelength are in inverse proportion and can be estimated roughly from the following formula:

$$E(eV) \approx 12.4/\lambda\ (Å) \quad (4)$$

The energy range of X-rays used in data verification in this study was set under 16 keV. This is because the characteristic X-rays of Mo that are used as the anticathode for X-ray generation lie in the range over 16 keV in our EDXRF instrument. The diffracted X-ray peaks produced in this energy range overlap the characteristic X-ray spectrum of Mo and make their verification more difficult.

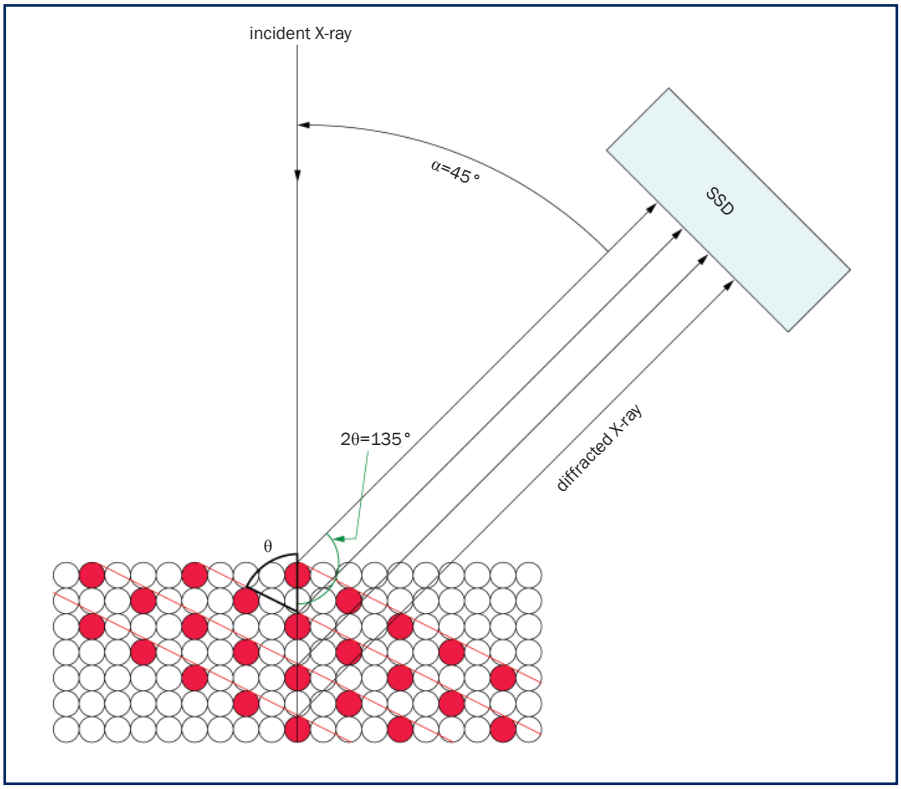

*Figure 7: The schematic diagram shows the angular relationship of the incident X-rays and the detector in our instrument, and the X-ray diffraction effect. Atomic planes of a crystal cause an incident beam of X-rays (if its wavelength is approximately the magnitude of the interatomic distance) to interfere with one another as they leave the crystal. At certain angles the X-rays diffracted from a set of planes are in phase, complementing each other and producing peaks of intensity on film or recorder. Diffraction occurs when Bragg's law is satisfied; this is calculated as $2d \sin\theta = n\lambda$, where **d** is the distance between the planes in the atomic lattice, **θ** is the angle between the incident X-ray beam and the atom planes, **λ** is the wavelength of the X-rays, and **n** is an integer. The atom positions coloured red lie in planes which generate the diffracted X-rays. The angle 2θ is the angle between the primary (transmitted) X-ray beam and the diffracted beam; the angle α is the angle between the incident X-ray beam and the fixed detector, and is 180°-2θ.*

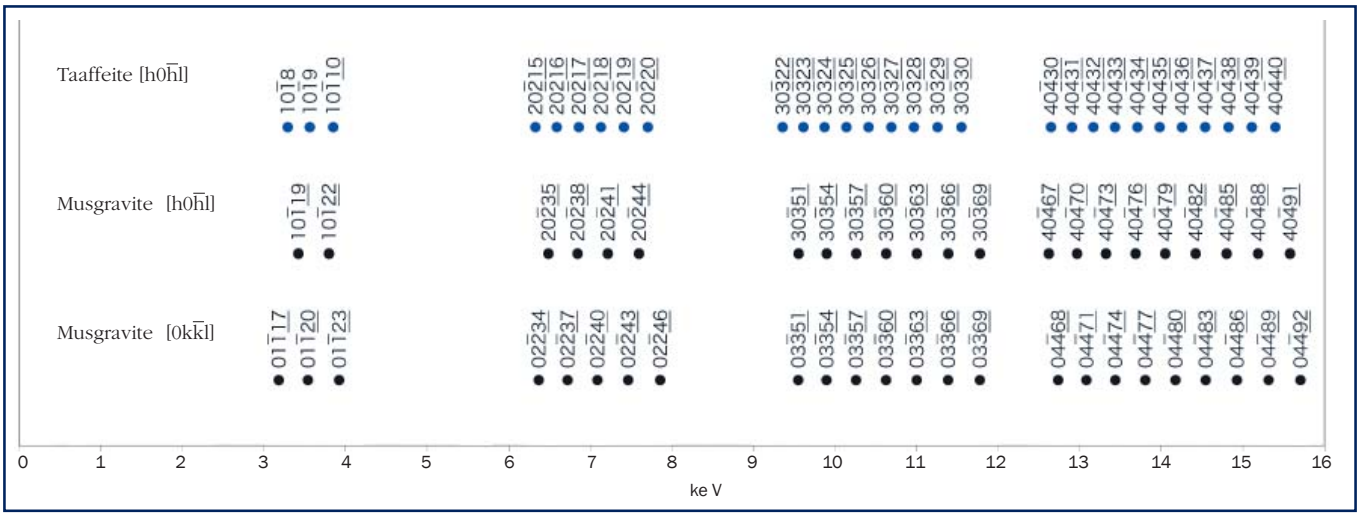

Figure 8: The energy values of peaks attributable to diffracted rather than fluorescent X-rays in an EDXRF spectrum when continuous X-rays are directed parallel to the c-axis of taaffeite and musgravite. The calculations from formulae (1) to (4) indicated that in both crystals, their diffraction spectra almost overlap in the energy ranges 3~4, 6.5~8, 9.5~11 and 12~14 keV. The peaks {h0h̄ l} and {0kk̄l} for musgravite are different, but for taaffeite they are the same. Estimation of the Miller index of a diffraction peak is only possible when orientation of the crystal is accurately set on the sample stage of the instrument.

Identification of taaffeite and musgravite

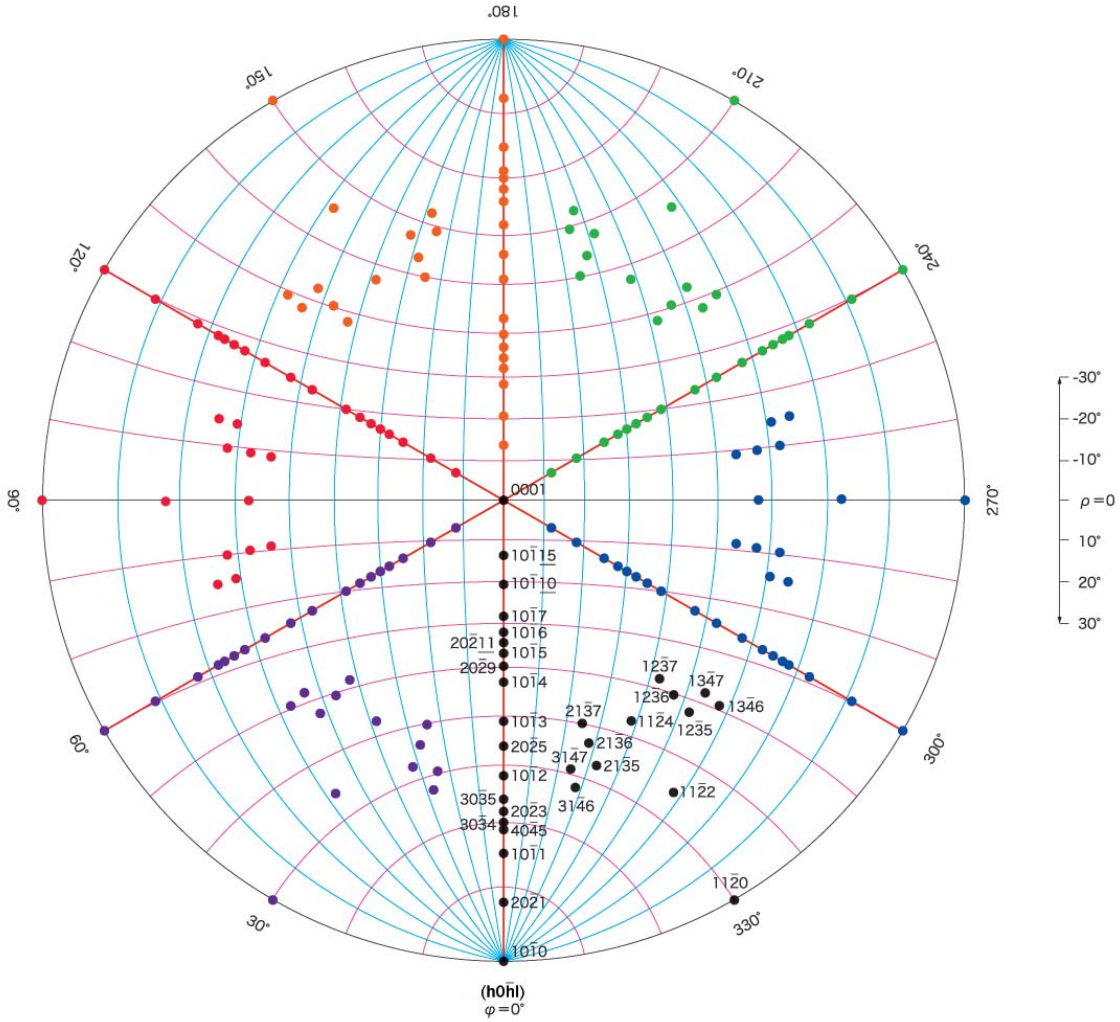

Figure 9a: The (0001) lattice plane standard pole of hexagonal taaffeite is indicated on a Wulff stereographic projection net. The Miller indices of taaffeite are labelled in black when the stage is set at ω=0°; on rotation each 60°, the Miller indices are labelled in the sequence violet, red, orange, green and blue.

The calculations from (1) to (4) above have shown that the energy ranges of both taaffeite and musgravite in which diffraction spectra will appear almost overlap in the regions 3~4, 6.5~8, 9.5~11 and 12~14 keV *(Figure 8)*. This is because both minerals have very similar values of the lattice constant a. In addition, their values of c are relatively large (although quite different) compared to common minerals. Therefore, the diffraction spectrum distribution of each mineral will be seen as a group of small peaks in a limited energy range, and this causes trouble in estimating a Miller index of the diffraction peaks. It is important to ensure that a crystal or stone is orientated precisely on the sample stage, or estimation of the Miller index of the diffraction peaks will be impossible.

The space group of taaffeite allows diffracted X-rays to be generated from lattice planes {h0$\bar{h}$l} and {0k$\bar{k}$l} under any conditions because the extinction rule does not apply. In contrast, the extinction rule does apply to musgravite and diffracted X-rays can be generated only when conditions –h+1=3n or k+1=3n are satisfied in lattice planes {h0$\bar{k}$l} and {0k$\bar{h}$l}. As a result, crystal lattice planes that have the spacing between {h0$\bar{h}$l} and {0k$\bar{k}$l} suitable for diffraction appear every 60° during rotation round the *c*-axis in taaffeite, while they only appear every 120° in musgravite. In other words, the {h0$\bar{h}$l} and {0k$\bar{k}$l} patterns are identical for taaffeite but different for musgravite. This is the most important feature to distinguish these two minerals.

Since the position of an incident X-ray beam, a sample face and an X-ray detector is almost fixed in a basic commercial EDXRF, it is most unlikely that a crystal at the X-ray irradiation spot will be in optimum orientation for diffraction. To prepare for this study, one author (A.A.) consulted a former study (Shimobayashi and Kitamura, 1998, 1999a,b and 2002), and improved our EDXRF JSX-3600 instrument by fitting a special stage to enable precise orientation of a crystal and obtain Miller indices. This special sample stage is placed on the X-Y movement stage on which a sample can be rotated through 360° about an axis parallel to the incident X-ray beam (ω-stage), and allows an inclination of up to 20°

Identification of taaffeite and musgravite

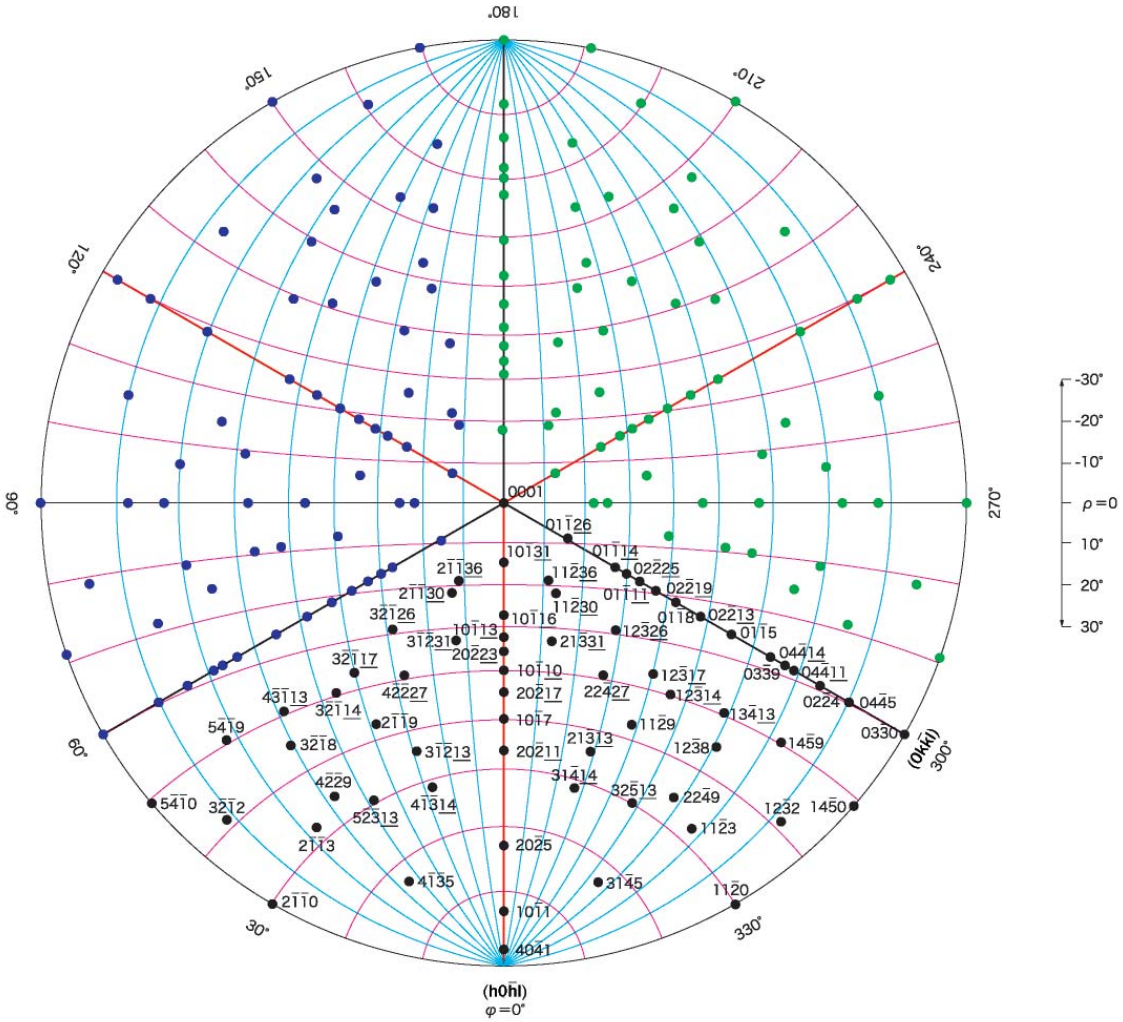

Figure 9b: The (0001) lattice plane standard pole of trigonal musgravite is indicated on a Wulff stereographic projection net. The Miller indices of musgravite are labelled black at 0° and on rotation, blue at 120° and green at 240°. φ is the rotation angle on the Wulff net; ρ is the tilting angle to the X-axis of the scanning stage.

(τ-stage). Each of these two sophisticated stages is powered by a motor, and the measurement and operation are done by a controller (see again *Figure 6b*).

Analysis process

1. The taaffeite or musgravite under investigation should be set with its optic axis, or *c*-axis, perpendicular to the sample stage of the EDXRF instrument, so that continuous X-rays can travel along the *c*-axis direction. The optic axis can be found by rotation of the stone between crossed polarizing filters with a converging lens until an interference figure of concentric rings with a black cross isogyre is found.
2. A convenient way to find the crystal orientation of taaffeite and musgravite is to plot the Miller indices of lattice planes in each crystal on a Wulff stereographic projection net *(Figure 9a,b)*. The sample rotation stage (ω-stage) is placed to correspond to the φ-axis of the Wulff net, and the tilting stage (τ-stage) is set to the ρ-axis. (φ is the rotation angle on a large circle; ρ is the interfacial angle (h0$\bar{h}$l) ∧(0001)). Miller indices of taaffeite are recorded in black at ω=0° on the stage, in pink at 60°, red at 120°, yellow at 180°, green at 240° and blue at 300°. For the Miller indices of musgravite, each is set up at 120° intervals and marked with black, blue or green. Then, measurements are taken with a constant setting ρ=0° on the Wulff net and a variable φ (this means that the sample is rotated without being tilted). Throughout this spectrum measurement, confirm that the diffraction spectra are within the energy range that has been calculated (see above). Set the angle at which that spectrum appears at 0 degree, and measure the spectra after every 60° rotation of the sample stage, then the spectra can be observed as a group of diffraction peaks in the same energy range. These are the diffracted X-ray spectra of the crystal lattice planes with Miller indices {h0$\bar{h}$l} and {0k$\bar{k}$l}.

Results

The oval mixed-cut violet sample T-001 and greyish violet M-10 were each

Identification of taaffeite and musgravite

Figure 10: The taaffeite T-001 of 1.72 ct on the left, and musgravite M-10 of 0.65 ct on the right, were analysed by EDXRF JSX-3600 for this study. Photos by Masaaki Kobayashi.

set on the goniometric sample stage without any coating preparation *(Figure 10)*. The optic axis of each stone was identified and set parallel to the direction of the incident X-ray beam. The surface of each stone was placed at the standard working distance (WD) of 1 mm from the bottom of X-ray beam window. The sample stage is then rotated from ω=0° to 360° gradually without any tilting (τ= 0°), and the diffracted X-ray spectra of the crystal lattice plane obtained as shown below.

In each diffraction spectrum of taaffeite at the successive setting angles of ω=0°, 60°, 120°, 180°, 240° and 300°, each pattern of diffraction peaks (h0$\bar{h}$l) and (0k$\bar{k}$l) occurs at an almost identical energy position *(Figure 11)*. This indicates that taaffeite possesses six-fold (hexagonal) symmetry about its *c*-axis.

On the other hand, the peak positions in the diffraction spectra of musgravite showed a slight difference between the first group of ω=0°,120° and 240° reflections and the second group of ω=60°, 180° and 300° *(Figure 12a,b)*. The results for the group ω=0°,120° and 240°, and for the group ω=60°, 180° and 300°, are detailed in the caption for *Figure 12*. These indicate that musgravite possesses three-fold (trigonal) symmetry about its *c*-axis.

From the above, it is clear that peak energy positions in the diffraction spectra of taaffeite and musgravite differ, and so, therefore, do the Miller indices of the lattice planes that cause these differences. All the Miller indices detected in this orientation lie between 20.4° and 26.4° away from the optic axis of the crystal (that is, lattice plane {0001}) (see *Figure 13a,b*).

For further verification, additional diffraction spectra of {h0$\bar{h}$l} and {0k$\bar{k}$l} were obtained from X-rays entering along a direction other than parallel to the *c*-axis, in the following way. The sample stage was tilted while the rotating stage was set at the angle at which spectra appeared in the first measurement (ω=0° and 60°). Then, X-rays entered under conditions of different tilt angles τ and spectra were measured. In other words, φ on the Wulff net was kept constant while ρ was varied, and this was continued until diffraction peaks appeared on a spectrum. When the τ-stage was tilted at about +9° several different diffraction peaks were detected in taaffeite and musgravite respectively *(Figures 14* and *15)*. When the τ-stage was tilted in the opposite way, at -9°, again different diffraction peaks were detected in taaffeite and musgravite *(Figures 16* and *17)*.

The energy positions of a series of these diffraction peaks were obtained and showed no overlap, and so the derived Miller indices were proved to indicate different lattice planes in the two minerals.

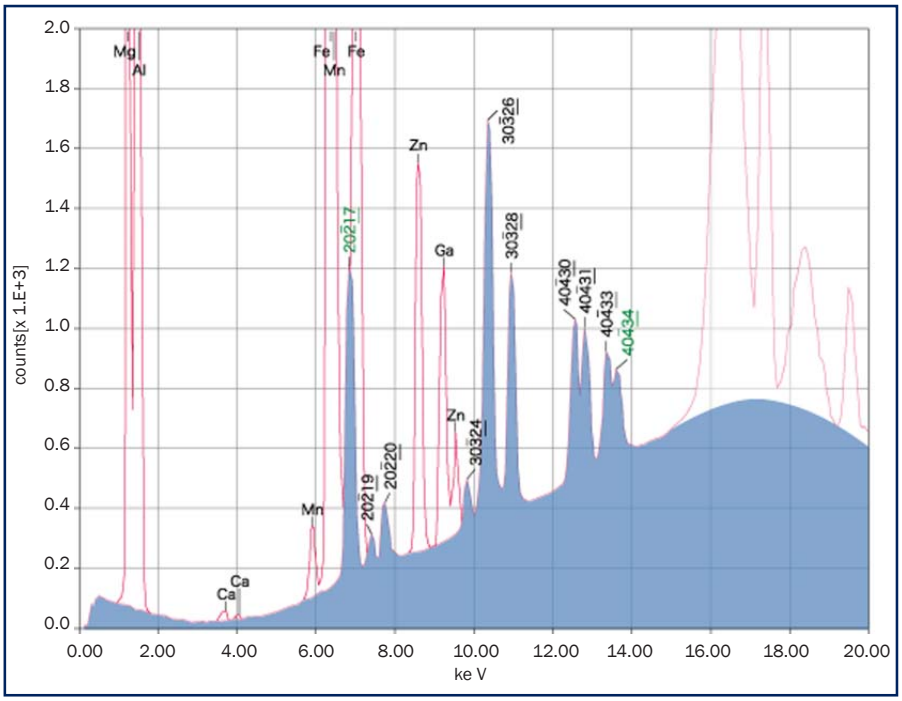

Figure 11: An energy dispersive X-ray spectrum with fluorescence peaks and diffraction peaks from lattice planes in taaffeite T-001. The diffracted X-ray peaks indicate Miller indices of (20$\bar{2}$17), (20$\bar{2}$19), (20$\bar{2}$20), (30$\bar{3}$24), (30$\bar{3}$26), (30$\bar{3}$28), (40$\bar{4}$30), (40$\bar{4}$31), (40$\bar{4}$33) and (40$\bar{4}$34) and were obtained at stage settings of ω= 0° and φ=0°. (20$\bar{2}$17) and (40$\bar{4}$34) is a doublet diffraction peak of (20$\bar{2}$17) which is indicated green.

Therefore, distinction between taaffeite and musgravite was successful using this method.

Summary

The chemical compositions of taaffeite and musgravite are very similar, and the differences in quantitative values of Be and Mg between the two are slight. Sophisticated analysis such as EPMA is required for accurate determinations. EDXRF analysis may help to separate these two minerals but the method is not sufficiently accurate for light elements, especially magnesium.

Taaffeite and musgravite also appear to have similar crystal structures but their lattice constants and space groups are different. Raman spectroscopy can be used to distinguish taaffeite from musgravite in gemmological laboratory testing, but some stones may be too fluorescent to provide useful Raman spectra. In such cases, one could resort to destructive, X-ray powder diffraction (using a few micrograms of sample from the gemstone's girdle). In this study, we have focused on this difficulty and have attempted to solve it in a non-destructive way by using a single crystal X-ray diffraction method. This exploits the differences in the crystal lattice planes between taaffeite and musgravite. While irradiating a sample with a continuous X-ray beam in a standard EDXRF instrument, both fluorescent X-rays and diffracted X-rays can be produced but since the X-ray detector is fixed in this instrument, accurate detection of diffracted X-rays from a certain lattice plane is very restricted. Therefore, our research group devised a special rotating and tilting stage to increase the detection capability and enable measurement of a range of crystal lattice planes. In this procedure, to run an effective analysis method, several processes should be confirmed during the operation. Firstly, take 2 or 3 spectra to place the *c*-axis exactly parallel to the X-ray beam. In this step, we have to rotate the sample every 2 or 3 degrees gradually within 30 degree ranges to get diffracted X-ray peaks during the analysis. Then measure the same diffraction spectra in

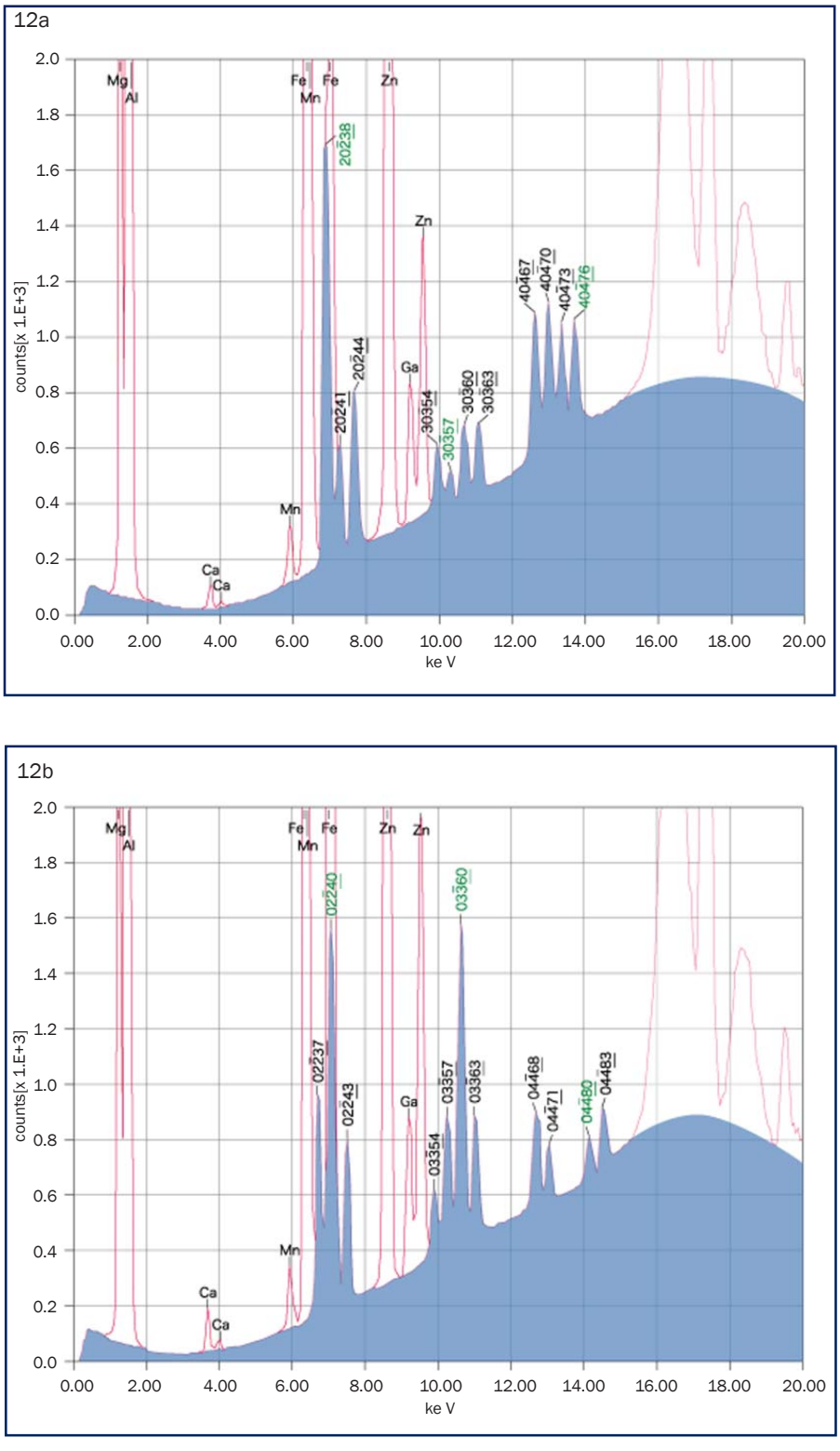

Figure 12: An energy dispersive X-ray spectrum with fluorescence peaks and diffraction peaks from lattice planes in musgravite M-10. (a) Diffraction peaks from lattice planes indicate Miller indices (20$\bar{2}$38), (20$\bar{2}$41), (20$\bar{2}$44), (30$\bar{3}$54), (30$\bar{3}$57), (30$\bar{3}$60), (30$\bar{3}$63), (40$\bar{4}$67), (40$\bar{4}$70), (40$\bar{4}$73) and (40$\bar{4}$76) with stage settings of ω= 0°, τ=0°. The peaks (20$\bar{2}$38), (30$\bar{3}$57) and (40$\bar{4}$76) comprise the triplet diffraction peak of (10$\bar{1}$19), and are marked in green. (b) (02$\bar{2}$37), (02$\bar{2}$40), (02$\bar{2}$43), (03$\bar{3}$54), (03$\bar{3}$57), (03$\bar{3}$60), (03$\bar{3}$63), (04$\bar{4}$68), (04$\bar{4}$71), (04$\bar{4}$80) and (40$\bar{4}$83) Miller indices are detected at stage settings of ω= 60°, τ=0°. The peaks (02$\bar{2}$40), (03$\bar{3}$60) and (04$\bar{4}$80) comprise the triplet diffraction peak of (01$\bar{1}$20), and are marked in green.

Identification of taaffeite and musgravite

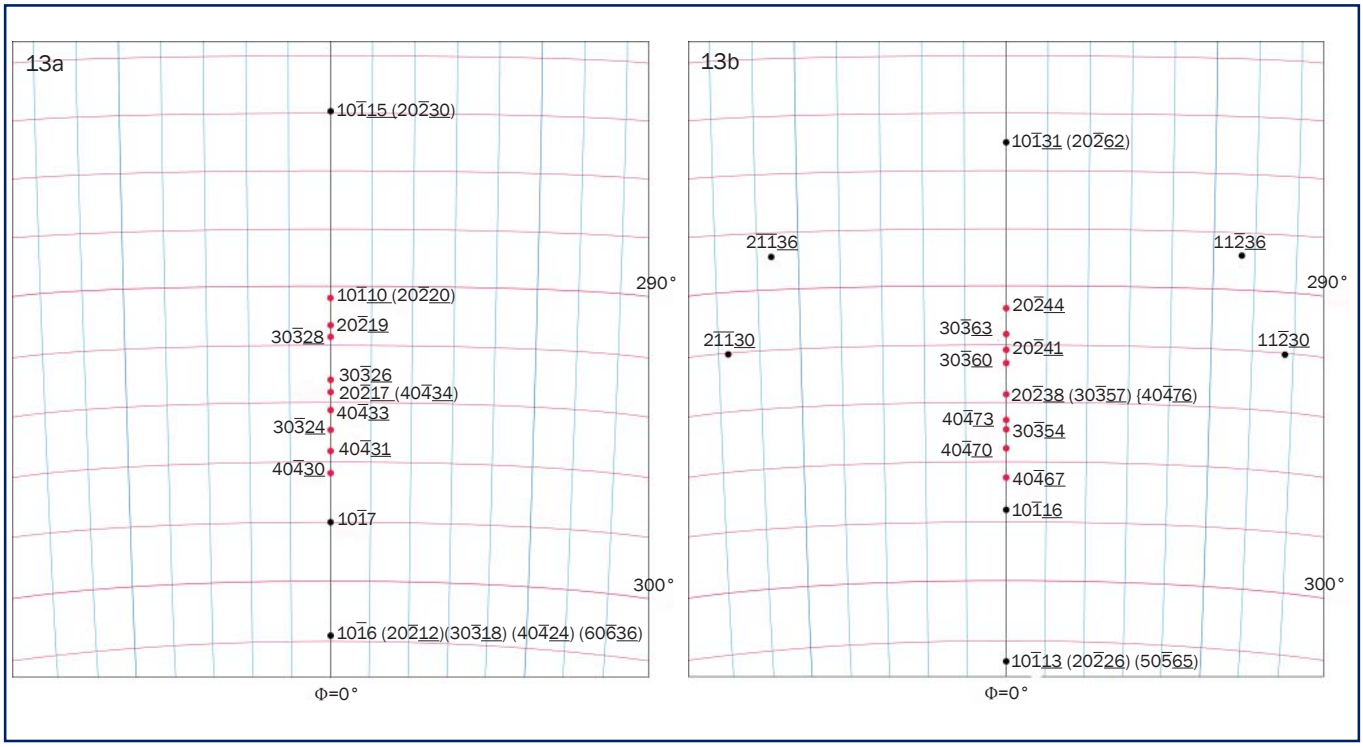

Figure 13: (a) The lattice planes with Miller indices (20$\bar{2}$17), (20$\bar{2}$19), (20$\bar{2}$20), (30$\bar{3}$24), (30$\bar{3}$26), (30$\bar{3}$28), (40$\bar{4}$30), (40$\bar{4}$31), (40$\bar{4}$33) and (40$\bar{4}$34) are indicated for taaffeite T-001 on a section of the Wulff net magnified near 290-300° in the central part of Figure 9a. (b) Miller indices (20$\bar{2}$38), (20$\bar{2}$41), (20$\bar{2}$44), (30$\bar{3}$54), (30$\bar{3}$57), (30$\bar{3}$60), (30$\bar{3}$63), (40$\bar{4}$67), (40$\bar{4}$70), (40$\bar{4}$73) and (40$\bar{4}$76) of musgravite M-10 plotted on an enlarged section of the Wulff net. The interfacial angles between these Miller indices and the standard pole [0001] indicate that φ=0° and that ρ has a range of 20.4° to 26.4°. The ρ angles just fall within the diffraction range detectable by the Si-semiconductor detector.

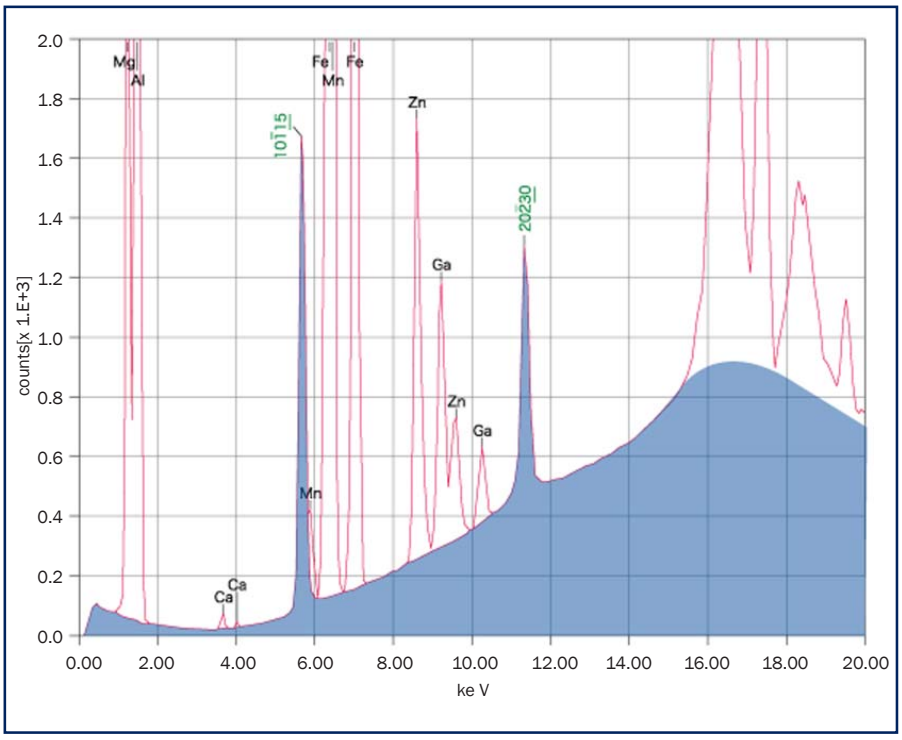

Figure 14: With the stage settings of ω= 0°, τ=+9°, the diffraction doublet peak indicating Miller indices of (10$\bar{1}$15) and (20$\bar{2}$30) of taaffeite T-001 was obtained and is marked green.

the same energy range on rotation of the sample every 60 or 120 degrees. If these diffraction peaks are initially not visible, further tilt is necessary by steps of 2 degrees and rotating again until they are. Second, set the diffraction peaks for the 0 degree position. Finally, rotate and then tilt if you want to further confirm. This process should take less than one hour. As a result, accurate distinction between taaffeite and musgravite is possible by determining their symmetry, which is 6-fold in taaffeite and 3-fold in musgravite. Most importantly for gems, the method is non-destructive.

Identification of taaffeite and musgravite

Figure 15: With musgravite at stage settings of ω= 0°, τ=+9°, the diffraction doublet peak indicating Miller indices of (10$\bar{1}$31) and (20$\bar{2}$62) was obtained and marked in green. These are clearly different from the taaffeite peaks shown in Figure 14.

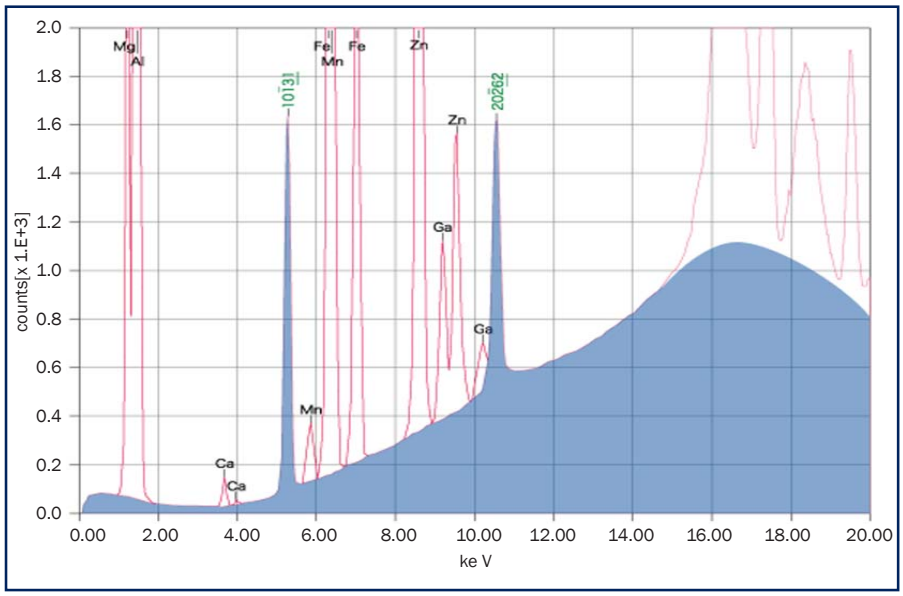

Figure 16: Diffraction X-ray peaks of taaffeite planes (20$\bar{2}$11), (20$\bar{2}$12), (30$\bar{3}$18), (40$\bar{4}$22), (40$\bar{4}$24) and (60$\bar{6}$36) were obtained with stage settings of ω= 0° and τ=-9°. The peaks (20$\bar{2}$12), (30$\bar{3}$18), (40$\bar{4}$24) and (60$\bar{6}$36) comprise the quadruple diffraction peak of (10$\bar{1}$6); the peaks (20$\bar{2}$11) and (40$\bar{4}$22) comprise the doublet diffraction peak of (20$\bar{2}$11).

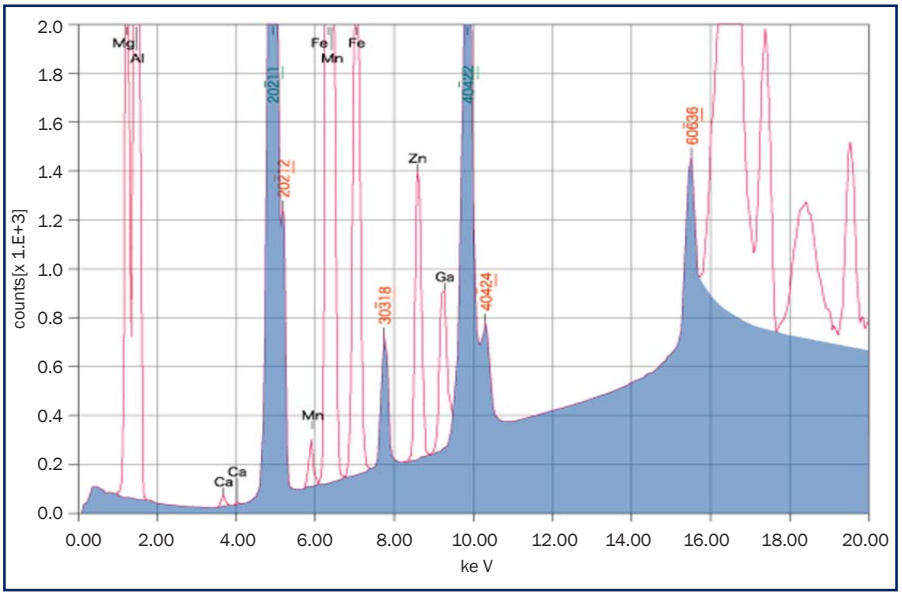

Figure 17: Diffraction X-ray peaks of musgravite planes (20$\bar{2}$26), (30$\bar{3}$39) and (50$\bar{5}$65) were obtained with stage settings of ω= 0° and τ=-9°. These three peaks comprise the triplet diffraction peak of (10$\bar{1}$13); the low intensities of (10$\bar{1}$13) and (40$\bar{4}$52) means that they may not be distinguishable from the peaks due to fluorescence.

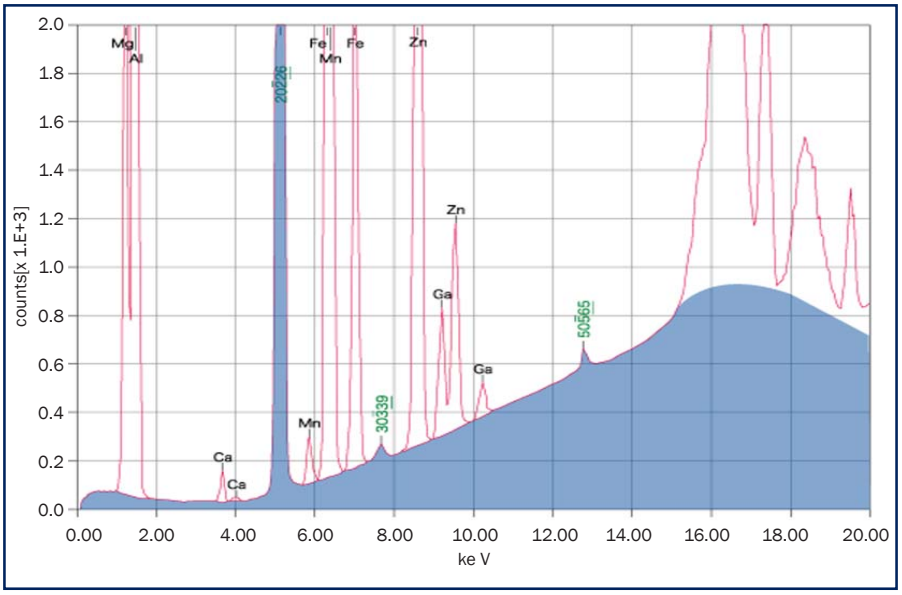

Acknowledgements

The authors are grateful to Dr Norimasa Shimobayashi (Kyoto University, Kyoto) for EDXRF stage construction, technical information and sample analysis advice, all of which made this non-destructive single-crystal X-ray diffraction study possible. We are also grateful to Dr Karl Schmetzer for discussion and critical comments, which helped improve the manuscript. Special thanks are due to Midori Jewellery for providing photographs of jewellery and to our sample supplier, the Magical Stone Lab. Finally, we thank our research colleagues Hiroshi Kitawaki FGA and Makoto Okano FGA at GAAJ for assistance with this work.

References

Abduriyim, A., Kobayashi, T., Fukuda, C., Okano, M., and Kitawaki, H., 2007a. Identification of taaffeite and musgravite with non-destructive single-crystal X-ray diffraction technique. *Annual meeting of the Gemmological Society of Japan,* 2007, Abstracts, pp.4-5

Abduriyim, A., Kobayashi, T., Fukuda, C., Okano, M., and Kitawaki, H., 2007b. Identification of taaffeite and musgravite with non-destructive single-crystal X-ray diffraction technique using EDXRF instrument. *Gemmology,* **38**(458), 11-15 (in Japanese)

Abduriyim, A., and Kobayashi,T., 2007c. Application of X-ray diffraction to identification of taaffeite and musgravite. *30th International Gemmological Conference (IGC), Moscow, Russia, 2007,* Abstracts, 5

Kiefert, L., and Schmetzer, K., 1998. Distinction of taaffeite and musgravite. *Journal of Gemmology,* **26**(3),165-7

Okano, M., Kitawaki, H., and Abduriyim, A., 2006. Taaffeite and musgravite <gemstones in the latest topics>. *Annual meeting of the Gemmological Society of Japan, 2006,* Abstracts, 11-12, and website http://www.gaaj-zenhokyo.co.jp/researchroom/2006/2006_10a-01en.html

Schmetzer, K., Kiefert, L., and Bernhardt, H.-J. 2000. Purple to purplish red chromium-bearing taaffeites. *Gems & Gemology*, **36**(1), 50-9

Schmetzer, K., Kiefert, L., Bernhardt, H.-J., Burford, M., and Gunasekara, D.P., 2005a. Iron-and zinc-rich gem-quality taaffeites from Sri Lanka. *Journal of Gemmology*, **29**(5/6), 290-8

Schmetzer, K., Kiefert, L., Bernhardt, H.-J., and Burford, M., 2005b. Two remarkable taaffeite crystals from Sri Lanka. *Journal of Gemmology,* **29**(7/8), 461-6

Schmetzer, K., Kiefert, L., Bernhardt, H.-J., and Burford, M., 2006. The variation of gemmological properties and chemical composition of gem-quality taaffeites and musgravites from Sri Lanka. *Australian Gemmologist*, **22**(11), 485-92

Schmetzer, K., Krzemnicki, M.S., Hänni, H.A., Bernhardt, H.-J., and Pettke, T., 2007. Gem-quality taaffeites and musgravites from Africa. *Journal of Gemmology,* **30**(7/8), 367-82

Shimobayashi, N., and Kitamura, M., 1998. Development and application of an X-ray analytical microscope, I. Characteristic of instrument (in Japanese). *Annual meeting of the Mineralogical Society of Japan, KyuSyu University 1998,* Abstracts, 103

Shimobayashi, N., and Kitamura, M., 1999a. Development and application of an X-ray analytical microscope, II. Crystal orientation mapping (in Japanese). *Annual meeting of the Mineralogical Society of Japan, Ibaraki University 1999,* Abstracts, 63

Shimobayashi, N., Minato, J., and Kitamura, M., 1999b. Application of an X-ray analytical microscope for the study of polycrystalline material. *Earth and planetary science using synchrotron radiation,* KEK proceedings 99-14, 83-6

Shimobayashi, N., and Kitamura, M., 2002. Modified X-ray analytical microscope for the study of polycrystalline materials. *18th General Meeting of the International Mineralogical Association,* Abstract, 154

The Authors

Ahmadjan Abduriyim, Taisuke Kobayashi and Chihiro Fukuda

Gemmological Association of All Japan (GAAJ), Zenhokyo Laboratory, 5-25-11 Ueno Taitoku, Tokyo, 110-0005 Japan.
email: ahmadjan@gaaj-zenhokyo.co.jp

Abstracts

Diamonds

Fluorescence spectra of colored diamonds using a rapid, mobile spectrometer.

S. Eaton-Magaña, J.E. Post, P.J. Heaney, R.A. Walters, C.M. Breeding and J.E. Butler. *Gems & Gemology,* **43**(4), 2007, 332-51.

A study is reported on numerous coloured diamonds from the Aurora Butterfly of Peace and other collections, using a new type of fluorescence spectrometer whose advantages include high portability, low cost and rapid collection times; for comparison, 10 irradiated diamonds were also studied. With only two exceptions, the natural colour diamonds could be separated into three categories (on the basis of the peak wavelength and the fluorescence spectra) that generally corresponded with their body colours: 1) ~ 450 and ~ 490 nm recorded mainly for pink, yellow and fancy white diamonds, 2) ~ 525 nm mainly for green-yellow or yellow-green and brown diamonds and 3) ~ 550 nm mainly for orange, grey-green (including chameleon) and type 1a blue-grey or grey-blue diamonds. A spectrum that is anomalous for the diamond's body colour may indicate that it has been treated; in some cases fluorescence spectroscopy can help to determine diamond type. R.A.H.

An examination of the Napoleon diamond necklace.

E. Gaillou and J.E. Post. *Gems & Gemology,* **43**(4), 2007, 352-7.

The intriguing history of the Napoleon necklace given by Napoleon Bonaparte in 1811 to his empress Marie Louise involves both royals and con artists (and one individual who was both), and it was ultimately donated to the Smithsonian Institution in 1962. IR absorption analysis of 101 stones in the necklace revealed that a high proportion of the larger diamonds are the relatively rare type IIa; most of the smaller stones are type IaAB. The luminescence behaviour of these diamonds to UV exposure correlates with their diamond type. R.A.H.

Lab notes.

T.M. Moses and S.F. McClure (Eds). *Gems & Gemology,* **43**(4), 2007, 358-65.

Notes are given on a 1.84 ct bright orange spessartine with dark blue-green inclusions of apatite, a 1.01 ct cut diamond with inclusions of garnet and omphacite, a natural black diamond with oriented etch channels and a 1.80 ct diamond cut in the shape of a fish. R.A.H.

A history of diamond treatments.

T.W. Overton and J.E. Shigley. *Gems & Gemology*, **44**(1), 2008, 32-53.

Although various forms of surface coatings intended to alter the colour of diamonds have long been in use, the modern era features more permanent colour alterations through irradiation and high pressure/high temperature annealing and improvements in apparent clarity with lead-based glass filling. Modern gemmologists are faced with a broad spectrum of colour and clarity treatments ranging from the simple to the highly sophisticated, and from the easily detected to the highly elusive. The history, characteristics and identification of known diamond treatments are reviewed. R.A.H.

Natural-color purple diamonds from Siberia.

S.V. Titkov, J.E. Shigley, C.M. Breeding, R.M. Mineeva, N.G. Zudin and A.M. Sergeev. *Gems & Gemology*, **44**(1), 2008, 56-64.

Twelve natural-colour purplish-pink to grey-purple diamond crystals from the Mir kimberlite field, Siberia, and seven round brilliants faceted from these crystals, were studied visually and by using UV-Vis-NIR, IR and photoluminescence spectroscopy. Aspects of their colour and the various structural defects in these purple diamonds are due to their post-growth plastic deformation in the earth. All the samples exhibited prominent parallel planar lamellae along which the purple colour is concentrated. R.A.H.

Natural type Ia diamond with green-yellow color due to Ni-related defects.

W. Wang, M. Hall and C.M. Breeding. *Gems & Gemology,* **43**(3), 2007, 240-3.

Commonly seen in HPHT-grown synthetic diamonds with a green component, Ni-related defects have now been found in a type Ia natural diamond with a strong green component. The 1.75 ct fancy green-yellow diamond shows a strong peak at 1332 cm^{-1} in the IR absorption spectrum, strong absorption from the 1.40 eV centre and the associated ~ 685 nm band in the Vis-NIR spectrum and very strong emissions from Ni-related defects in the photoluminescence spectra – all of which indicate that nickel is the primary cause of the green colour. R.A.H.

[Morphology of diamonds from kimberlite pipes of Catoca field (Angola).]

V.N. Zinohenko. *Proceedings of the Russian Mineralogical Society,* **136**(6), 2007, 91-102. (Russian with English abstract.)

The morphology of more than 3200 diamond crystals from kimberlite pipes of the Catoca field in the Lunda diamond-bearing province of NE Angola, has been studied in detail, Diamond crystals from different pipes in this field have distinguishing peculiarities in their morphology and in their physical-

Abstracts

mineralogical properties. Octahedral forms predominate in crystals from the Catoca and Kamitogo pipes, which are considered to be indicative of conditions more favourable for diamond growth and preservation, in comparison with diamonds from the Kakele pipe, where rhombododecahedra are the commonest forms. These morphological and other mineralogical peculiarities of diamond crystals may be used to appraise the diamond-bearing potential of their primary source in NE Angola. R.A.H.

***European Journal of Mineralogy,* 20(3), 2008.**

This special issue devoted entirely to diamonds is in honour of Vladimir S. Sobolev who first suggested that diamonds might be found in the rocks of the northern Siberian platform. He followed this up with the use of indicator minerals such as Cr-rich pyrope to locate kimberlite which led to the discovery of the famous Mir pipe and to several hundred kimberlite pipes in Yakutia. Nikolai V. Sobolev is the eldest son of V.S. Sobolev. The issue contains a total of ten papers, five of which are abstracted below.

Nanometre-sized mineral and fluid inclusions in cloudy Siberian diamonds: new insights on diamond formation.

A.M. Logvinova, R. Wirth, E.N. Fedorova and N.V. Sobolev. *European Journal of Mineralogy*, **20**(3), 2008, 317-31.

Nm-sized isolated inclusions have been studied in four cloudy octahedral diamonds from the internationalnaya and one for the Yubileynaya mines, Yakutia. TEM, AEM, EELS and HREM were applied as well as line scan and elemental mapping of the samples. All the crystals exhibit an octahedral habit with opaque central cuboid cores with numerous nano-inclusions (between 30 and 800 nm). They are composed of multi-phase assemblages which include silicates, oxides, carbonates, brines (KCl) and fluid bubbles. Distinguishable crystalline phases include: a crystalline high-Mg silicate, dolomite, Ba-Sr carbonate, phlogopite, ilmenite, ferropericlase, apatite, magnetite, K-Fe sulphides (djerfisherite ?) and kyanite. Carbonates were identified in TEM foils from all the diamonds, studied, and show a general enrichment in incompatible elements such as Sr and Ba. Some elemental variations may be explained by fractional crystallization of fluid/melt or mixing of fluids with different compositions. R.A.H.

Diamond potential of metamorphic rocks in the Kokchetav Massif, northern Kazakhstan.

V.A. Pechnikov and F.V. Kaminsky. *European Journal of Mineralogy*, **20**(3), 2008, 395-413.

There are two known diamondiferous bodies in Kazakhstan, the Kundy-Kol deposit and the Barchi-Kol occurrence; both are located in the western part of a metamorphic belt outcropping in the centre of the Kokchetav Massif. This metamorphic belt is interpreted as a mega-mélange that comprises structural units underlain by HP and UHP rocks. Diamondiferous UHP rocks in the Hundy-Kol deposit form a narrow (~ 1 km thick) band; they comprise less than 1% of the total UHP rock volume. Garnet-biotite gneiss makes up about 80% of the diamondiferous zone. A certain regularity is discernible in the spatial distribution of the diamonds, linear diamond-rich zones alternate with barren ones. The diamond grade ranges from several carats per ton (cpt) to several hundreds of cpt. Different morphological varieties of diamonds include octahedral, cubes, cubo-octahedral forms, skeletal and spheroidal crystals. A wide range of $\delta^{13}C$ (–8.9 to –27 ‰) and $\delta^{15}N$(+5.3 to +25 ‰ values have been measured. Diamonds from different rock types differ in their isotopic patterns: those from gneiss have 'lighter' isotopic compositions relative to those of pyroxene-carbonate and garnet-pyroxene rocks. Graphite, coesite, clinopyroxene, rutile, titanite, kyanite, K-feldspar, biotite, phengite, phlogopite, quartz, albite, apatite, chlorite and carbonates are minerals forming intergrowths with diamonds; the most frequent being graphite + diamond. It is concluded that a model of crustal fluid-metasomatic formation of diamonds in metamorphic rocks best reflects the observations. This model presumes that the formative process occurred at relatively low temperature and pressure within an open disequilibrium catalytic system; it does not exclude an UHP episode in the geological history of the metamorphic rocks. R.A.H.

Monitoring diamond crystal growth, a combined experimental and SIMS study.

V.N. Reutsky, B. Harte, Y.M. Borzdov and Y.N. Palyanov. *European Journal of Mineralogy,* **20**(3), 2008, 365-74.

Detailed ion microprobe measurements were made on two synthetic diamond crystals grown by the metal catalyst technique under identical *P-T* conditions of 1450°C and 5.5 GPa, but with different source nitrogen abundances. Measurements of the C and N isotope compositions and nitrogen abundances were made in traverses across the crystal sectors, which included cubic and octahedral sectors of both relatively rapid and relatively slow growth. In both crystals an early growth phase dominated by falling $\delta^{13}C$ and rising N is followed by an extensive growth phase with moderately constant $\delta^{13}C$ and gradually descending N. This change in $\delta^{13}C$ has been modelled numerically; the stabilization is achieved once a steady state is attained and diamond grows with the same $\delta^{13}C$ composition as the graphite source. The decreasing N values appear to be a product of Rayleigh fractionation. The nitrogen isotope compositions show major differences of ~ 30 ‰ between octahedral and cubic sectors, possibly representing a consistent difference in N isotope adhesion between the two faces. R.A.H.

Olivine inclusions in Siberian diamonds: high-precision approach to minor elements.

N.V. Sobolev, A.M. Logvinova, D.A. Zedgenizov, N.P. Pokhilenko, D.V. Kuzmin and A.V. Sobolev. *European Journal of Mineralogy*, **20**(3), 2008, 305-15.

At depths in the continental lithospheric mantle exceeding 120–150

Abstracts

km there are two types of geological environment which support diamond formation. They are ultramafic or peridotitic (U-type) and eclogitic (E-type) environments, as shown by minerals found as inclusions in diamonds and which make up xenoliths of diamondiferous peridotites and eclogites in kimberlites. In primary diamond-bearing kimberlite and lamproite rocks the ratio of diamonds from these two geological environments varies widely between localities. U-type diamonds predominate, however, in the great majority of diamond occurrences worldwide. Olivine is the most typical inclusion in U-type diamonds, along with enstatite, pyrope and chromite in harzburgitic or dunitic assemblages. More than 260 olivine inclusions from major Siberian mines were studied and compared with olivine from diamonds of the Snap Lake dyke system in Canada. Olivine composition in eight xenoliths of diamondiferous peridotites from Udachnaya pipe representing the rarest mantle samples, were also re-examined. Inclusions were analysed for major and minor elements by electron microprobe to obtain high-precision and accuracy, especially for Ni, Ca, Mn, Cr, Co and Al. Minor element abundances in most of the olivines vary in the following ranges: (wt %): NiO 0.320–0.408, CaO 0.005–0.045, MnO 0.079–0.131, Cr_2O_3 0.013–0.115, Co 0.009–0.022 and Al_2O_3 0.007–0.039. About 70% of the olivines were very low in CaO, reflecting a relatively low equilibration temperature of the lherzolitic paragenesis, or lack of clinopyroxene associated with olivine. R.A.H.

Diamondiferous xenoliths from crystal subduction: garnet oxygen isotopes from the Nyurbinskaya pipe, Yakutia.

Z.V Spetsius, L.A. Taylor, J.W. Valley, M.T. Deangelis, M. Spicuzza, A.S. Ivanov and V.I. Banzeruk. *European Journal of Mineralogy,* **20**(3), 2008, 375-85.

The newly developed Nyurbinskaya kimberlite pipe in Yakutia has yielded an unprecedented array of xenoliths, each containing diamonds. Some 121 of these xenoliths were studied and garnets were separated from the different types of xenoliths, including mostly eclogites, but also some pyroxenites and peridotites. The $\delta^{18}O$ ratios of most of the peridotitic garnet samples lie within the range of the average mantle, except for one with a $\delta^{18}O$ value of 6.57 ‰. Garnets from pyroxenites (websterites) in general have $\delta^{18}O$ values above 6.0 ‰, with two samples as high as 7.3 and 8.50, and only two samples as low as 5.9 and 6.0 ‰. Eclogitic garnets have a $\delta^{18}O$ range of 4.7 to 9.7 ‰, with > 80% about 6 ‰. These new garnet oxygen-isotope ratios are not only evidence for subduction of oceanic crust, but also evidence for a major involvement of the upper, low-temperature metasomatized portion of the crustal section. R.A.H.

Gems and Minerals

The Minh Tien tourmaline mine, Luc Yen mining district, Yenbai Province, Vietnam.

D. Blauwet. *Mineralogical record,* **38**, 2007, 443-52.

Account of a visit to the Minh Tien mine in Yenbai Province, Vietnam. The recovery of specimen-quality tourmaline crystals is described. M.O'D.

A study of nail-head spicule inclusions in natural gemstones.

G. Choudhary and C. Golecha. *Gems & Gemology,* **43**(3), 2007, 228-35.

Nail-head spicules are inclusions that have traditionally been associated with hydrothermal synthetic quartz and emerald. They are caused primarily by rapid growth conditions and disturbances during crystallization of their host. These or similar-looking inclusions, however, have also been found in natural emerald and sapphire. A yellow sapphire, spinel, diamond and quartz have also been found with inclusions that strongly resemble them. Nail-head spicules remain a notable feature of rapid and disturbed growth, but their presence does not confirm a stone's natural or synthetic origin without further examination. R.A.H.

Mineralogical and geochemical characterization of the 'bituminous' agates from Nowy Kościół (Lower Silesia, Poland).

M. Dumanska-Slowik, L. Natkaniec-Nowak, M.J. Kotarba, M. Sikorska, J.A. Rzymelka, A. Loboda and A. Gawel. *Neues Jahrbuch für Mineralogie Abhandlungen,* **184**(3), 2008, 255-68.

The agates from Nowy Kościół, Lower Silesia, exhibit mainly horizontally stratified structures often developed as typical multiradial stars. These agates are mainly spherical with diameters of 2 to 40–70 cm; most are brownish red, 'honey-black' or red. The dark colour of their banding is mainly caused by Fe-compounds, REE-bearing minerals, Zn sulphides and organic matter. The content of organic matter is relatively low (0.15 wt %) but is dispersed within the silica matrix. It forms thin laminae or irregularly shaped drops or lenses. Asphaltenes are the dominant bitumen (56 %), with the remainder varying between 10 % aromatic hydrocarbons, 16 % resins and 18 % saturated hydrocarbons. Stable carbon isotope ($\delta^{13}C$) analysis (saturated hydrocarbons -28.9 ‰, aromatic hydrocarbons -28.3 ‰, resins -28.6 ‰, asphaltenes -28.3 ‰, whole organic matter -25.9 ‰) revealed its algal or mixed algal/humic origin. R.A.H.

Copper-bearing tourmalines from new deposits in Paraíba State, Brazil.

M. Furuya. *Gems & Gemology,* **43**(3), 2007, 236-9.

Two newly discovered pegmatites with Cu-bearing tourmaline are described, not far from the original locality of Mina da Batalha. The Glorious mine has produced a limited amount of gem-quality material with a composition similar to the blue tourmaline from the Mina da Batalha, but the second mine has not yet produced any gem-quality tourmaline. Violet material from the Glorious mine becomes blue on heat treatment, producing faceted stones of 0.15–0.34 ct. R.A.H.

Abstracts

Amethystfund aus dem Zemplen-Gebirge.

D. Grolit. *Mineralien Welt,* **29**(1), 2008, 55-61.

Amethyst of possible ornamental quality is described from Zemplén, Hungary, where it has been found with clinoptilolite. M.O'D.

Perlenzucht mit Pinctada maxima in Süost-Asien – ein Beispiel.

H.A. Hänni. *Gemmologie. Z. Dt. Gemmol. Ges.,* **56**(3/4), 2007, 83-96. 13 photographs, bibl. (German with English abstract.)

This is an update on modern farming methods used in south east Asia, mainly in north Bali and West Papua, under the supervision of marine biologists and geneticists from the James Cook University. Culturing oysters from fertilized eggs has replaced wild oyster collection. The larvae and spat are developed in hatcheries under scientifically controlled conditions. It takes two years for the oyster to grow to about 12 cm and be ready for the operation. Donor oysters for tissue graft and host oysters are carefully controlled with regular cleaning and X-ray checks. The first harvesting begins when the oyster is four years old. Most of the oysters are not re-seeded; their muscles are processed as seafood and the shells used as nacre. The pearls are processed, quality graded and marketed in Australia. E.S.

Gemmologische Kurzinformationen. Imitation für Feuerachat.

U. Henn. *Gemmologie. Z. Dt. Gemmol. Ges.,* **56**(3/4), 2007, 127-9, 5 photographs. (German with English abstract.)

A fire agate necklace offered in the trade was shown to be agate with thermally induced fractures. Milky-white zones were found alongside these fractures due to dehydration. The typical botryoidal structure of fire agate was also missing. E.S.

Gem news international.

B.M. Laurs (Ed.). *Gems & Gemology,* **43**(3), 2007, 252-74.

News is given of the development of a large diamond mine in the Fort a Corne kimberlite field some 60 km E of Prince Albert, Saskatchewan; exploration drilling and processing has already led to the recovery of 10,251 diamond crystals (~ 1270 ct) from 40,000 tonnes of kimberlite. Other items include an unusual colour-zoned axinite from Pakistan, with distinctly more Ti and Mn in the blue zone than in the light brown zone, Cr-V-bearing kyanite from Madagascar (with La-ICP-MS analyses of trace elements in kyanite from four countries) and a Cr-V-bearing light yellow-green spodumene from Afghanistan. R.A.H.

Gem news international.

B.M. Laurs. Lab notes. *Gems & Gemology,* **43**(4), 2007, 366-91.

Items mentioned include the soaring prices obtained at auction for coloured diamonds or flawless colourless cut diamonds, the marine diamond deposits in Namibia, magnesioaxinite and ferro-axinite from Tanzania (EPMA results given), yellow-green clinohumite and yellow chondrodite from Tanzania (with EPMA), sinhalites (1.35–3.20 ct) from Mogok, Myanmar, variously coloured Cu-bearing tourmalines from Mozambique and Nigeria, and new Russian synthetic beryl simulating 'Paraíba' Cu-bearing tourmaline. R.A.H.

Gem news international.

B.M. Laurs (Ed.). *Gems & Gemology,* **44**(1), 2008, 74-94.

Descriptions are given of an unusually large 76.27 ct cut titanite showing a vibrant display of dispersion, a 59.58 ct jeremejevite from Madagascar and an orange spessartine from Loliondo, Tanzania. Mention is made also of faceted blue afghanite and greenish-blue hauyne, both from Badakshan, Afghanistan, and a piece of light blue rough manganaxinite with MnO 6.9 wt % and with V_2O_3 ~ 0.1 wt % as the chromophore. R.A.H.

Yellow Mn-rich tourmaline from the Canary mining area, Zambia.

B.M. Laurs, W.B. Simmons, G.R. Rossman, E.A. Fritz, J.I. Koivula, B. Anckar and A. U. Falster. *Gems & Gemology,* **43**(4), 2007, 314-31.

Yellow gem-quality elbaite has been quarried in the Canary mining area of Zambia since 1993, both from pegmatites and eluvial/alluvial deposits, in colours ranging from yellow-green to yellow to orange and brown. Much of the orange-to-brown material is heated to attain a 'golden' or 'canary' yellow colour. The tourmaline is Mn-rich (up to 9.18 wt % MnO; EPMA results are given for 11 samples: ε 1.623–1.625, ω 1.645–1.649; SG 3.11–3.17) and contains traces of Ti and little or no Fe. Its distinctive composition is probably the result of the crystallization of abundant schorl from an unusual B-rich, Li-poor pegmatite magma, which depleted Fe while conserving Mn until the late-stage crystallization of gem pockets. R.A.H.

Copper-bearing (Paraíba-type) tourmaline from Mozambique.

B. Laurs, J.C. Zwaan, C.M. Breeding, W.B. Simmons, D. Beaton, K.F. Rijsdijk, R. Befi and A.U. Falster. *Gems & Gemology,* **44**(1), 2008, 4-30.

Cu-bearing tourmaline is found in alluvial pebbles beneath about 5 m of overburden, on the eastern side of the Alto Ligonha pegmatite district, Mozambique. They occur in a wide range of colours, typically pink to purple, violet to blue and blue to green or yellowish-green. Heat treatment of all but the green to yellowish-green stones produces Paraíba-like blue-to-green hues by reducing the absorption at ~ 520 nm caused by the presence of Mn^{3+}. The gemmological properties are typical of those for Cu-bearing tourmaline; the most common inclusions are partially healed fractures and elongate hollow tubes. Electron microprobe analyses are given; the stones have relatively low Cu contents and very low amounts of Fe and Ti. R.A.H.

Zirkone aus dem Reichsforst im Fichtelgebirge.

S. Meier and S. Weiss. *Lapis,* **32**(12) 2007, 20-8, 33-4.

Gem-quality transparent to translucent pink to reddish zircon is described from the Reichsforst in the Fichtelgebirge, Bavaria, Germany. M.O'D.

Abstracts (continued)

Notes from the DSEF gem lab.
C.C. Milisenda. *Gemmologie. Z. Dt. Gemmol. Ges.,* **56**(3/4), 2007, 79-82, 6 photographs.

A new Brazilian occurrence of gem-quality emeralds has been found near the town of Lages in the state of Rio Grande do Norte. Fifty specimens weighing between 0.3 and 10 ct were examined. They had standard physical properties. Mica formed the most characteristic inclusion, but there were also two- and, very rarely, three-phase inclusions. Healing cracks, hollow tubes, growth and colour zoning were observed.

A transparent faceted colourless stone with blue inclusions, purchased in Brazil, was shown to be rock crystal with gilalite inclusions. This material has been known since 2003 and comes from a deposit in Paraíba. Some yellow-green faceted stones weighing 7–10 ct had several absorption lines between 500 and 750 nm. These are typical features of Maxixe-type beryls which owe their colour to artificial irradiation. A specimen of 14.7 ct offered as scapolite cat's-eye had an RI 1.58 and SG 2.72. It showed strong dichroism and its infrared spectrum indicated it to be beryl. Its absorption spectrum showed the characteristic bands of irradiated Maxixe-type beryl. An octagonal faceted stone of 12.19 ct offered as bicoloured tourmaline had an RI 1.543-1.552, and thus was shown to be quartz. It was found to be a triplet consisting of colourless quartz and colourless beryl connected by a bicoloured green and pink adhesive binding. E.S.

Lab Notes.
T.M. Moses and S.F. McClure (Eds). *Gems & Gemology,* **43**(3), 2007, 244-51.

Items noted include an unusually large (201.18 ct) cat's-eye aquamarine, an unsuccessful attempt at diamond deception (in which an HPHT-treated diamond had been purposely cut and inscribed to match a previous GIA report of a diamond with a natural origin of colour), an intense blue 8.54 ct kyanite initially mistaken for sapphire and a large (67.94 ct) crystal of phenakite masquerading as a diamond. R.A.H.

Lab notes.
T.M. Moses and S.F. McClure (Eds). *Gems & Gemology,* **44**(1), 2008, 66-73.

Items noted include a square-cut 5.29 ct fancy brownish greenish yellow diamond which had experienced multiple growth/dissolution stages during its formation, the first CVD synthetic diamond submitted for grading, and an orange zircon which contained a melted inclusion indicating that the zircon had been subjected to an unusually high-temperature heat treatment possibly when mixed in with corundum subjected to such heat treatment. R.A.H.

Spodumenes from Nuristan, Afghanistan.
L. Natkaniec-Nowak. *Australian Gemmologist,* **23**(2), 2007, 51-7, 8 figures, 3 tables, 1 map.

Chemical analysis, Mössbauer spectroscopy and X-ray diffraction were used to investigate coloured spodumenes from the Nilaw mine. The authors found that Fe and trivalent Cr were responsible for the colour of green-yellow spodumene. A mixture of Mn, Fe and possibly Cr is thought to produce the violet-pink colour of kunzite. The spodumenes are found associated with the alkaline igneous rocks being products of post-magmatic pegmatitic-pneumatolytic processes. L.J.

Sealant impregnated rubies.
G.M. Pearson. *Australian Gemmologist,* **23**(2), 2007, 58-61, 14 figures.

Natural rubies are suggested to be impregnated with lead glass based on their appearance in transmission X-radiographs. L.J.

The formation of precious opal: clues from the opalization of bone.
B. Pewkliang, A. Pring and J. Brugger. *The Canadian Mineralogist,* **46**(1), 2008, 139-49.

The composition and microstructure of opalized saurian bones (Plesiosaur) from Andamooka, South Australia,have been analysed and compared to saurian bones that have been partially replaced by magnesian calcite from the same geological formation, N. of Coober Pedy, South Australia. Powder XRD shows that they are essentially pure SiO_2 (88.59–92.69 wt %), with minor Al_2O_3 (2.02–4.04 wt %) and H_2O (3.36–4.23 wt %). No traces of biogenic apatite remain after opalization. The opal is depleted in all trace elements relative to Post-Archaean Australian Shale composite (PAAS). During the formation of the opal, the coarser details of the bone miscrostructure have been preserved down to the level of the individual osteons (~ 100 μm), but the central canals and boundary area have been enlarged and filled with chalcedony, which postdates opal formation. These chemical and microstructural features are consistent with the opalization process being a secondary replacement after partial replacement of the bone by magnesian calcite, and also with the opal forming first as a gel in the small cavities left by the osteons, and the individual opal spheres growing as they settle within the gel. Changes in the viscosity of the gel provide a ready explanation for the occurrence of colour and potch banding in opals. The indication that opalization is a secondary process after calcification in the Australian opal fields is consistent with a Tertiary age of formation. R.A.H.

Dobova, die klassische Lokalität des Dravit.
A. Recnik, A. Hinterlechner-Ravnik and G. Niedermayr. *Mineralien Welt,* **29**(1), 2008, 48-53.

Well-formed dravite crystals are described from the Dobova area of Slovenia. M.O'D.

Lipovka: German Vein oder Vein for Germans?
M. Sehrig. *Lapis,* **33**(4), 2008, 29-34.

Pegmatite in the 'German Vein' in the geological park at Lipovka, central Urals, Russia, has produced specimens of pink tourmaline and chrysoberyl. M.O'D.

From single source to global free market: the transformation of the cultured pearl industry.

Abstracts

R. Shor. *Gems & Gemology,* **43**(3), 2007, 200-26.

Over the past fifteen years a combination of market forces, environmental events and scientific research has radically changed the cultured pearl industry from a single commodity dominated by one producer to a highly diverse industry operating throughout the Pacific region. The new products, consistent quality and broader marketing programmes in turn led major designers and retailers in the west to take a much greater interest in cultured pearls. During this period, consumer interest has expanded from the traditional small and medium white round Japanese akoya cultured pearl to the larger South Sea and Tahitian products, and to previously unfashionable shapes and colours. R.A.H.

Mineralogical investigations of dentine from African elephant, Siberian mammoth, hippopotamus, walrus and sperm whale tusks.

T. Sito, L. Natkaniec-Nowak, M. Pawlikowshi and M. Dumanska-Slowik. *Gemmologie. Z. Dt. Gemmol. Ges.,* **56**(3/4), 2007, 117-26, 14 photographs, 17 diagrams, bibl.

The tusks/teeth from African elephants, Siberian mammoth, hippopotamus, walrus and sperm whale were macro-and microscopically examined, including both the mineral matrix (dahllite) and the organic component (collagen). The thickness of single collagen fibres, bunches of fibres and the size of the nutritious channel were measured. The characteristics of the dentine should be helpful in the identification of zoological discoveries in archaeological sites. E.S.

Infrared spectroscopic study of modern and ancient ivory from sites at Jinsha and Sanxingdui, China.

L. Wang, H. Fan, J. Liu, H. Dan, Q Ye and M. Deng. *Mineralogical Magazine,* **71**(5), 2007, 509-18.

Anicent ivory from the Chengdu Jinsha and Guanghan Sanxingdui sites in China has been buried for several thousand years. These ancient ivory samples have been compared with modern ivory, using IR spectroscopy in the 400–4000 cm^{-1} range. By combining these results with XRF analytical data, the crystallinity and crystal chemistry of the apatite component as well as the structural characteristics of the ivory have been compared. The ancient ivory consists almost entirely of hydroxyl-carbonate apatite. Compared with modern ivory, the PO_4^{3-} and CO_3^{2-} bands are stronger, the PO_4RF values are obviously greater and an extra OH^- band at 3569 cm^{-1} is observed. These results imply that there is a greater degree of apatite crystallinity in the ancient apatite and that there has been incorporation and recrystallization of CO_3^{2-} in the apatite during burial. Positive correlations are found between the apatite crystallinity, CO_3^{2-} and OH^- ion contents and burial time. The organic matter in ancient ivory has been lost or decomposed, which may be the main reason for ancient ivory being easily dewatered and readily friable after being unearthed. R.A.H.

Vaterit in Süßwasser-Zuchtperlen aus China und Japan.

U. Wehrmeister, D.E. Jacob, A.L. Soldati, T. Häger and W. Hofmeister. *Gemmologie. Z. Dt. Gemmol. Ges.,* **56**(3/4), 2007, 97-116, 13 photographs, 5 graphs, 1 table, bibl. (German with English abstract.)

Japanese and Chinese tissue and bead nucleated cultured freshwater pearls of good quality were investigated with Raman spectroscopy and LA-ICP-MS. In 50% of the investigated tissue-nucleated samples vaterite could be identified near the centre of the cultured pearls as well as in little blemishes on the surface. Continuous growth structures transect both vaterite and aragonite areas. Sodium and strontium are significantly lower in vaterite areas while Mg is significantly higher. The high amount of good quality cultured pearls implies that the formation of vaterite during growth may be a major factor affecting the quality of freshwater cultured pearls. E.S.

Tourmaline from the Minh Tien pegmatite, Luc Yen mining district, Yenbai Province, Vietnam.

W.E. Wilson. *Mineralogical Record,* **38,** 2007, 453-7.

Tourmaline from the Minh Tien pegmatite in Yenbai Province, Vietnam, has occurred in divergent clusters from pink to raspberry-red to yellow green and yellow-orange. Discussion continues on the composition which may be elbaite, rossmanite or liddicoatite. M.O'D.

The 100-year history of the benitoite gem mine.

W.E. Wilson. *The Mineralogical Record,* **39**(1), 2008, 13-42.

The history, working and production of the Dallas benitoite gem mine, San Benito County, California, are described with notes on some of the personalities who were instrumental in establishing the recovery of gem-quality benitoite. It would appear from this account that the mine is now opened occasionally for rockhound access rather than for the regular production of gem-quality material. M.O'D.

American mineral treasures.

W.E. Wilson. *The Mineralogical Record,* **39**, 2008, 171-222.

Overview of a near-50 case mineral display featuring fine and often rare American mineral specimens, many of ornamental quality, displayed at the 2008 Tucson Gem and Mineral Show. Brief descriptive notes include present ownership. M.O'D.

Instruments and Techniques

AGIL refractometer with LED light source.

T. Linton and R. Beattie. *Australian Gemmologist,* **23**(2), 2007, 62-63, 2 figures.

A moderately priced critical angle refractometer with light source produced by the Asian Gemmological Institute and Laboratory (AGIL) in Hong Kong is reviewed. The authors conclude that this is a quality instrument with a clear and easy to read scale. It provided accurate results when tested. L.J.

Abstracts

Synthetics and Simulants

Latest generation CVD-grown synthetic diamonds from Apollo Diamond Inc.
W. Wang, M.S. Hall, K.S. Moe, J. Tower and T.M. Moses. *Gems & Gemology,* **43**(4), 2007, 294-312.

Gemmological and spectroscopic properties of 43 chemical vapour deposition (CVD) synthetic diamonds (0.14–1.20 ct) from Apollo Diamond Inc. of Boston, Massachusetts, have been examined to characterize this latest generation (2006-2007) of their products. Relative to those examined in 2003, the new samples showed considerably improved size, colour and clarity. In addition to colourless and near-colourless material, fancy orange-to-pink colours are now produced. These high-quality CVD-grown diamonds are comparable in colour and clarity to natural diamonds; they can be identified by the use of a combination of gemmological and spectroscopic properties. R.A.H.

Abstractors

R.A. Howie – R.A.H. L. Joyner – L.J. M. O'Donoghue – M.O'D. E. Stern – E.S.

Letters

Tables of Gemstone Identification

A letter from R. Dedeyne, I. Quintens and J. Hyršl expressing concern about the review of their book Tables of Gemstone Identification (*Journal of Gemmology*, **30**(7/8), 2007, 463), was forwarded to me with a request for a second opinion.

After a very brief introduction together with a list of the abbreviations used, this book is basically a series of tables, of which the more important are those listing refractive index, opaque and translucent stones, density, spectra and an alphabetical index with supplementary data. Once a reader has gained familiarity with the abbreviations used, these tables are seen to contain a wealth of information. The problem of dealing with a mineral species with widely varying compositions is tackled by giving it several entries. This contributes to the length of some of the tables (the density table extends over a daunting 115 pages with, for example, baddeleyite getting 43 entries and hyperstene [sic] at least 30). It is also unfortunate that a few odd names such as hematine (sintered iron) and rock names (anyolite, nuumite, unakite, verdite) crop up: not many, but they inevitably appear several times in the refractive index and density tables. There are also brief tables showing the relationship between refractive index and density of glasses, minerals of the garnet group and on the isotropic and anisotropic imitations of diamond. The tables end with short lists of books and journals dealing specifically with gem minerals and gemmology.

Books dealing with tabulated determinative features of minerals and gemstones are popular with readers. The test here will be whether the main tables presented are found to be suitable for identifying unknown gemstones despite their length and the complexities of multiple entries. The work is thus rather massive for bench use, but the price seems eminently reasonable.

Professor R.A. Howie
Matlock, Derbyshire

Proceedings of the Gemmological Association of Great Britain and Notices

Conference and Graduation Ceremony

The 2007 Gem-A Conference was held at the Renaissance London Heathrow Hotel on Sunday 28 October. Speaking on the theme 'Gems of the Orient – Pearls and Jade' were Shigeru Akamatsu, Japan, George Bosshart, Switzerland, Professor Henry A. Hänni, Switzerland, Roger Keverne, London, Mimi Ou Yang Chiu Mei, Hong Kong, Kenneth Scarratt, Thailand, and Elisabeth Strack, Germany.

A programme of events and workshops was arranged to coincide with the Conference including a private viewing of the Crown Jewels with David Thomas, and group visits to the School of Earth Sciences, Kingston University, to view and learn about the equipment used to research gems and minerals.

The Graduation Ceremony was held at Goldsmiths' Hall in the City of London on Monday 29 October. Gem-A Chairman Professor Alan Collins presided and David Thomas MVO, Crown Jeweller from 1991 to July 2007, presented the awards and diplomas. In his address David Thomas gave a brief résumé of his career in the jewellery trade and his role as Crown Jeweller. Stressing the importance of education to the trade, he told the graduates: "In these days of modern technology with so many of our ancient crafts and traditions disappearing, it is only by your dedication and studies that the trade will survive." The ceremony was followed by a reception for graduates, members and their guests.

A special award was made during the Graduation Ceremony of an Honorary Life Membership to Ms Mimi Ou Yang Chiu Mei, in recognition of her substantial contribution to the world of gemmology and to the Association. Ms Ou Yang is founder and director of the Hong Kong Gems Laboratory and the Hong Kong Institute of Gemmology, one of Gem-A's largest Allied Teaching Centres. She has conducted numerous studies on jadeite jade, lectures in gemmology and jdaeite, and has produced four books and numerous articles on the subject.

Reports of the Conference, the Graduation Ceremony and the award of the Honorary Life Membership were published in *Gems & Jewellery*, 2007, **16**(5), 8-14.

Gem-A President Alan Jobbins awarding Ms Mimi Ou Yang Chiu Mei with an Honorary Life Membership during the Graduation Ceremony. Photo courtesy of Lewis Photos Ltd.

Gem-A Awards

Gem-A examinations were held in October 2007 and January 2008. In the Examinations in Gemmology 156 candidates sat for the Diploma Examination of whom 72 qualified, including one with Distinction and nine with Merit. In the Foundation Gemmology Examination, 163 candidates sat of whom 120 qualified. In the Gem Diamond Examination 70 candidates sat of whom 34 qualified, including one with Distinction and one with Merit. The names of the successful candidates are listed below.

Examinations in Gemmology

Gemmology Diploma

Qualified with Distinction

Rasche, Elizabeth, London

Qualified with Merit

Hansson, Maria Charlotte, Lannavaara, Sweden
Kyaw Swar Htun, Yangon, Myanmar
Lau Pui Ting, Kowloon, Hong Kong
Li Jingna, Guilin, Guangzi, P.R. China
Qu Gang, Beijing, P.R. China
Underwood, Antonia Charlotte, London
Vignal, Patrick, Ampus, France
Wang Jian Xing, Wuhan, Hubei, P.R. China
Xu Chong, Wuhan, Hubei, P.R. China

Qualified

Baker, David Mark, Bath, Avon
Bieri, Willy Peter, Escholzmatt, Switzerland
Bracey, Anne Christine, Birmingham, West Midlands
Brichet, Leonore, Vernouillet, France
Chan Chi Wai, Wah Fu Estate, Hong Kong
Chan Wing Kwok, New Territories, Hong Kong
Chen, Sisi, Wuhan, Hubei, P.R. China
Cheung Chi Shing Peter, Lam Tin, Kowloon, Hong Kong
Cheung Pui Shan, Alicia, Tsuen Wan, New Territories, Hong Kong
Chien, Lien Chin, Taichung, Taiwan, R.O. China
Chitty, Warne William, Aspen, Colorado, U.S.A.
Chong, He, Wuhan, Hubei, P.R. China
De Alwis Dissanayake, M. D., Colombo, Sri Lanka
Ding Hui, Surbiton, Surrey
Dowden, Simon, Chadds Ford, Pennsylvania, U.S.A.
Driscoll, Brian John, New York, U.S.A.
Gerrard, Belinda Louise, Sydney, New South Wales, Australia
Gunnarsson, Camilla Elizabeth, Norrtälje, Sweden
Hon Wai Ching, Hung Hom, Hong Kong
Hou Xukui, Guilin, Guangxi, P.R. China
Hsu Juiwen, Taipei, Taiwan, R.O. China
Jeavons, James, Geebung, Queensland, Australia
Lai Sau Han, Winnie, Hong Kong
Lau Ka Yan, Hong Kong
Lau Yuen Yee, Simmy, Kowloon, Hong Kong
Lee Chi-Ju, Taipei, Taiwan, R.O. China
Li LiuFen, Guangzhou, P.R. China
Li Yan, Beijing, P.R. China
Liang Rong, Guilin, Guangxi, P.R. China
Lin Chun-Yen, Taipei, Taiwan, R.O. China
Lin Yu Chi, Taipei, R.O. China
Maclellan, Kiki, London
Mak, Bing Lan, Fanling, New Territories, Hong Kong
Meninno, Marco, London
Mi Zhiwei, Guilin, Guangxi, P.R. China
Mitchell, Andreas, London
Mu, Yujing, Shanghai, P.R. China
Netsah, Maayane, London
Overton, Thomas William, Carlsbad, California, U.S.A
Partridge, Jennifer Anne, Cambridge
Raguin, Odiane, Eguilles, France
Raimundo Da Silva, Aldina, Verdun, Quebec, Canada
Ringhiser, Barbara G., Lake Worth, Florida, U.S.A.
Russell, Marie, Worcester, Worcestershire
Sheng Ran, Beijing, P.R. China
Shpartova, Irina, London
Sikkema, Ariane, Almelo, The Netherlands
Strafti, Kalliopi-Maria, Athens, Greece
Tan Koon Oi, Beijing, P.R. China
Tsang Wai Ming, Causeway Bay, Hong Kong
Vigneron, Charlotte, Boulogne-Billancourt, France
Wan Moli, Guangzhou, P.R. China
Wang Yinjie, Shanghai, P.R. China
Wong Ling Ling, Tseung Kwan O, New Territories, Hong Kong
Wong Man Yuen, Daniel, Pokfulam, Hong Kong
Xia Qiang, Wuhan, Hubei, P.R. China
Xu Hui, Guilin, Guangxi, P.R. China
Yang Xi, Wuhan, Hubei, P.R. China
Yu Xiubing, Shanghai, P.R. China
Zhang Minghui, Guilin, Guangxi, P.R. China
Zhao Na, Beijing, P.R. China
Zheng Xin Zi, Wuhan, Hubei, P.R. China

Proceedings of the Gemmological Association of Great Britain and Notices

Foundation Certificate in Gemmology

Qualified

Agarwal, Kamal Kishore, Jaipur, Rajasthan, India
Al-Saif, Manar, Wembley, Middlesex
Amrit, Paveet, Northolt, Middlesex
Ang, Pamela Co, Shanghai City, Shanghai, P.R. China
Araujo Cartwright-Jepson, Maria Claudia, London
Asplund, Jan Olof, Kiruna, Norrbotten, Sweden
Baek, Kyung Ha, Jeollabuk-do, Korea
Baethe, Vanessa, Saint-Maur-Des-Fosses, France
Berezovsky, Florence Paulette Marie, Zurich, Switzerland
Bhatia, Esha, Gujarat, India
Blagg, Natalie, London
Bondar, Ilona, London
Branting, Andreas, London
Cai Min, Guangxi, P.R. China
Carre, Stephanie, Rambouillet, France
Chan Kin Chung, San Po Kong, Kowloon, Hong Kong
Chang, Shao-Ling, Taipei, Taiwan, R.O. China
Cheng Ming Yee, Kristy, Kowloon, Hong Kong
Chong, Ronald R.K.K., Amstelveen, The Netherlands
Deng Jianrong, Guangzhou, P.R. China
Dionne, Jean-Sebastien, Ste-Catherine-Jacques-Cartier, Quebec, Canada
Duraffourg Valerie, Belle Fontaine, France
Empson, Laura, Knaresborough, North Yorkshire
Flaxman Johnson, Edmund, Windsor, Berkshire
Fontaine, Josee, St-Basile-le-Grand, Quebec, Canada
Freeman, Derek, Hove, East Sussex
Gao, Xiaohuan, Shanghai, P.R. China
Geahel, Annemarie Charles, Montreal, Quebec, Canada
Gonzalez, Olga M., London
Goubert David, Les Avignon, France
Gritsenko, Anastasia, London
Harson, Docteur Jean Claude, Porto Vecchio, Corsica
Hoeu, Atitmuni Samnang, Phnom Penh, Cambodia
Hong, Nabin, Shanghai, P.R. China
Honour, Kevin J., Yeading, Middlesex
Huang Jinming, Guangxi, P.R. China
Jakkawanvibul, Jirapit, Bangkok, Thailand
Jamieson, Pauline, Edinburgh
Jaugeat Blaise, Vanves, France
Ji Qiusong, Guangxi 541004, China
Joannou, Christina, Ilford, Essex
Khounchanh, Marisa, Pointe-Claire, Quebec, Canada
Kim, Min Ji, Busan, Korea
Kuo Jia-Wen, Taipei, Taiwan, R.O. China
Lapsiwala, Foram Pravin, Gujarat, India
Law King Man, Kennedy Town, Hong Kong
Lee, Yun Jung, Ulsan, Korea
Lee Suk Chong, Yan Tong, Hong Kong
Lee Wan Ho, New Territories, Hong Kong
Li, Zhuonan, Shanghai, P.R. China
Liang, Jie, Birmingham, West Midlands
Lin, Sheau Lan, Taipei, Taiwan, R.O. China
Lin, Chun-Yen, Taipei, Taiwan, R.O. China
Liu, Feng-I, Taipei, Taiwan, R.O. China
Liu, Huijing, Shanghai, P.R. China
Louy, Olivier, Montreal, Quebec, Canada
Loye, Edward R., Plymouth, Devon
Lu, Sisi, Richmond, British Columbia, Canada
Lu, JR-Yang, Taipei, Taiwan, R.O. China
Lundvall, Linn, Lannavaara, 98013, Sweden
Luo Han, Guangzhou, P. R. China
Lust, Nathalie, Les Pennes Mirabeau, France
Lyons, Louise, London
Manasse, Daniele, Rome, Italy
Manuelli, Piero, Genoa, Italy
Matsukawa, Kent, Gampaha, Sri Lanka
Mayne, Edwina L., London
Mergalet, Caroline, Villefranche Sur Mer, France
Mitchell, Andreas, London
Muhhamedjanova, Jelena, Tallinn, Estonia
Ng Fei Yeung, Kowloon, Hong Kong
Noronha Muthu, Mrs Sunita Karen, Gujarat, India
Nwe, May Moe, Yangon, Myanmar
O'Cock, Sabrina, London
Park, Jin Hui, Busanjin-Gu, Busan, Korea
Park, Hey Kyung, Daegu, Korea
Park, Jin Hee, Daegu, Korea
Peng, Hsiang Chieh, Taipei, Taiwan, R.O. China
Peyron Alain, Nice, France
Poore, Sarah, Worthing, West Sussex
Pwint Phyu Win, Yangon, Myanmar
Rasche, Elizabeth, London
Rousseville, Prisca, London
Samaratunge, Punyadevi, Horana, Sri Lanka
Seo, Sun Mi, Daejeon, Korea
Shah, Prachi Hirenbhai, Surat, India
Sharma, Anita, Haryana, India
Simonsson, Kim, Stockholm, Sweden
Skalwold, Elise Ann, Ithaca, New York, USA
Soh Lip Sim, Johor Bahru, Malaysia
Soh Shi Hong, Johor Bahru, Malaysia
Son, Hye Jin, Masan-Si, Gyongsangnam-do 631-862, Korea
Soumare, Myriam, Paris, France
Spauwen, Tim, Mechelen, The Netherlands
Tan Huay Sian, Michelle, Singapore
Tan Kiat Choo, June, Johor Bahru, Malaysia
Teng, Ying, Shanghai, P.R. China
Teng Yongqing, Guangxi, China
Thinn, Jessica Myint, London
Thomas, Jane, Skipton, North Yorkshire,
Tran-Vinh, Caroline, Issy-Les-Moulineaux, France
Underwood, Antonia Charlotte, London
Wang, Wenyi, Guangzhou, P. R. China
Wang Hongmei, Guangxi, P. R. China

Wang Hui, Guangxi, P. R. China
Wang Liling, Guangxi, P. R. China
Wang Zongyu, Guangxi, P. R. China
Watrelos, Celine, Paris, France
Weng Chuxin, Guangxi, P. R. China
Win, San San, Singapore
Wu Dehe, Dehe, Guangzhou, P. R. China
Ye Ying, Singapore
Yim, Hye Jung, Gypmgsamgnam-do, Korea
Yip Long Ching, New Territories, Hong Kong
Yow, Kitty, Island South, Hong Kong
Zavadnikova, Valeria, London
Zhang Jieqin, Guangxi, P. R. China
Zheng, Wenting, Shanghai, P. R. China
Zhong Xiangtao, Guangxi, P. R. China
Zhu, Ye, Shanghai, P. R. China

Gem Diamond Examination

Gem Diamond Diploma

Qualified with Distinction
Rowley, Elaine, London

Qualified with Merit
Vefa, Jale Aydin, Sidcup, Kent

Qualified
Chan Che Min, Tsuen Wan, Hong Kong
Chan Po Ling, Kowloon, Hong Kong
Chan, Oi-Yan, Kowloon, Hong Kong
Cheng Chong Chuen, Tsuen Wan, New Territories, Hong Kong
Dollond, Steven, London
Drummond, Jean, Farnham, Surrey
Ferneyhough, Ella Jane, Leamington Spa, Warwickshire
Ho Wing Yi, Kowloon, Hong Kong
Hui, Hau Kan, Feltham, Middlesex
Huijbrechts, Thomas N., Salisbury, Wiltshire
Ji, Shuming, Beijing, P.R. China
Kai, Li, Beijing, P.R. China
Kan Sau Mei, Abby, Kowloon, Hong Kong
Kearney, Sonny Michael, Kimberley, Nottinghamshire
Khaing, Win Win, Bahan Township, Yangon, Myanmar
Lam Lai Kam, Kowloon, Hong Kong
Lee, Kitty Wai Yin, Tuen Mun, New Territories, Hong Kong
Lin, Chun-Yen, Taipei, Taiwan
Monogyios, John, Athens, Greece
Ng, Che Keung, New Territories, Hong Kong
Shaw, Martin Mackenzie, Kowloon, Hong Kong
Shaw, Bianca Debbie Fung Yee, Kowloon, Hong Kong
Shen, Huanqun, Shanghai, P.R. China
Stefani, Helen, Athens, Greece
To Siu Lun, New Territories, Hong Kong
Tong Sen Yue, Sandy, Central, Hong Kong
Wang, Qian, Beijing, P.R. China
Wang Hongbin, Wuhan, Hubei, P.R. China
Wong Fung Ha, New Territories, Hong Kong
Wong Lai Pui, Tuen Mun, New Territories, Hong Kong
Wong Wing Suet, Kowloon, Hong Kong
Xing Yingying, Hubei, P.R. China

Members' Meetings

Gem Discovery Club Specialist Evenings

The Gem Club meets every Tuesday evening at the Gem-A London headquarters when Club members have the opportunity to examine a wide variety of stones, and once a month a guest gem or mineral specialist is invited to give a presentation.

The November guest speaker was Diane Flora who gave Club members an introduction to the AGS Diamond Grade Cutting System. The guest in January was Mohammed Jabir who gave a presentation entitled 'Pearls, a natural history', explaining the origin and history of pearls before describing the growing interest in natural pearls and the resulting increase in demand and prices. In February Helen O'Neill of PMC Studio Ltd gave a talk and demonstration on precious metal clay with particular reference to the *in situ* firing of natural gemstones. Haji Abdul Hajid Butt, former general manager of J & K Minerals, the Indian Government Agency responsible for the Kashmir sapphire mines, was the March specialist, who gave a talk about the Kashmir sapphire mines, their location, geology, potential and the problems of working at 16,000 feet! Gem Club members were treated to a second specialist evening in March, when Guy Clutterbuck gave a talk on Zambian emeralds and aquamarines. He buys substantial quantities of emerald and aquamarine at source in Zambia, in addition to investing in small-scale mining operations. The April guest speaker, Alexandra Russell-Stoneham, shared her knowledge on the Russian diamond market in her presentation 'From Yakutia with Love'. She had delved into the world of the Russian diamond market, tracing its history from the discovery of the first kimberlite pipe to the present day, whilst studying in St Petersburg. In May, Anton Vasiliev from the LAL Stone-cutting Company, Russia, presented a special report on the Russian emerald mines, followed by a presentation on his facet design software.

Many of the Gem Club presentations have been reported in *Gems & Jewellery*.

Midlands Branch

The Branch Annual General Meeting was held on 25 January 2008 at the Earth Sciences Building, University of Birmingham, at which Paul Phillips, Elizabeth Gosling and Stephen Alabaster were re-elected Chairman, Secretary and Treasurer respectively. The AGM was followed by a Team Quiz and a Bring and Buy Sale. Other events held at the Earth Sciences Building included a presentation by Gwyn Green on 30 November 2007 on the observations of bubbles as an aid to gem identification, a talk on 29 February 2008 entitled 'Birmingham silver and the history of the Assay office' by Dr Sally Baggott, Curator at the Birmingham Assay Office, and a presentation by Doug Garrod on natural, treated and synthetic corundum on 25 April. At a meeting on 18 November 2007 held at Barnt Green, Alan Hodgkinson gave a talk on opals and provided many interesting specimens to examine. The Branch's 55th Anniversary Dinner was held on 8 December, also at Barnt Green.

North East Branch

Meetings held at the Ramada Jarvis Hotel, Wetherby, included a talk by Don Ariyaratna on the gems and the gem industry of Sri Lanka on 13 September 2007 and 'It's all in the cut', a presentation by James Riley of Backes & Strauss on pricing held on 2 April 2008. Doug Garrod gave a talk on the colour in diamond on 1 May at the Pavilion Hotel, Fulford, York.

North West Branch

On 17 April organics expert Maggie Campbell Pedersen spoke on organics and their fakes. James Riley of Backes & Strauss gave a talk on diamonds on 15 May entitled 'It's all in the cut'. Both meetings were held at the YHA Liverpool International, Wapping, Liverpool.

Scottish Branch

The Scottish Branch Conference was held at the Queen's Hotel, Perth, from 2 to 5 May. Speakers included George Rossman (keynote), David Callaghan, Alan Hodgkinson, Brian Jackson, Harold Killingback, Elisabeth Strack, Anton Vasiliev and Stephen Whittaker. The Sunday afternoon was devoted to workshops and displays, and the Conference concluded on the Monday with a field trip to collect haggis rock and visit Lauriston House to view the Blue John collection. (A report of the Conference was published in June 2008 issue of *Gems & Jewellery*.)

On 26 November 2007 Branch members visited auctioneers Lyon & Turnbull for a preview of their Fine Jewellery and Silver Sale. Meetings held at the British Geological Survey, Edinburgh, included a talk by Tracy Jukes on 16 October 2007 on coloured gemstone valuation in the twentieth-first century; Louise Johnson gave a presentation entitled 'Samba, topaz, lemurs and sapphires' on 22 January 2008; and James Riley gave a talk entitled 'It's all in the cut', explaining how the cut of a diamond affects the price, on 1 April. On 25 February at Napier University, Edinburgh, Margaret Sax gave a talk on techniques of Chinese and Mughal jade carving.

South East Branch

The Branch Annual General Meeting was held on 27 March at the Grange Holborn Hotel, London WC1, when Veronica Wetten, Liz Taylor and Roderick Booth were elected Chairman, Secretary and Treasurer respectively. The AGM was followed by a lecture on jade by Alan Jobbins.

South West Branch

Branch meetings held at the Bath Royal Literary and Scientific Institution included a hands-on session on 8 October 2007 with Doug Garrod looking at the colours of gemstones and how we see them; a talk on Scottish gemstones by Brian Jackson on 24 February, and a talk and practical session with Gwyn Green entitled 'Is it a diamond?' on 18 May.

Membership

Between 1 November 2007 and 31 May 2008, the Council approved the election to membership of the following:

Fellowship (FGA)

Abduriyim, Ahmadjan, Japan. 2007
Bieri, Willy Peter, Escholzmatt, Switzerland. 2008
Bracey, Anne Christine, Birmingham, West Midlands. 2008
Bryl Gaudet, Lou-Pierre, Montreal, Quebec, Canada. 2007
Dowden, Simon, Chadds Ford, Pennsylvania, U.S.A. 2008
Gunnarsson, Camilla E., Norrtälje, Sweden. 2008
Hansson, Maria Charlotte, Lannavaara, Sweden. 2008
Hossenlopp, Patricia, Chene – Bougeries, Switzerland. 2007
Luzuriaga Alvarez, Hugo Vicente, Montreal, Quebec, Canada. 2007
Munoz-Vasquez, Alejandra, London, 2007
Naing, Soe Moe, Southall, Middlesex. 1999
Sarraf, Kundan, Kathmandu, Nepal. 2007
Sourendre Shah, Rupal, Antananarivo, Madagascar. 2006
Stevenson, Laura, North Vancouver, British Columbia, Canada. 2007
Tovey, Kevin, Newport, Gwent. 1987

Educational Sponsorship and the 100 Club

This year Gem-A is celebrating One Hundred Years of Gemmological Education. To ensure that we remain the provider of the highest status gem education through our second century, we have ambitious plans for the expansion and increased accessibility of Gem-A courses worldwide. This can only be achieved with the support of our Fellows and members, and the gem and jewellery trade.

To encourage donations, two new fundraising schemes have been introduced. The first is the 100 Club aimed at Fellows and members of the Association; a donation of a minimum of £1000 is required to join the Club. The second is Educational sponsorship. Gem and jewellery companies, trade organizations and all those who support gem education have been invited to become sponsors with a choice of three levels: Diamond Sponsorship (over £10,000), Ruby Sponsorship (£5000–£9999) and Pearl Sponsorship (£1000–£4999).

The Council of the Association is most grateful to the following who have already joined the 100 Club or become Educational Sponsors.

100 Club

Canadian Gemmological Association, North York, Ontario, Canada
Terry M.J. Davidson FGA, Coln St Aldwyn, Gloucestershire
David Gann Ltd, London
Gemological Institute of America, Carlsbad, California, U.S.A.
Dr Roger R. Harding FGA, Avebury, Wiltshire
Andrew F. Hinds FGA, London
Harold Killingback FGA, Oakham, Leicestershire
Shinko Katayama FGA, Colombo, Sri Lanka
Robert J. Maurer FGA DGA, Redhill, Surrey
Dr Jack M. Ogden FGA, London
James Riley, Knutsford, Cheshire
Scottish Branch of the Gemmological Association of Great Britain
Simon A. Stoodley FGA, Alton, Hampshire
Unni Trolle FGA DGA, Eslov, Sweden
John O. Vince FGA, West Adderbury, Oxfordshire

Educational Sponsorship

Ruby Sponsorship

The Accredited Gemologists Association, San Diego, California, U.S.A.

Pearl Sponsorship

Mohammed Idris Jabir, Kuala Lumpur, Malaysia
Sanaullah Khan, Peshawar, Pakistan
K.K. Sharma, Indian Diamond Institute, Surat, India
Benjamin Zucker, new York, U.S.A.

Diamond membership (DGA)

Austen, Katelyn, Birmingham, West Midlands. 2007
Martins, Miki, Burnaby, British Columbia, Canada. 2007
Thomas, David John, Milton Keynes, Buckinghamshire. 2007

Associate membership

Akerlund, Sophia, Lidingo, Sweden
Akinfenwa, Ayodeji, London
Astley, Mark, London
Awad, Elizabeth, Reading, Berkshire
Blake, Andrea, Chevy Chase, Maryland, U.S.A.
Chen Wei-Ting, London
Chitty, Warne, Aspen, Colorado, U.S.A.
Coppack, Flavia, London
Corbett, John, East Grinstead, West Sussex
Drayson, Marie Lule, London
Dungler, Pierre, Beziers, France
Duval, Pauline, France
Feldheim, Yinon, Israel
Florio, Daniela, London
Fowell, May, London
Franklin, Peter Nigel, Shenfield, Essex
Fujii, Hideo, Soka City, Saitama Pref., Japan
Gamley, Alistair, Hullbridge, Essex
Gandulfo, Veronica, Teofilo Otoni, Minas Gerais, Brazil
Gerrard, Edward Francis, Nealon, Western Australia, Australia
Glendening, Sarah Louise, Eastbourne, East Sussex
Gordon, Richard, Farningham, Kent
Hamston, Janet, Old Basing, Hampshire
Hara, Shintarou, Sasebo City, Nagasaki Pref., Japan
Hardy, Sarah, Middlesbrough, North Yorkshire
He Xiaoyu, London

Gifts and Donations

The Association is most grateful to the following for their gifts and donations for research and teaching purposes:

Haji Abdul Majid Butt, Kashmir, for a piece of Kashmir sapphire mine rock containing sapphire crystals
Maggie Campbell Pedersen FGA, London, for a selection of organic beads including natural, dyed and simulated coral, and carved bone, jet, opercula and spikey shells
Steven Collins FGA DGA, Letchworth, Hertfordshire, for a selection of pezzottaite cabochons
Branko Deljanin BSc FGA DGA, Vancouver, British Columbia, Canada, for a piece of rough diamond crystal weighing 0.69ct
Eric Emms BSc FGA DGA, London, for a two-pan balance
Alexey Eremen, Russian Colored Stone Company, Genesee, Colorado, U.S.A., for a piece of Russian chromian diopside
Chaman Golecha FGA, Chennai, India, for pieces of sapphire and ruby with a trapiche-like appearance
Mohammed Idris Jabir, Kuala Lumpur, Malaysia, for a selection of natural and cultured pearls, in memory of his father Mohammed Idris
Dominic Mok FGA DGA, Hong Kong, for a range of refractometers for Gem-A's examinations in Hong Kong and a box of yu hua shi (Chinese agate)
Paula Preston, London, for two boxes of yu hua shi (Chinese agate)
Sara Ritchie GG, Glen Ridge, New Jersey, U.S.A., for three pieces of operculum
Alexandros Sergoulopoulos FGA DGA, Athens, Greece, for four rough diamond crystals
Jason Williams FGA DGA, London, for a collection of natural and synthetic cut stones
Zhili Qiu FGA, Guangzhou, P.R. of China, for a selection of rough B jade

Montetary donations were gratefully received from:

Raed Al-Hadad FGA, Abu Dhabi, United Arab Emirates
Alexander Armati DGA, Sonning Common, Berkshire
Eisuke Ashida FGA, Kyoto, Japan
Petra C. Bardehle FGA, Holzhausen, Munsing, Germany
Bjorn Bendikssen, Sto, Norway
L.M. Bevers-Reinders.FGA, Rotterdam, The Netherlands
Burton A. Burnstein., Los Angeles, California, U.S.A.
Susan Deacon FGA, London
Dennis Durham., Kingston upon Hull, East Yorkshire
Gwyn Green FGA DGA, Birmingham, West Midlands
Masao Kaneko FGA, Tokyo, Japan
John C.A. Kulukundis FGA, London
Heli Kuulman FGA, Tallinn, Estonia
Sandra Lear FGA, Morpeth, Northumberland
Torbjorn Lindwall FGA DGA, Lannavaara, Sweden.
Caroline E. Maclachlan FGA DGA, Edinburgh, Scotland
Stefanos Mourtzanos FGA, Crete, Greece
Sara Naudi FGA, London
Edward Nealon, Booragoon, Western Australia, Australia
Robert L. Rosenblatt FGA, Salt Lake City, Utah, U.S.A.
Elaine Rowley FGA DGA, London
David J. Sayer FGA DGA, Wells, Somerset
Moe Moe Shwe FGA, Singapore
Monika Sinagra FGA, Shanghai, P.R. China
Elisabeth Strack GG FGA, Hamburg, Germany
Annaliese J.C. Stubbs DGA, London
Stasia-Mae Tereszczuk, Little Horwood, Buckinghamshire
Francoise Tschudin FGA, Neuchatel, Switzerland
William J. Tucker FGA, Douglas, Isle of Man
U Myint Tun FGA, Lulea, Sweden
Michael Vaughan FGA, Elesmere Port, South Wirral
Keith P. Whitehouse BSc(Hons) FGA DGA, Nr Church Eaton, Staffordshire
Christine M. Woodward FGA DGA, London

Henderson, Ian M., Windsor, Ontario, Canada
Horner, Peter James, Hallkirk, Caithness, Scotland
Jagne, Kura, London
Kerremans, Yves, Lier, Belgium
Kitami, Kumiko, Yokohama City, Kanagawa Pref., Japan
Langdon-Smith, Elizabeth, Luxembourg
Leger, Emmanuelle, Amiens, France
Madhu, Bindiya, Hatfield, Hertfordshire
Mamada, Ikuko, Taito-ku, Tokyo, Japan
Marais, Eugene, Stevenage, Hertfordshire
Masaki, Furuya, Kofu-shi, Yamanashi-ken, Japan
Mathews, Thomas, Freeport, Illinois, U.S.A.
Matsuk, Daria, London
Mergalet, Caroline, Villefranche Sur Mer, France
Mithaiwala, Priyanka, London
Mizukami, Yusuke, Saitama City, Saitama Pref., Japan
Mo, Zhuangguo, London
Monkute, Vilita, London
Mullins, David, Van Wert, Ohio, U.S.A.
Nishikawa, Takamichi, Kusatsu City, Shiga Pref., Japan
O'Neill, Helen E.J., Amersham, Buckinghamshire
O'Sullivan, Gary, Newbury, Berkshire
Oudy, Myriam, Opio, France
Pace, Elizabeth Julia Mitchell, Carmarthen, Dyfed
Paige, Denise, London
Parry, Lucy, Widnes, Cheshire
Phipps, Jane Margaret, Addlestone, Surrey
Prendergast, Lorna, Great Missenden, Buckinghamshire

Russell, Peter, Cheltenham, Gloucestershire
Sano, Taiki, Himeji City, Hyogo Pref., Japan
Savchenko, Elena, London
Segurado, Taynara Leão, Glasgow, Scotland
Simm, Charlotte, London
Small, Robert Charles, Kilembe, Uganda
Stockbridge, John, Windsor, Berkshire
Sturman, Darko, Toronto, Ontario, Canada
Sugihara, Toshiyuka, Osaka City, Osaka, Japan
Thein Thein Win, Rosy, London
Voltaire, Barbra, San Francisco, California, U.S.A.
Webb, Gordon Phillip, London
Whiffin, Andrew Stafford, Meopham, Kent
Yamaguchi, Nao, Shikonawate City, Osaka, Japan

Transfers

Associate Membership to Fellowship and Diamond Membership (FGA DGA)

Lin Chun-Yen, Taipei, Taiwan, R.O. China. 2008

Fellowship to Fellowship and Diamond Membership (FGA DGA)

Drummond, Jean, Farnham, Surrey. 2008
Ferneyhough, Ella Jane, Leamington Spa, Warwickshire. 2008
Rowley, Elaine, London. 2008

Diamond Membership to Fellowship and Diamond Membership (FGA DGA)

Baker, David Mark, Bath, Avon. 2008
Chan Chi Wai, Wah Fu Estate, Hong Kong. 2008
Netsah, Maayane, London. 2008

Associate Membership to Fellowship (FGA)

Chitty, Warne W., Aspen, Colorado, U.S.A. 2008
Gerrard, Belinda Louise, Sydney, New South Wales, Australia. 2008
Jeavons, James, Geebung, Queensland, Australia. 2008
Mitchell, Andreas, London. 2008
Rasche, Elizabeth, London. 2008
Ringhiser, Barbara G., Lake Worth, Florida, U.S.A. 2008
Shpartova, Irina, London. 2998
Underwood, Antonia Charlotte, London. 2008

Associate Membership to Diamond Membership (DGA)

Dollond, Steven, London. 2008
Hui Hau Kan, Feltham, Middlesex. 2008
Huijbrechts, Thomas N., Salisbury, Wiltshire. 2008
Shen, Huanqun, Shanghai, P.R. China. 2008

Erratum

In *J. Gemm.*, 2007, **30**(7/8), p.450, right-hand column, in equations I-1 and I-2 the term should be $\tan^2 V_z$, not $\tan 2V_z$

Obituaries

Professor Chen Zhonghui
1935–2007

Professor Chen was born in Shanghai on 1 October 1935 and died on 6 November 2007 at the age of 73 (sadly, just before I was due to meet him in Beijing where he lived in the university district).

Chen trained as a geologist and studied the geology of coal in the Ukrainian Coalfield where he also learnt Russian. On his return he taught coal geology at the China University of Geosciences (CUG) in Beijing and wrote many articles on the economic geology of coal. In 1980 he rose to Principal in CUG and, at that time, he moved with part of the university to Wuhan on the Yangtze River (Chang Jiang) and soon afterwards was made Professor. Professor Chen established the first gemmological education in Mainland China, with the first Gem-A course starting in 1989. Thus he initiated the Association's excellent relations with so many people in the gem and jewellery industry in Mainland China, following the pioneering visits of E. Alan Jobbins (now President of the Association) and Dr Jamie B. Nelson who introduced the Association's curriculum and practical gem testing programme during the previous year. Their introduction to Professor Chen and his wife Professor Yan Weixuan, who had established the mineralogical museum at the university, came through their good friend Ms Mimi Ou Yang Chiu Mei, President of the Hong Kong Institute of Gemmology – a Gem-A Allied Teaching Centre. In order to achieve this historic start in 1989, Professor Chen sought and obtained funding from many sources throughout Mainland China and Taiwan, and through his efforts the Wuhan school became the first of our Allied Teaching Centres in Mainland China. He followed this with plans for a jewellery institute, established in 1992. He established the Association's Gem Diamond Diploma course in China in 1993 with funding from the chemical industry.

Throughout this time and afterwards through his retirement and up until his death, Chen Zhonghui was tireless in his translation work and in producing a translation glossary, course notes and handbooks. His huge effort to support the Association's examination system throughout China established and ensured its safety and integrity. He also produced the *Chinese-English Dictionary of Jewellery*, now in its third edition.

Chen was highly regarded in international gemmology; he set up the annual conference of the Gemmological Institute of China at the Wuhan campus and later elsewhere in China, attracting many important gemmologists from more than twenty countries, increasing China's relationships with international gemmology. In 1997, Chen and his wife were invited by the Association to visit London for Chen to present the Diplomas and

Professor Chen and his wife Professor Yan Weixuan during their visit to London in 1997.

Prizes at the annual Awards Ceremony at Goldsmiths' Hall, where he delivered a speech which brought the connections with the Far East that bit closer to the home of gemmological education. In 2004–5 Chen organized the 29th International Gemmological Congress in Wuhan which, after a year's delay brought about by the SARS outbreak, attracted gemmologists from more than thirty countries.

Through these past two decades, Chen remained in very close contact with me in my role as Director of Education and with the members of our team, some of whom he met during our periodic visits to China, and his welcome and ready discussions leave a legacy of continuity in our programme of work in China. Without his effort and support, it is hard to see how such good relations and success for the Association in China could have come about and continue in a way that enables us to develop further our close contact and our education and membership programmes.

For his great service to gemmology and gem education, Professor Chen was awarded an Honorary Fellowship of the Association in 1999, one of only four in the world at that time. His great care and his extremely high standards, his attention to detail, his readily-given advice and his warm sense of humour, are all attributes so valuable in someone who I am pleased to have known as a good friend as well as a truly valuable supporter of the Association and its education staff.

Ian Mercer

Grahame Brown
1935–2008

Grahame Brown, long-time Editor of the *Australian Gemmologist*, passed away on 15 January 2008, after a long battle with cancer.

Graham joined the Queensland division of the Gemmological Association of Australia (GAA) in 1973. His many achievements in the world of gemmology included the award in 1974 of the Australia Prize, having achieved the highest marks in Australia in the GAA Diploma of Gemmology examinations. He was elected a Fellow of the Gemmological Association of Great Britain in 1975, having qualified for his Diploma in Gemmology with Distinction. In 1978 he was awarded the first Research Diploma of the GAA for a thesis entitled 'Investigations into the structure and properties of precious corals'.

It would be hard to find a group of several gemmologists and gem materials authors and gem enthusiasts who together could begin to take the place of someone like Grahame. And he made his expertise available, worldwide, to gemmologists, enthusiasts and students. He gave great support to students of Gem-A and to its exam candidates, by giving student support, arranging exam facilities and taking great care of the detail and security of the Association's exam system. Grahame's talks in London demonstrated his straightforward approach to information and its sharing, opening further the discussion on the huge variety of organic gems or, as he correctly insisted for very logical reasons, 'gem materials of organic origin'.

My all-too-brief chats and discussions with Grahame, in London, in China and in his own home just last October, left me with a pleasant feeling that here is a bloke who's in touch and, crucially, one who kept in touch with the fullest use and enjoyment of the literature and the communicators in the world of gems. Grahame's passing is a huge loss to the international gem world.

Ian Mercer

William (Bill) F. Ferguson
1931–2007

Bill Ferguson FGA DGA (D. 1956), Balloch, Strathclyde, died following a short illness in 2007.

Bill served a five-year horological apprenticeship with John Hudson in Alexandria, Dunbartonshire, prior to his National Service from 1952–54. He was an Inspector for Westclox for one year before taking over the jewellery business of John Hudson. He started teaching part-time, but later took on a full-time position teaching gemmology and horology at Barmulloch College, Glasgow, leaving his wife May to run the shop during the week.

Bill won the admiration of countless students by his encouragement and compassionate concern to pass on all he knew.

Bill Ferguson is survived by his wife May and son Neil, who carries on the jewellery tradition in Rhode Island.

* * *

Robin Ian McKay FGA DGA (D.1957), Harmans Cross, Dorset, died on 5 December 2007.

Evelyn Sim FGA DGA (D.1990), Edinburgh, died in 2007.

Gem-A Events

Monday 30 June	**ANNUAL GENERAL MEETING** followed by **Surviving a Life Sentence at Christie's** by **David Warren**
Thursday 3 July	**GEM-A CENTENARY DINNER**
Wednesday 9 July	**GEM DISCOVERY CLUB** **Identification of Small, Colourless and Fancy Colour HPHT-grown and CVD-grown Diamonds** with **Branko Deljanin** of EGL Canada
Tuesday 16 September	**HONG KONG GRADUATION AND AWARDS DINNER** Venue: Royal Palace Chinese Restaurant, Kowloon (see p30 for further details)
Thursday 18 September	**NORTH WEST BRANCH** **Fakes and Forgeries in the Silver Markets** by **Andrew Spicer**
Friday 26 September	**MIDLANDS BRANCH** **Reflections on Gem Cutting** by **Doug Morgan**
Thursday 16 October	**NORTH WEST BRANCH** Branch AGM followed by **Gems in Archaeology** by **Jo Jones**
Thursday 23 October	**NORTH EAST BRANCH** **Identifcation of Colourless Gems in jewellery** by **Gwyn Green**
Saturday 25 and Sunday 26 October	**GEM-A CENTENARY CONFERENCE AND EUROPEAN GEMMOLOGICAL SYMPOSIUM** Venue: The Hilton London Kensington (see p.14 for further details)
Monday 27 October	**GRADUATION CEREMONY AND PRESENTATION OF AWARDS** Venue: Goldsmiths' Hall, Foster Lane, London EC2V 6BN
Friday 31 October	**MIDLANDS BRANCH** **British and European Hallmarking, Birmingham Silver and the Influence of Matthew Boulton** by **Dr Sally Baggott**
Friday 28 November	**MIDLANDS BRANCH** **Eighteenth-Century Jewellery: Buttons, Bows and Bones** by **John Benjamin**
Saturday 29 and Sunday 30 November	**MIDLANDS BRANCH** **Anniversary Dinner (Saturday) and Centenary Conference (Sunday)** Venue: Menzies Strathallan Hotel, Birmingham
Sunday 7 December	**NATURE'S TREASURE: MINERALS AND GEMS** A joint Gem-A/Mineralogical Society one-day seminar Venue: The Flett Theatre, Natural History Museum, London

Contact details

Gem-A Headquarters:	Olga Gonzalez on 020 7404 3334 email olga.gonzalez@gem-a.com
Midlands Branch:	Paul Phillips on 02476 758940 email pp.bscfgadga@ntlworld.com
North East Branch:	Mark Houghton on 01904 639761 email sara_e_north@hotmail.com
North West Branch:	Deanna Brady on 0151 648 4266
Scottish Branch:	Catriona McInnes on 0131 667 2199 email scotgem@blueyonder.co.uk
South East Branch:	Veronica Wetten on 020 8577 9074 email veronica@wetten.co.uk
South West Branch:	Richard Slater on 07810 097408 email richard@fellows.co.uk

For up-to-the minute information on Gem-A Events visit our website at **www.gem-a.com**

One hundred years 1908 2008

OF GEMMOLOGICAL EDUCATION

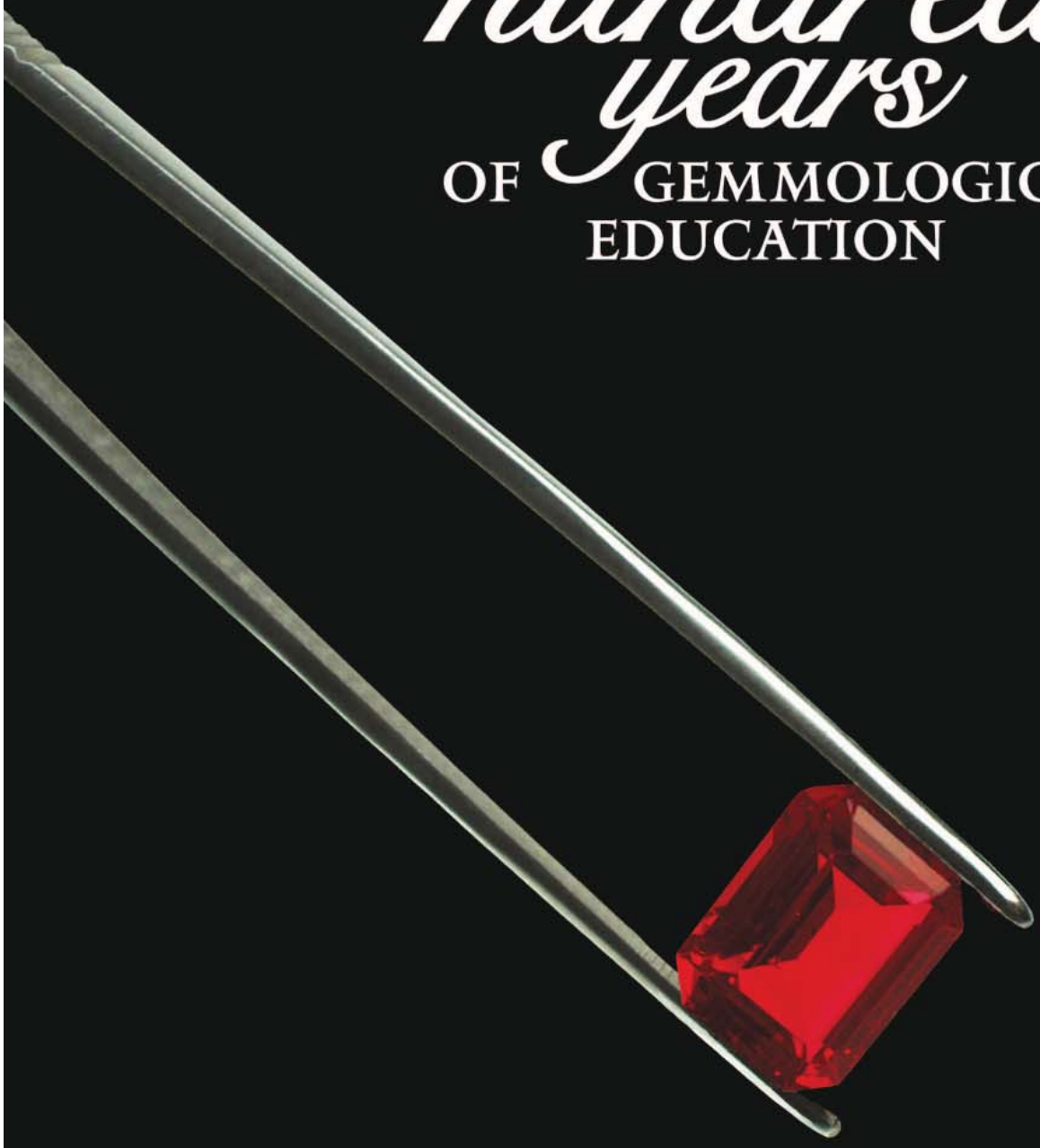

Gem-A

THE GEMMOLOGICAL ASSOCIATION
OF GREAT BRITAIN

The Journal of
Gemmology
2008 / Volume 31 / Nos. 1/2

Contents

Cover Picture: Faceted thortveitite in daylight (top) and incandescent light (lower right). (See Thortveitite – a new gemstone, p. 1.)

The Gemmological Association of Great Britain

27 Greville Street, London EC1N 8TN
T: +44 (0)20 7404 3334 **F**: +44 (0)20 7404 8843
E: information@gem-a.com **W**: www.gem-a.com

Designed and printed by DG3 (Europe) Ltd
ISSN: 1355-4565